VISVESVARAYA TECHNOLOGICAL UNIVERSITY

Jnana Sangama, Belagavi,Karnataka - 590 018

A Dissertation Report on

Title

Numerical and Experimental Analysis of Automotive Exhaust Gas Thermoelectric Generator

Submitted in partial fulfillment of the requirements for the award of the degree of

Doctor of Philosophy

in

Mechanical Engineering

by

RAVINDRA KONDAGULI
USN:2BL16PMJ04

Under the Guidance of

Supervisor

Prof. P V Malaji M.Tech.,Ph.D.

Co-Supervisor

Prof C R Hiremath M.Tech.,Ph.D.

Department of Mechanical Engineering

BLDEAs V.P Dr. P.G Halakatti College of Engineering and Technology

Vijayapura 586103.

1980

VISVESVARAYA TECHNOLOGICAL UNIVERSITY

Jnana Sangama, Belagavi-590 018.

BLDEAs V.P Dr. P.G Halakatti College of Engineering and Technology

Vijayapur-586103.

CERTIFICATE

This is to certify that the project work entitled **"Numerical and Experimental Analysis of Automotive Exhaust Gas Thermoelectric Generator"** is a bonafide work of **Ravindra Kondaguli(2BL16PMJ04)** carried out in the Department of Mechanical Engineering , BLDEAs V.P Dr. P.G Halakatti College of Engineering and Technology, Vijayapur

Signature of the Co-Guide

Signature of the Guide

Signature of Head of Research center

HOD
Mechanical Engg. Dept.
BLDEA's V.P.Dr. P.G.Halakatti
College of Engg. & Tech., Vijayapur

Signature of Head Institute

Principal
B.L.D.E.A's. V.P. Dr. P.G.H.
College of Engg & Tech.

External Viva

Name of the examiner

Signature with date

1.

2.

DECLARATION

I hereby declare that, the research work embedded in this doctoral thesis entitled, **"Numerical and Experimental Analysis of Automotive Exhaust Thermoelectric Generator"**, submitted for the award of degree of Doctor of Philosophy in Mechanical Engineering, has been carried out by me under the guidance of **P V Malaji**, Associate Professor,Department of Mechanical Engineering , BLDEAs V.P Dr. P.G Halakatti College of Engineering and Technology, Vijayapur. I declare that the contents of this thesis and the results of this research work has not been submitted in part or full for the award of any diploma or degree of this or any other university. This research has good contributions justified through simulation results and authenticated through standard publications in good quality journals and conferences.

Ravindra Kondagul
USN: 2BL16PMJ04

ACKNOWLEDGMENTS

First and foremost, I would like to express my sincere gratitude to my supervisor, Prof. Pradeep Malaji, for his constant guidance throughout my PhD. He introduced me to the exciting field of thermoelectrics and also taught the necessary experimental skills to carry out the work. He has always pushed me to think more scientifically and carry out a deeper analysis of the data, which was crucial in uncovering important physics and helped me in writing the papers. I have learnt many scientific as well as non-academic things from him, for which I am very fortunate and thankful.

I would like to thank my co-supervisor Prof. C R Hiremath for constant guidance throughout my PhD and also taught the necessary experimental skills to carry out the work. He has always pushed me to think more scientifically and carry out a deeper analysis of the data, which was crucial in uncovering important physics and helped me in writing the papers.

I wold like to thank Prof. Ramesh Chandra Mallik Department of Physics Indian Institute of Science Bangalore for teaching me how to do research and allowing to use resources at IISC to do experiments.

I would like to thank my doctoral committee members Dr. Syed Abbasali(SIET, Vijayapur), Dr.S G Cholake (BLDEACET, Vijayapur).) for their fruitful suggestions and comments. I would like to acknowledge the Head of research center the mechanical department, Prof.R N Jeergal and Dr. V G Sangam Head of Institute.

Last but not the least, I acknowledge my wonderful parents: Shreeshail Kondaguli and Suvarna Kondaguli for inspiring me to pursue PhD, and for their constant love and support. I thank my wife, my confidant Smita for her encouragement and providing me the strength to get through some difficult times. I thank my brothers Chandrashekar,Basavaraj and my sister-in-laws Priya,Anupama. I thank my daughters Samyuktha,Nakshatra and my Sons Sanskar,Siddhartha and all my family members for their support and affection.

ABSTRACT

This present study focuses on the utilization of waste heat from internal combustion engines through the use of automotive exhaust gas thermoelectric generators (AETEGs). The inefficiency of internal combustion engines, where approximately 70% of the heat produced is wasted, presents an opportunity to increase the efficiency of automobiles by converting this waste heat into useful electricity. TEGs, which are solid-state devices that directly convert heat to electricity, have the potential to harness the heat energy from automotive exhaust gases. However, these devices are currently less explored and have lower efficiency, typically below 10%. Despite their lower efficiency, even the extraction of a small amount of energy from waste heat can have a significant impact.

The objective is to evaluate the properties and performance of a commercially available thermoelectric generator module and analyze the efficiency of AETEGs. The present work involves designing and fabricating heat exchangers to analyze AETEGs. Theoretical, numerical, and machine learning approaches are employed for analysis, and experimental methods validate results.

The current study delves into the concepts of equivalent and effective material properties, considering contact resistance and heat loss during experimentation. Equivalent material properties are influenced by temperature, making their theoretical and numerical modeling intricate. On the other hand, effective material properties remain unaffected by temperature, making them more suitable for theoretical and numerical modeling. The experimental analysis results of power output are compared with those obtained from theoretical and numerical modeling using effective material properties; they are comparable with a maximum deviation of 13% and 12% , respectively. As a result, chapter 4 and 5 adopts the use of effective material properties. Skuttrudite ($CoSb_3$) is a promising thermoelectric material for AETEGs; in the present work, it produced low voltage output due to electric contact resistance and a metal-semiconductor junction. Hence AETEG analysis is conducted on the commercially used bismuth telluride (Bi_2Te_3) Modules.

A commercially available TEG module (TEM-12706) is simulated, and its performance under different conditions is studied. For commercial TEG 12706, the hot side temperature is maintained at 70^0 C, and the cold side temperature is maintained at 30^0 C. The peak power produced is 168 milliwatts at a load resistance of 2.4Ω. The analysis includes the effects of load resistance, source and sink temperatures, and leg length. The present study also explores the impact of TEG shape on internal resistance and efficiency,

suggesting that square-shaped TEGs are more suitable for low load resistance, while circular cross-sections are better for high load resistance due to load and internal resistance tuning. Different shapes of uni-couple thermoelectric generators are examined, revealing the advantages of trapezoid cross-sections in terms of increased efficiency. The variation in sink temperature is found to have a greater effect on performance compared to source temperature. The concept of segmented legs is applied to increase power output.

The study highlights the role of heat exchangers in power production from AETEGs. Heat exchangers are designed and fabricated, with one experiment involving blowing hot air from a hot air gun on one side and circulating cold water on the other side of the heat exchanger. The results demonstrate a peak power of approximately 59 watts when 24 TEGs are connected in series with an 81 Ω load resistance. The analysis considers the effects of hot side temperature, load resistance, cold side temperature, and mass flow rate. Theoretical and numerical simulation results are compared with experimental results, showing close agreement with minor deviations attributed to heat losses and assumptions regarding effective material properties.

Furthermore, a heat exchanger is designed, fabricated, and mounted on the exhaust of a single-cylinder diesel engine to evaluate the performance of AETEG, the effect of temperature, the flow rate of hot exhaust gases, cold fluid, and the number of TEGs on the performance of AETEG are studied for exhaust gas mass flow of 12gm/s. The power of 10 TEG in series at matched load resistance is 35 watts. The matched load resistance is 24Ω.

In summary, this present work contributes to the understanding and improvement of AETEGs, providing insights into their properties, performance, and potential for increasing the efficiency of AETEGs. The findings emphasize the importance of material properties, heat exchanger design, and AETEG system tuning for maximizing power generation from waste heat.

Moreover, the present study validates effective material properties for thermoelectric generator simulations, enabling more accurate modeling and analysis. The optimization of the thermoelectric generator shape and the emphasis on the role of heat exchangers contribute to improved performance and power production from AETEGs.

Keywords: Thermoelectric generator,AETEG,Numerical Analysis,Characterization; —

Contents

List of Figures

List of Tables

Table 1: Nomenclature

Symbol	Description
ZT	Device Figure of merit
α	Seebeck Coefficient
κ	Thermal Conductivity
ρ	Resistivity of material
A	Cross section area
L	Length of Leg
$\dot{Q}_{out}$	Heat flow rate out from cold junction
$\dot{Q}_{in}$	Heat flow rate into hot junction
R_{in}	Internal resistance
R	Total resistance
R_L	Load Resistance
T_h	Hot Junction Temperature
T_c	Cold Junction Temperature
P_{out}	Power output from Thermoelectric generator
ZT	Device Figure of merit
zt	Material figure of merit
α	Seebeck Coefficient
κ	Thermal Conductivity
ρ	Resistivity of material
V_{opn}	open circuit voltage
η_{th}	Thermal Efficiency
L	Length of Leg
A	Cross section area
$\dot{Q}_{out}$	Heat flow rate out from cold junction
$\dot{Q}_{in}$	Heat flow rate into hot junction
$\dot{m}_{exh}$	mass flow rate of exhaust gases
$\dot{m}_c$	mass flow rate of cold fluid
R	Total resistance
R_L	Load Resistance
R_{in}	Internal resistance
T_c	Cold Junction Temperature
P_{out}	Power output from Thermoelectric generator
T_h	Hot Junction Temperature
η_{th}	Thermal Efficiency
K, σ	Thomson effect
J	current density
Pi	Peltier coefficient
$\dot{Q}_h$	Heat flow at the hot side

Continued on next page

Table 1 – continued from previous page

Symbol	Description
$\dot{Q}_c$	Heat flow at the cold side
P_{out}	Electric power generated by the TEG
T_h	Temperature at the hot side
T_c	Temperature at the cold side
α	Seebeck coefficient
I	Electric current
R	Internal resistance
K	Thermal conductivity
R_L	Load resistance
Z	Figure of merit
$\overline{T}_c$	Average temperature between the hot and cold sides
$\dot{Q}_{\text{in}}$	Heat input to the element
P_{max}	Maximum power
η	Efficiency
N	Number of thermoelectric material pairs
A_{leg}	Cross-sectional area of a single leg of the TEG
k_{leg}	Thermal conductivity of a single leg of the TEG
ΔT_{pair}	Temperature difference across each thermoelectric material pair
$\dot{S}_T$	Source term in the TEG equation
S	Seebeck coefficient
σ	Electrical conductivity
μ	Dynamic viscosity
ρ	Fluid density

Chapter 1

Introduction

Energy harvesting involves converting ambient energy into electrical energy through various methods, including solar, thermal, mechanical, and vibration approaches. Solar energy harvesting relies on solar cells to convert sunlight into direct current electricity. Mechanical energy harvesting employs piezoelectric generators to convert mechanical motion into electricity, while vibration energy harvesting utilizes electromagnetic generators to convert vibrations into electrical power. Thermal energy harvesting utilizes heat tranfer to generate electricity.

There are two main types of thermal energy harvesting: thermoelectric generators (TEGs) and pyroelectric generators. However, there are several other types of thermal energy harvesting methods with their unique applications. Thermophotovoltaic (TPV) cells use semiconductor materials to convert heat into electricity by emitting photons that are absorbed by photovoltaic cells. Thermoacoustic generators, made of materials with high acoustic impedance like aluminum, generate electricity from heat through the expansion and contraction of gases, producing sound waves. Thermogalvanic generators use the electrochemical reaction between two different metals, such as zinc and copper, to convert heat into electricity. Selecting the best thermal energy harvesting method depends on specific application requirements, with TEGs being suitable for large temperature differences and pyroelectric generators for applications with frequent temperature changes, such as in the human body. Examples of thermal energy harvesting applications include self-powered sensors, wearable devices, IoT devices in remote locations, telecommunications equipment, building energy management systems, and spacecraft using solar heat. As technology advances, thermal energy harvesting is likely to see increased adoption in a broader range of applications.

This chapter reports an introduction to the thermoelectric generator and its basic

principle. The automotive vehicle exhaust system is discussed. The possible location and potential of an Automotive exhaust thermoelectric generator are discussed. Statement of problem is made and objectives are defined. In the end outline of the thesis and the interconnection between chapters are briefed.

In the 21^{st} century, energy is a predominant factor in defining the economy of a country. The economy of the country is driven by electrical energy. According to IEA [1] about 65% of electricity is produced from coal, oil, and natural gas as shown in Fig. 1.1. The chemical energy associated with fossil fuels is initially converted to heat energy before converting to electricity. Heat is low-grade energy; about 66% of energy is lost in the form of waste heat, as shown in Fig. 1.2. From Fig. 1.3 it can be observed that, during various applications such as residential, Commercial, Industrial, and transportation, about 65.4% of energy is rejected.

Automotive vehicles are an integral part of modern human life. On average automotive vehicles can convert about 25% of available fuel energy into useful. About 5% is lost to friction, and the rest 70% is lost to exhaust gases and coolant. This waste heat can be trapped and converted to useful electrical energy using a solid-state device called a thermoelectric generator. Figure 1.4 shows the progress of research in the field of automotive vehicles. The research is focused not only to increase the efficiency of vehicles with present vehicles but also explore new technology like hybrid electric vehicles and hydrogen technology.

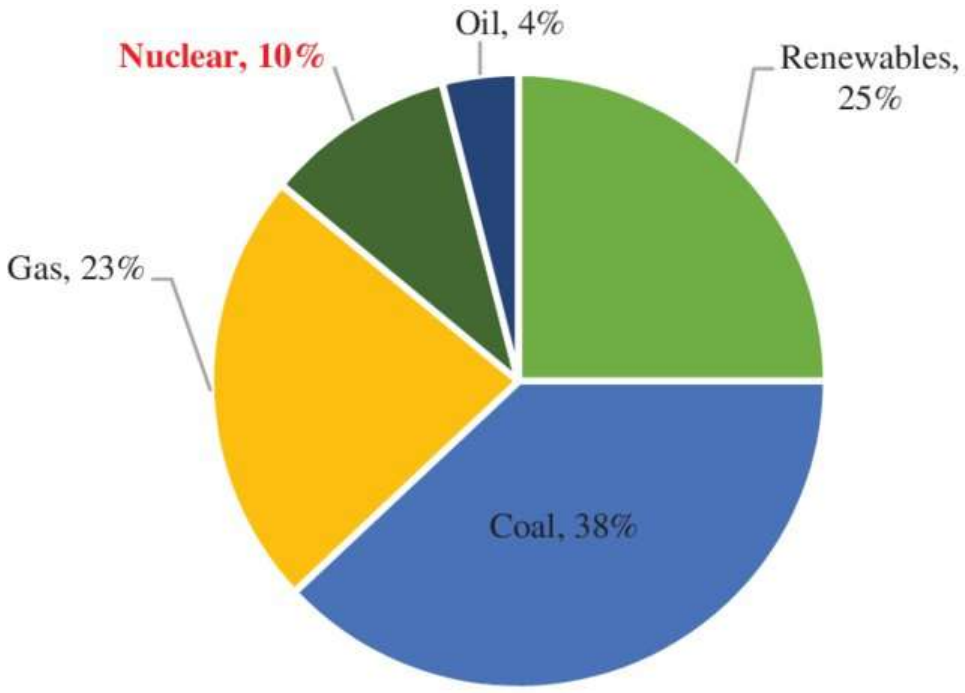

Figure 1.1: IEA 2017 World Energy scenario [1]

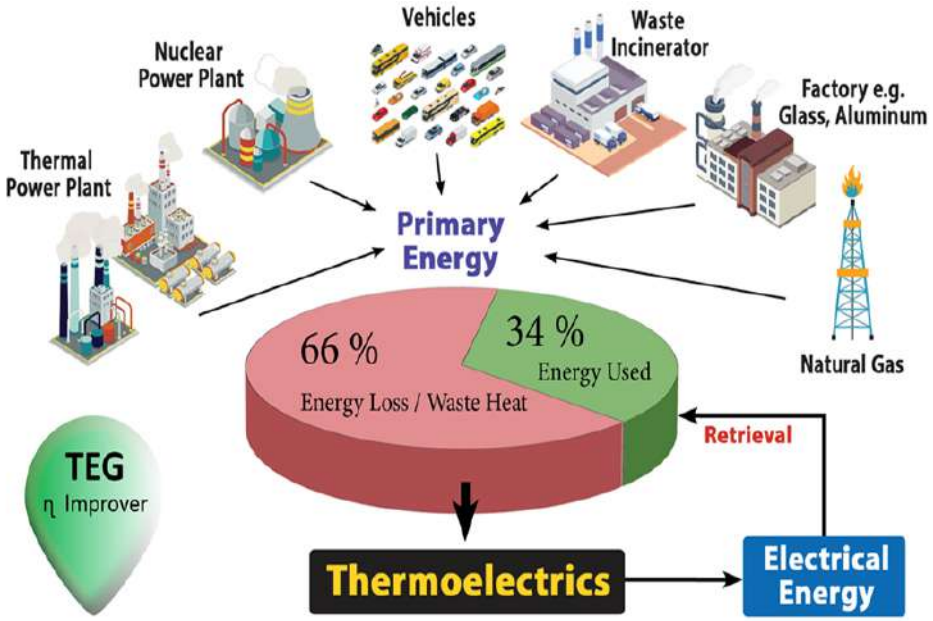

Figure 1.2: Waste heat to electricity [2]

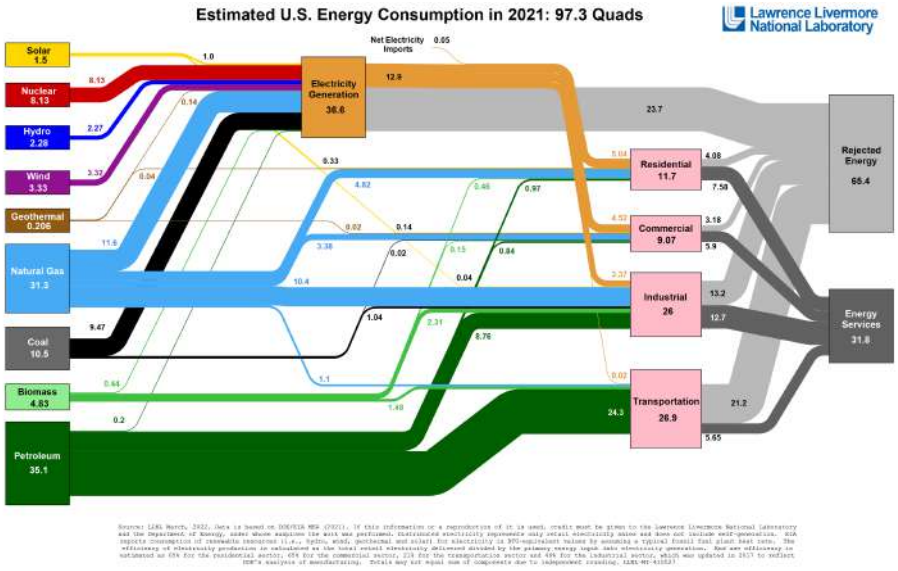

Figure 1.3: US Energy use in 2021 [3]

1.1 Increase Electrification in Automotive Vehicles

With the increase in technology, more electric components are included in Automotive vehicles, as shown in Fig. 1.5. An increase in electrification doesn't only mean electric vehicles. The electric components of conventional vehicles are also increasing. For conventional vehicles, waste heat recovery is best suited. This is done by Thermoelectric generator.

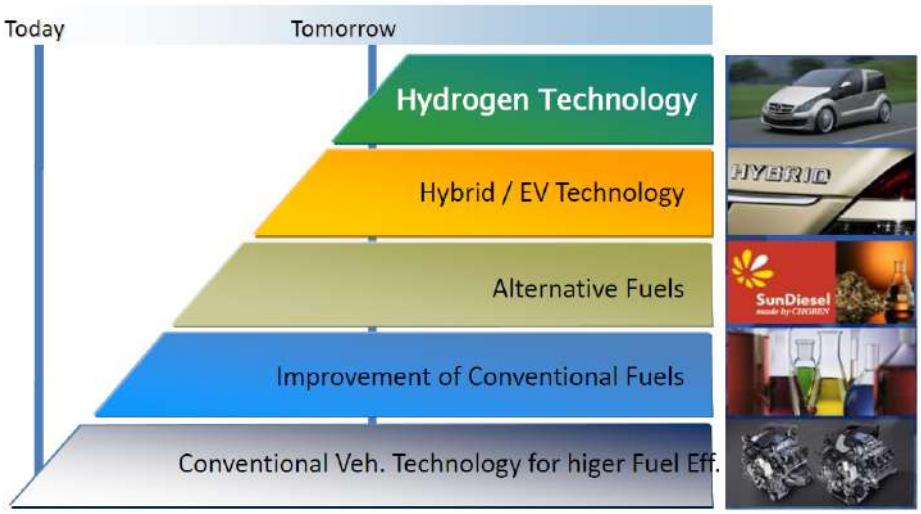

Figure 1.4: Progress of Automotive vehicle

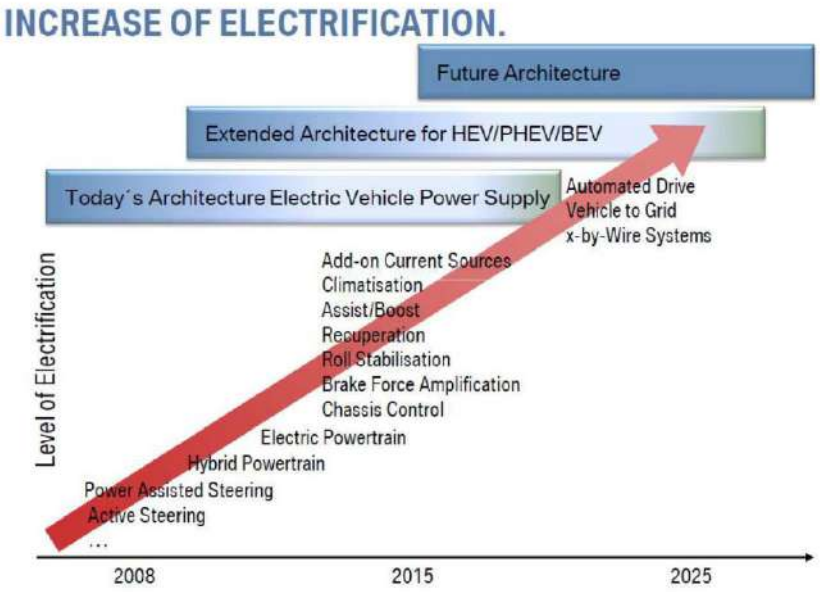

Figure 1.5: Increase electrification in vehicles [4]

1.2 Introduction to thermoelectrics

A Thermoelectric generator is a solid-state device. It converts heat to electricity directly without any moving parts. About 200 years ago, this phenomenon was discovered by Seebeck. It mainly consists of P & N type of semiconductors connected by metal electrodes sandwiched between the ceramic substrate. The problem with these devices is they are less efficient. The efficiency of the TEG device is less than 10%. The thermoelectric generator works on the Seebeck principle. When the junction of two dissimilar materials is kept at different temperatures EMF is generated. The performance of a thermoelectric generator mainly depends on the Seebeck coefficient(S), Electrical conductivity σ, Thermal conductivity κ, and Peltier effect π. A thermoelectric material should have a high Seebeck coefficient, Low thermal conductivity, and electrical resistivity. These terms can be combined to form a term called a figure of merit as $zT = \frac{\alpha^2}{\rho\kappa}T$. A material having a high figure of merit will produce more power and is considered a good thermoelectric material. Previously it was believed that zt of material will not cross 1. Because all good thermal conducting materials are electrical conducting materials. With invent of nanotechnology. New materials are being discovered of zt=2 in bulk materials. In thin films Scientists at TU Wien (Vienna) [15] have now got success in inventing a material with a ZT value of 5 to 6. In thin films, high zt has been reported in the literature.

1.3 History of Thermoelectrics

In 1823 Seebeck [16] reported the deflection of a compass needle in the vicinity of the closed loop formed by two dissimilar conductors when one is heated. In 1834 Peltier [17] discovered that when voltage is applied to the junction of two dissimilar materials temperature difference is observed at the ends. He could not co-relate this to the Seebeck effect. In 1838 Lenz [18] explained the Peltier effect. In 1851 Thomson [19] discovered the third thermoelectric effect, which describes the generation or absorption of heat in a current-carrying conductor having a temperature gradient. Altenkrich [20] explained theory of thermoelectric generator in 1905. A thermoelectric material should have a high Seebeck coefficient, low electrical resistivity and thermal conductivity. The above three terms can be combined in a term $Z = \frac{\alpha^2}{\rho\kappa}$. Z is having a unit of K^{-1} it is usually expressed by a non-dimensional term called ZT figure of merit. In 1950 Lofee [18] found that doped semiconductors produce good thermoelectric with low thermal conductivity

and high Seebeck coefficient. Maria Telkes [21] during research on solar energy harvesting, developed the first Thermoelectric generator. Several experiments failed to increase zt in 1960s many believed that it is not possible to produce materials with high electrical conductivity and low thermal conductivity. Hence zt of materials has reached its highest value and the efficiency of TEG cannot be increased further. In the 1990s after nanotechnology started developing. Scientists started to think of producing new engineered materials of high zt.

1.4 Principle of Thermoelectric Generator

The thermoelectric generator works on the principle of the Seebeck effect. If the junction of two dissimilar materials is kept at two different temperatures an EMF is generated. The EMF is directly proportional to the temperature difference between the hot and cold sides. Figure 1.6 shows the working principle of a thermoelectric generator. P-Type and N-Type semiconductors are connected by a metal electrode. One side is maintained at higher temperature T_h other side at lower temperature Tc. A load resistance R_l connected across the uni-couple TEG. Power is delivered across the load. The power produced by a thermoelectric generator depends on material properties such as the Seebeck coefficient, Electrical conductivity, and thermal conductivity. The thermoelectric generator works mainly on three effects Seebeck Effect, the Peltier effect & Thomson effect. Theses effects are explained in this section.

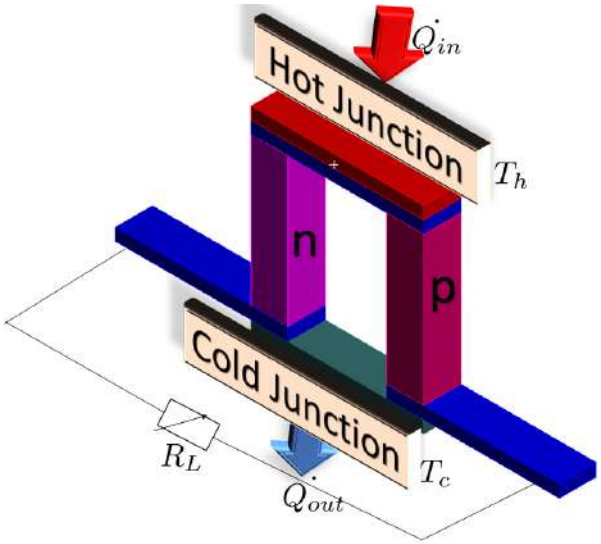

Figure 1.6: Principle of working of thermoelectric generator

1.4.1 Seebeck Effect

When the junctions of two dissimilar materials are kept at different temperatures ($T_1 > T_2$) a voltage is developed and is measured with a voltmeter as in Fig.1.7. Material A and B are two dissimilar materials. As the junctions are at two different temperatures ($T_1 > T_2$) EMF is developed. Seebeck coefficient is denoted by α. Seebeck coefficient is given by Eqn. 1.1

$$\alpha = \lim_{\Delta T \to 0} \frac{\Delta V}{\Delta T} \tag{1.1}$$

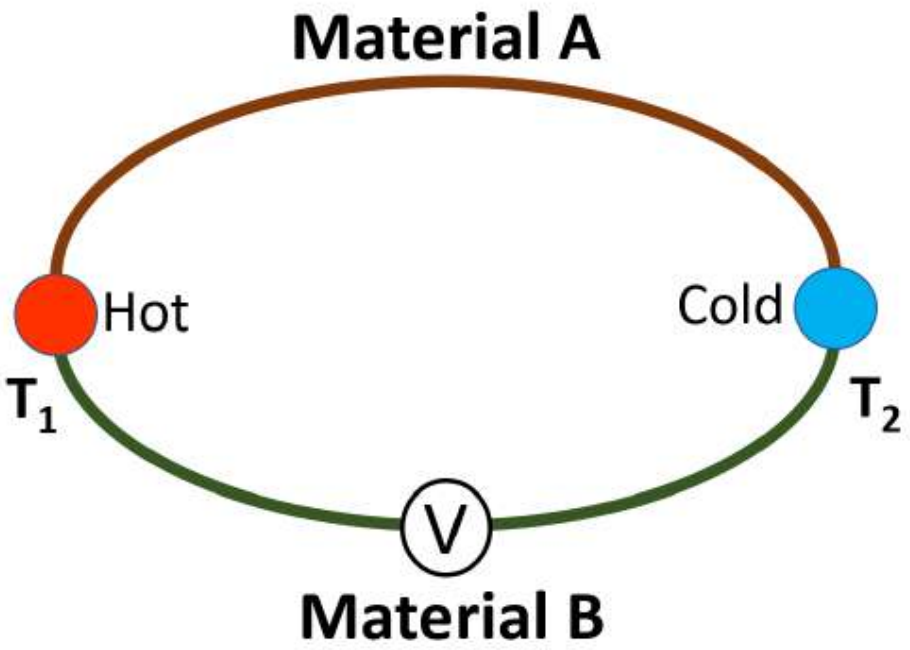

Figure 1.7: Seebeck effect

1.4.2 Peltier Effect

When an electric potential is applied across the junction of two dissimilar materials heat is absorbed or liberated at the junction. Heat is directly proportional to the current flowing through it. The Peltier effect is as shown in Fig. 1.8. The rate of heat transfer is given by Eqn 1.2. The Peltier effect occurs due to the different chemical potentials of the charge carriers in the material on either side of the junction.

$$Q = (\Pi_A - \Pi_B) = \Pi_{AB} I \tag{1.2}$$

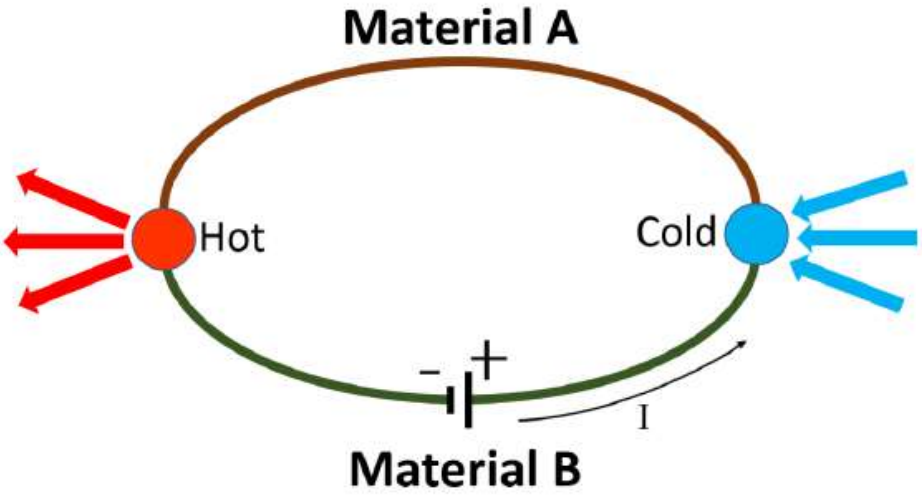

Figure 1.8: Peltier effect

1.4.3 Thomson effect

When current is flowing through temperature gradient single material. The heat is liberated or absorbed not only at the junction but throughout the material. This is the reversible effect. Heat is proportional to both electric current and temperature gradient.

The Thomson effect is observed in a single material with current flowing in a circuit having a temperature gradient. The rate of heat liberated or absorbed is given in Eqn. 1.3. Where ΔT is a temperature difference. K is the Thomson coefficient and J is the current density.

$$\frac{dQ}{dT} = KJ\Delta T \tag{1.3}$$

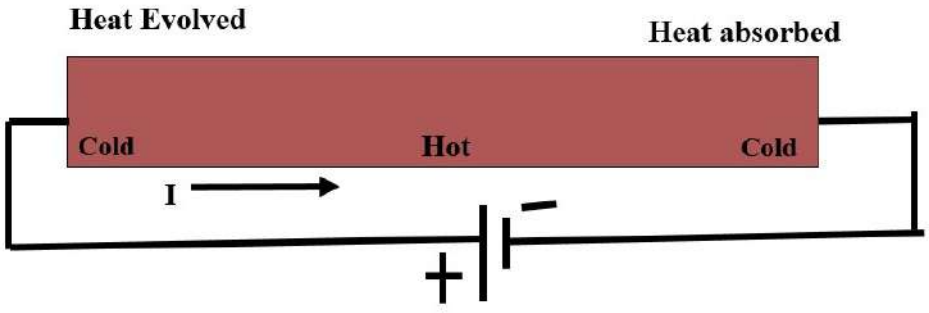

Figure 1.9: Thomson effect

1.5 Figure of merit

A thermoelectric material needs a high Seebeck coefficient, low thermal conductivity, and low electrical resistivity. The above transport properties are combined in one term $z = \frac{\alpha^2}{\rho\kappa}$. The unit of z is K^{-1}. It is good to express by a non-dimensional term called zt material figure of merit, the higher the zt value the best is the material suitable for a thermoelectric generator. Thermal conductivity has two parts one is the Lattice part of thermal conductivity other is the electronics part, the lattice part of thermal conductivity can be decreased with some techniques [22]. With nanotechnology, a high figure of merit materials can be produced by nano inclusion [23]. [24] reported Tin selenide p-type thermoelectric material of zt 2.6 and [25] Shang et al. reported n-Type material of zt 2.8 in bulk thermoelectrics.

Fabrication of a thermoelectric generator is a challenging task. A thermoelectric generator consists of semiconductors connected by metal electrodes. When metal and semiconductors are joined electrons will not flow properly due to band bending. Hence a proper connection is required to join metal with semiconductors. The device figure of merit is given by Eqn. 1.4.

$$ZT = \frac{(\alpha_p - \alpha_n)^2}{[(k_p\rho_p)^{\frac{1}{2}} + (k_p\rho_p)^{\frac{1}{2}}]^2}T \tag{1.4}$$

If the device figure of merit ZT is 4 then they can work as efficiently as currently available mechanical devices. If ZT reaches infinity then the efficiency of the thermoelectric device reaches Carnot efficiency. Presently all commercially available thermoelectric generators are made of Bismuth Telluride.

1.6 Current State of Art of Thermoelectric material

A thermoelectric material should have a high Seebeck coefficient low electrical resistivity and thermal conductivity. The above three terms can be combined in one term $z = \frac{\alpha^2}{\rho\kappa}$.z is having a unit of K^{-1} it is usually expressed by a non-dimensional term called zt called material figure of merit, the higher the zt value the better is the thermoelectric material. A thermoelectric generator consists of P-Type & N-Type semiconductors. Figure 1.10 shows the variation of the figure of merit of material with temperature. It can be observed that the zt of the material is high for small temperatures. $Bi2Te3$ is a low-temperature thermoelectric material. Its zt is high at a temperature of around 60 C.

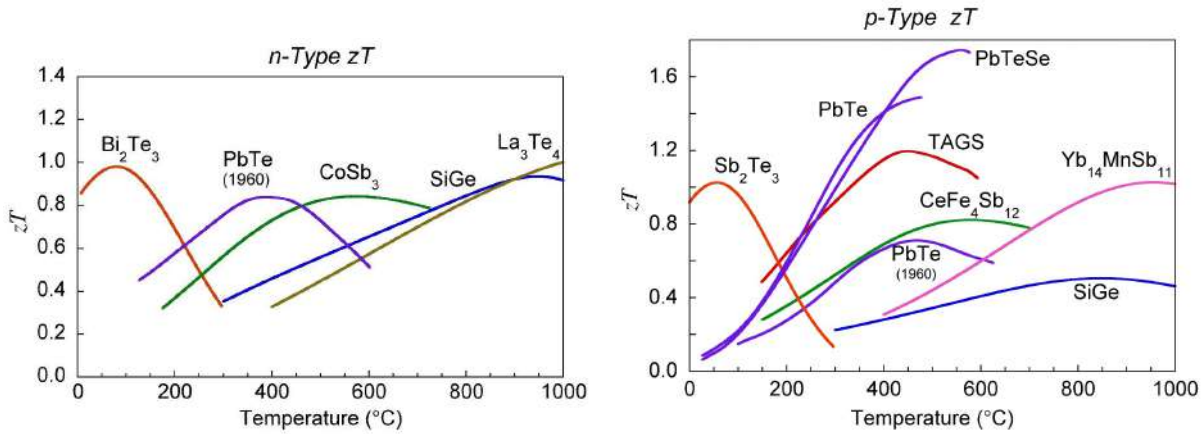

(a) zt as a function of temperature for n-type material

(b) zt as a function of temperature for p-type material

Figure 1.10: Variation of zt with temperature [5]

1.7 Interface resistance

Several promising zt materials are available now but the ZT of the device is very low compared to the zt of the material. A TEG consists of P & N type semiconductors connected electrically in series with help of metal electrodes. The joint will be between a metal-semiconductor junction, due to which band bending will take place and electrical resistance will be high. The interface resistance are shown in the Fig.1.11. At hot junction diffusion of material takes place hence diffusion barrier is used. The metallization layer and bonding layers act as bonding layers. For the low-temperature application of Bismuth telluride. Metalized contact layer is bonded with Cu/Ni electrode by soldering. Soldering won't work at higher temperatures [26]. For high-temperature applications of lead telluride-based thermoelectric modules, new joining methods are brazing [27], soldering with nickel-based paste [28] and lead-free soldering [29] is used. Ajay Singh et al. [30] developed a low electrical contact resistance on N-type lead telluride and TAGs as P-type TEG elements. It reports an efficiency of 6%. It also reports that as the number of TE elements increases internal resistance increases. Zhonglin Bu et al. [31] developed a GeTe alloy-based thermoelectric generator. It reports a peak efficiency of 14%. It has low chemical diffusion and electrical contact resistance.

1.8 TEG Fabrication Process

The TEG fabrication process involves the joining of metal with semiconductors. After metallization legs are cut into the required shape. For wire cutting, EDM, Chemical

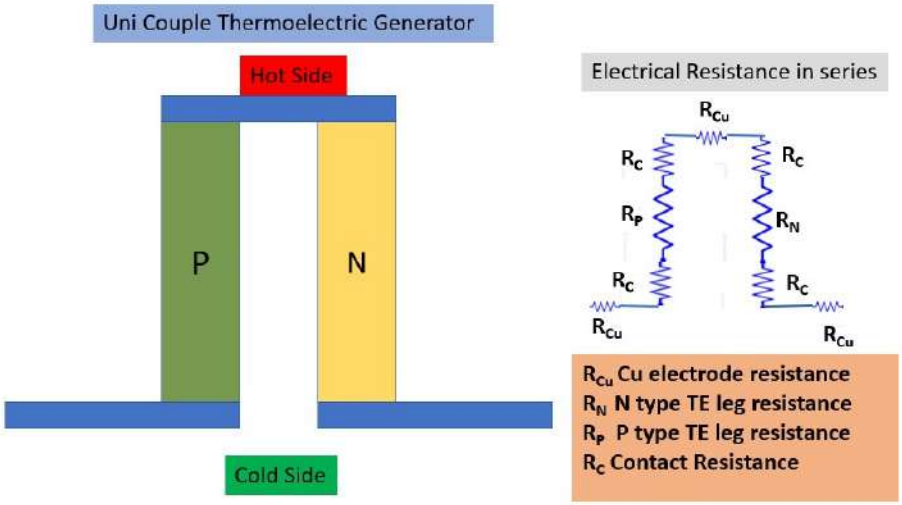

Figure 1.11: TEG electrical resistance

etching methods are used. Then they are joined by soldering, brazing, etc. Finally, electrical leads are attached and a quality check is carried out. The block diagram of steps for fabrication of TEG are given in Fig.1.12. Most commercially available thermoelectric modules are made of Bi_2Te_3 material. They can work reliably till 200 C. These use Ni as a metallization layer [32]. Soldering is carried with SAC 305 and Zinc Aluminium solder [33] [34]. In 2016 Alphabet Energy made a tetrahydrate and magnesium silicate-based TEG with 6W power at 300K temperature difference [35]. TEG Canada sells PbTe/TAGS-based TEG devices. HiZ [36], and Marlow [37] are other companies that supply TEG. These all are highly expensive.

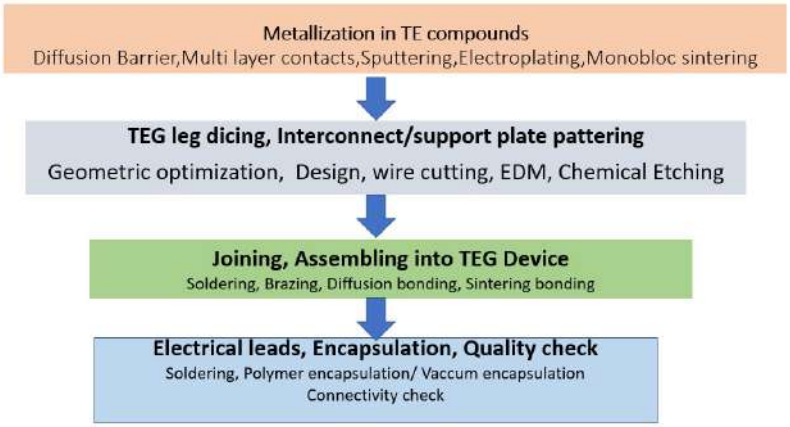

Figure 1.12: TEG fabrication process

1.9 Thermodynamics of Thermoelectricity

Seebeck coefficient, Peltier coefficient, and Thomson effect have been discussed in the previous section.

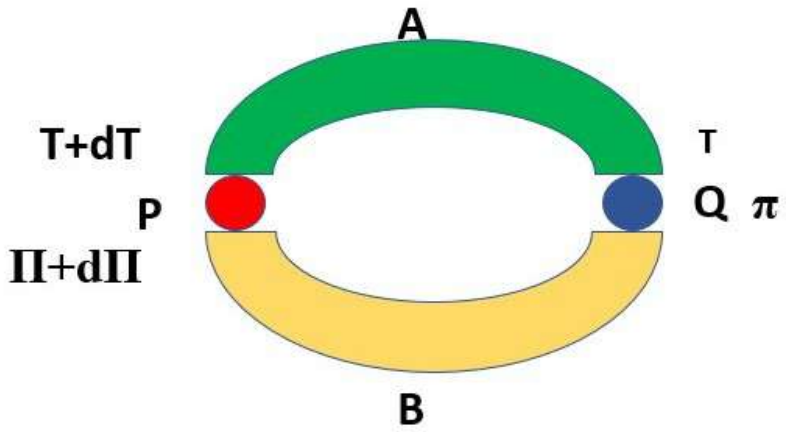

Figure 1.13: Junction of hot and cold side

Both Peltier and Thomson effects are reversible.
Due to the Peltier effect, the amount of energy absorbed is $\Pi + d\pi$, and the amount of energy liberated is π, where $\Pi + d\pi$ and π are Peltier coefficients at points P and Q, respectively. The Thomson coefficients at points A and B are denoted as K_A and K_B, respectively.

Due to the Thomson effect, the amount of heat absorbed is $(K_A - K_B) \cdot dT$. Applying the second law of thermodynamics, we have:

$$\frac{\Pi + d\pi}{T + dT} - \frac{\pi}{T} + \frac{(K_A - K_B) \cdot dT}{T} = 0 \tag{1.5}$$

Simplifying Equation 1.5, we get:

$$d\pi + (K_A - K_B) \cdot dT = \frac{\pi \cdot dT}{T} \tag{1.6}$$

The algebraic sum of the Peltier EMF and the Thomson EMF is equal to the Seebeck EMF:

$$dE = d\pi + (K_A - K_B) \cdot dT \tag{1.7}$$

By comparing Equation 1.6 and the Seebeck coefficient equation, we can conclude that the Peltier coefficient is $\pi = T \cdot \frac{dE}{dT}$.

1.10 Exhaust system of Automotive Vehicle

Different components of the exhaust system are shown in Fig. 1.14. The function of the exhaust system is it is used to silence the noise caused by high-pressure exhaust gases leaving the engine and transporting hot and toxic gases away from the driver's compartment. It acts as an integral part of combustion and emission control. It converts harmful & toxic gases to non-harmful gases to meet emission norms and reduce pollution. It will stop leakage upstream of the catalytic converter. The main components of the Exhaust system are the Exhaust manifold, catalytic convertor Mufflers, and tailpipe.

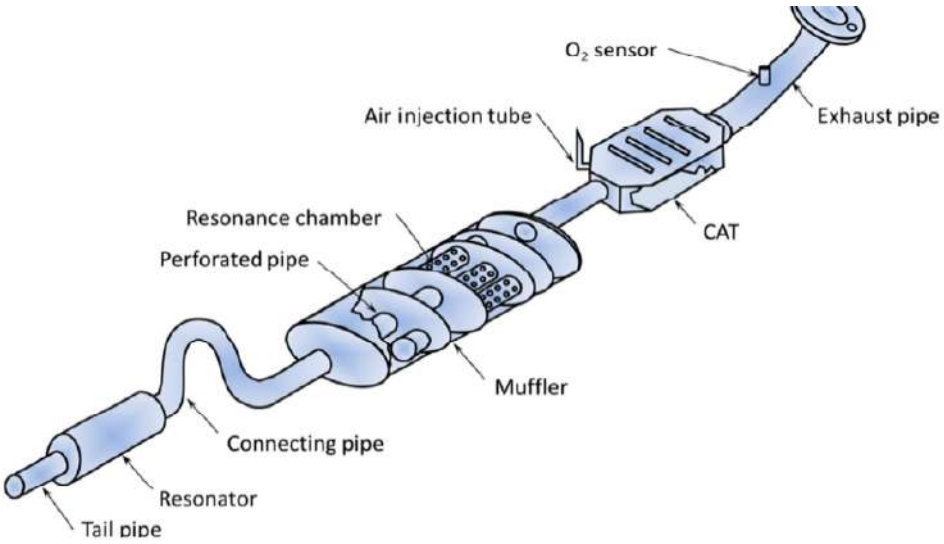

Figure 1.14: Components of exhaust system [6]

1.11 Possible location of TEG on an Automotive Vehicle

For an automotive vehicle, TEG can be placed at different locations as shown in Fig.1.15. The temperatures at different locations are given in the Table. 1.1. Location 1 is at the outlet of the engine exhaust at the exhaust manifold the temperature is high. High-temperature TE materials like Lanthanum telluride can be used. Location 2 is after the exhaust manifold and before the catalytic converter, the temperature is high and nano-structured skutterudite and silicon germanium can be used as TE material. Location 3 is

Table 1.1: Temperature in different locations of an automotive exhaust system

Location	Gasoline	Diesel
1	750-1100 C	600-850 C
2	400-750 C	350-600 C
3	200-400 C	150-350 C
4	300-500 C	100-400 C

after the catalytic converter medium temperature TE materials like skutterudites, Half Heusler can be used. Location 4 with Exhaust gas re-circulation TEG can be used.

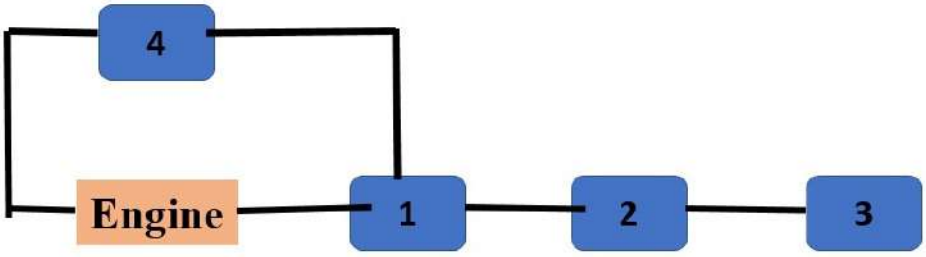

Figure 1.15: Possible location of TEG on an Automotive vehicle

1.12 Potential for Exhaust gas energy recovery

In an automotive vehicle from Fig. 1.16 it can be observed that about 40% of energy is lost in exhaust gases. Due to thermodynamic limitations, we cannot convert all energy in the exhaust to useful electrical energy. If we can trap a small segment of the waste heat of exhaust gases it will increase the efficiency of an automotive vehicle. Exhaust gas temperatures vary with time. For the New European drive cycle(NEDC) exhaust gas temperature and mass flow rate are reported as shown in Fig. 1.17 [8].

In conventional IC engines alternator is used to charge the battery. The conversion efficiency of the alternator is 60% [9]. The conversion efficiency of an IC engine is 25% hence the efficiency of conversion of chemical energy of the fuel to electrical energy is 16% [38]. The thermoelectric generator will reduce the load on the alternator.

The temperature of the exhaust system varies from the exhaust manifold to the tail pipe. The temperature profile of the exhaust system for full load and part load is shown in Fig. 1.18 and Fig. 1.19. The temperatures of the SI engine exhaust system are higher compared to CI engine

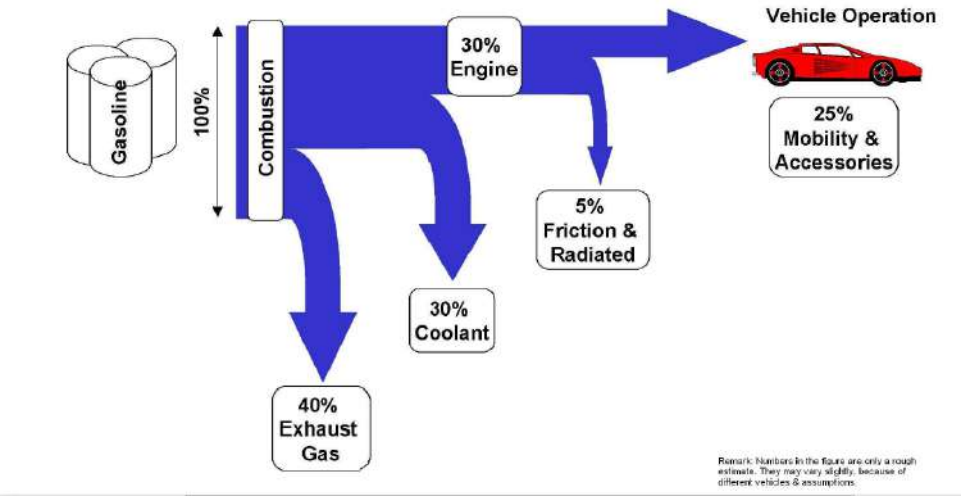

Figure 1.16: IC Engine energy balance [7]

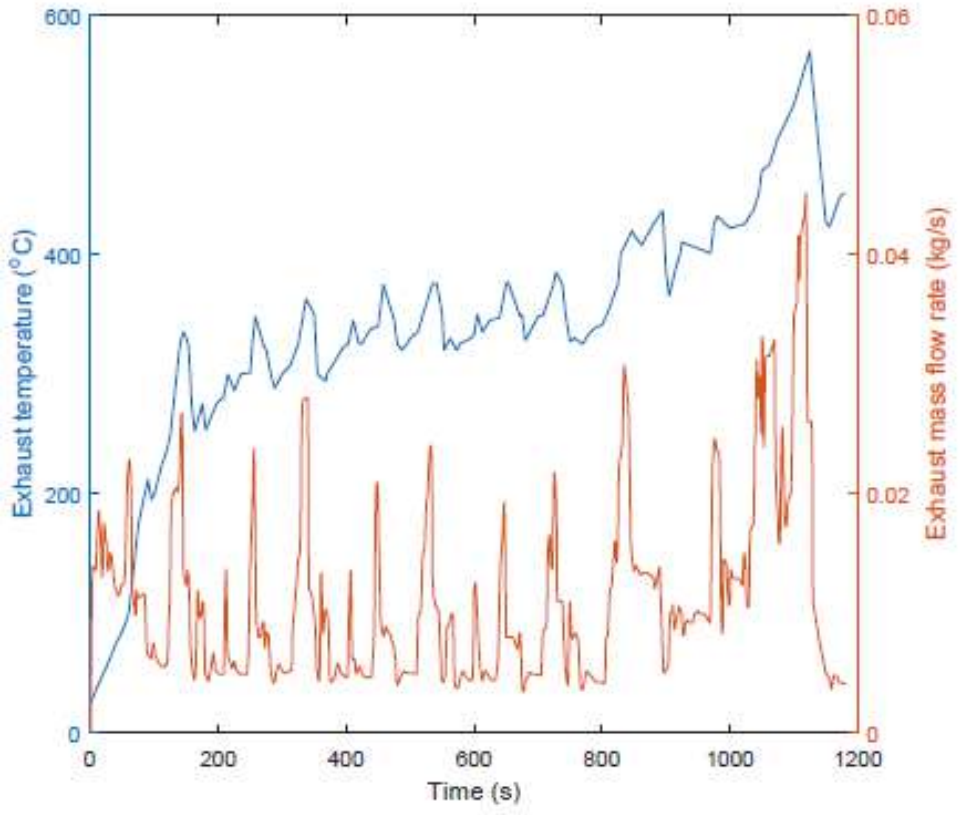

Figure 1.17: Exhaust temperature and mass ow rate downstream of the three-way catalyst for a 3L-BMW-gasoline engine [8]

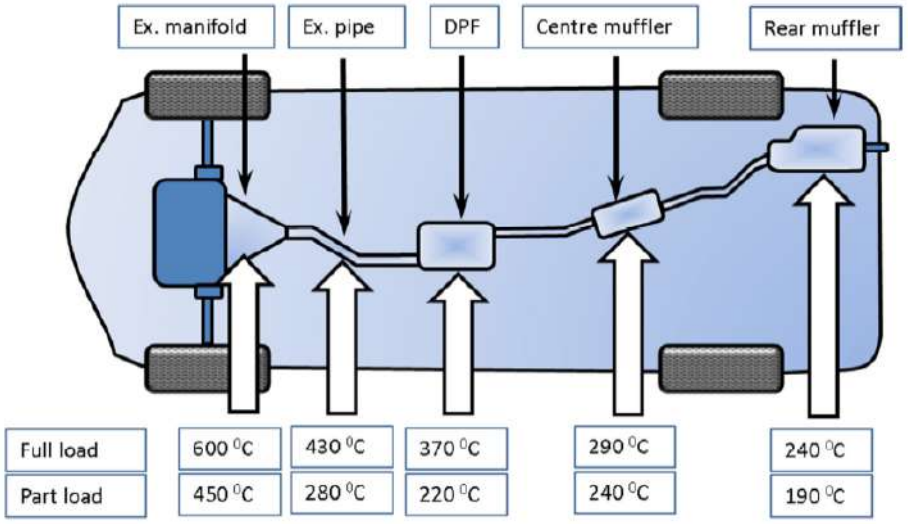

Figure 1.18: BMW 3-series exhaust temperature profiles of a Compression Ignition (CI) engine [9]

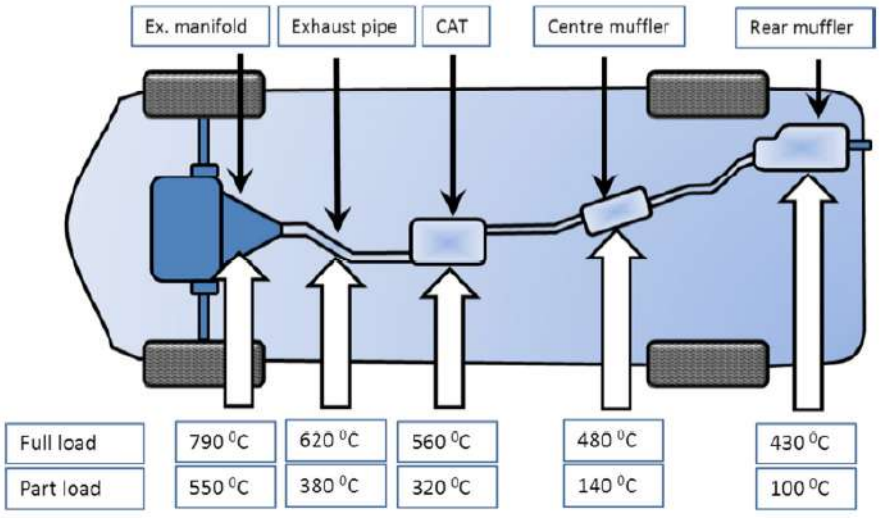

Figure 1.19: BMW 3-series exhaust temperature profiles of a Spark Ignition (SI) engine [9]

1.13 Integration of TEG on Automotive Vehicle

In automotive vehicles battery supplies power to electrical components. In the conventional vehicle, the battery is charged by an alternator. A thermoelectric generator will produce dc power from a temperature gradient. Using a DC-DC converter the power from TEG is converted to the required level. DC power is used to charge the battery as shown in Fig.1.20.

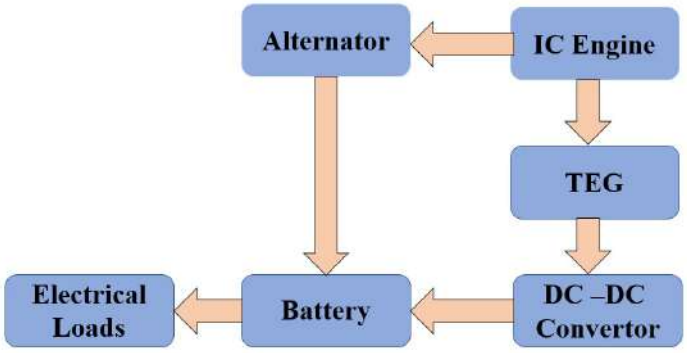

Figure 1.20: Integration of TEG on Automotive vehicle

1.14 Problem Statement

The objective of this research is to investigate and analyze various aspects of Thermoelectric Generators (TEGs) and Automotive Exhaust Gas Thermoelectric Generators (AETEGs). Specifically, the research aims to characterize the transport properties of TEGs and evaluate their performance. Theoretical and numerical analysis will be conducted to gain insights into the behavior of both TEGs and AETEGs. Furthermore, the research will focus on the design optimization and modeling of TEGs and AETEGs. The performance of the automotive exhaust gas thermoelectric generator will be evaluated and validated through experimentation. The ultimate goal is to enhance the understanding of TEGs, optimize their design, and assess their effectiveness in utilizing automotive exhaust gases.

1.15 Objectives of present work

1. Characterization of transport properties, Theoretical and numerical analysis of TEG and AETEG
2. Design optimization and modeling of TEG and AETEG.
3. Performance evaluation of automotive exhaust gas thermoelectric generator and validation.

1.16 Outline of Thesis

The organization of the thesis and a brief description of each chapter is given below.

Chapter 1: Introduction

This chapter gives introduction to thermoelectric generator. It introduces basic principles of the thermoelectric material, device and its application to AETEG. Statement of problem is made and objectives are defined.

Chapter 2: Literature Review

This chapter gives a literature review of Thermoelectric Generators and Automotive Exhaust Thermoelectric Generators. Based on the literature review research gaps are identified.

Chapter 3: Research Methodology

This chapter explains the theoretical modeling and numerical modeling of TEG and AETEG. Performance analysis of TEG and AETEG and validation of theoretical and numerical results with experimental results.

Chapter 4: Design Optimization and modeling of Thermoelectric Generator

This chapter focuses on the characterization of commercially available thermoelectric generators (TEGs) using both experimental and theoretical methods to evaluate their effective and equivalent material properties. Specifically, the Skutterudite thermometric module is thoroughly studied and presented. The optimization of TEGs is performed for both HiZ and uni-couple TEGs, considering various TEG shapes. Moreover, the study

includes an investigation of segmented leg TEGs to enhance power output. Additionally, the chapter reports on the analysis of TEGs with a heat exchanger mounted on a hot air blower.

Chapter 5: Application of TEG to Automotive Exhaust Thermoelectric Generator(AETEG)

In this chapter automotive exhaust gas thermoelectric generator mounted on exhaust of IC engine is reported. A neural network model is trained using the experimental data and analysis results are reported.

1.17 List of contributions

This research work contributes to the field of thermoelectric generators (TEG) and automotive exhaust gas thermoelectric generators (AETEG) in the following ways:

1. Characterization of TEG: The research analyzes the transport properties of TEG through experimental analysis. This characterization provides insights of transport properties such as seebeck coefficient,electrical conductivity and thermal conductivity

2. Design Optimization and Modeling of TEG: The research optimizes the geometry using numerical modeling, resulting in enhanced efficiency.

3. AETEG Performance Evaluation and Validation: Experimental performance evaluation of AETEG and validation with results by theoretical and numerical methods.

These contributions advance the understanding of TEG systems, optimize TEG device design, and assess the viability of AETEG for automotive use. The research has implications for the development of more efficient and sustainable energy conversion technologies, particularly in waste heat recovery and automotive energy systems.

Chapter 2

Literature Review

2.1 Introduction

This chapter reports the literature review of work done on the thermoelectric generator. Since 2000 the work on thermoelectrics has gained momentum due to nanotechnology. High zt materials are developed. Decent efficient devices are developed now. this chapter also reports the use of literature on automotive exhaust thermoelectric generators and machine learning techniques for the analysis of thermoelectric generators.

2.2 Thermoelectric Generator

A thermoelectric generator is a solid-state device. It directly converts heat to electricity without any moving parts. It can be observed that about 60% of energy is lost as waste. Figure 2.2 shows the development of thermoelectric material with time. From 1960 to 1990 there is no growth in the performance of TE materials. With Nanostructured thermoelectric materials, the zt of materials has reached around 3. The performance of thermoelectric material is based on the material property called figure of merit $zt = \frac{\alpha^2\sigma}{\kappa}$. A good thermoelectric material should have a high Seebeck coefficient and electrical conductivity but low thermal conductivity. Most of the thermoelectric materials research is based to reduce thermal conductivity.

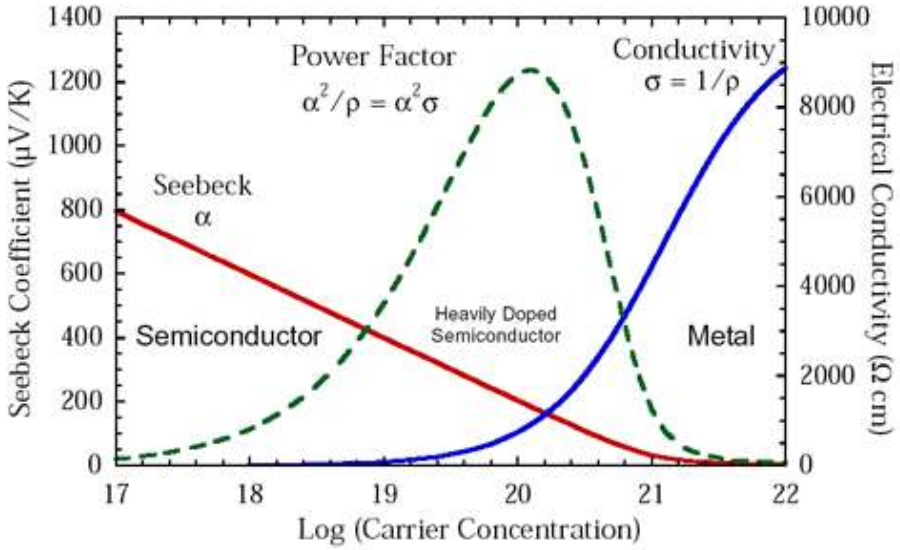

Figure 2.1: Seebeck coefficient as a function of charge carriers

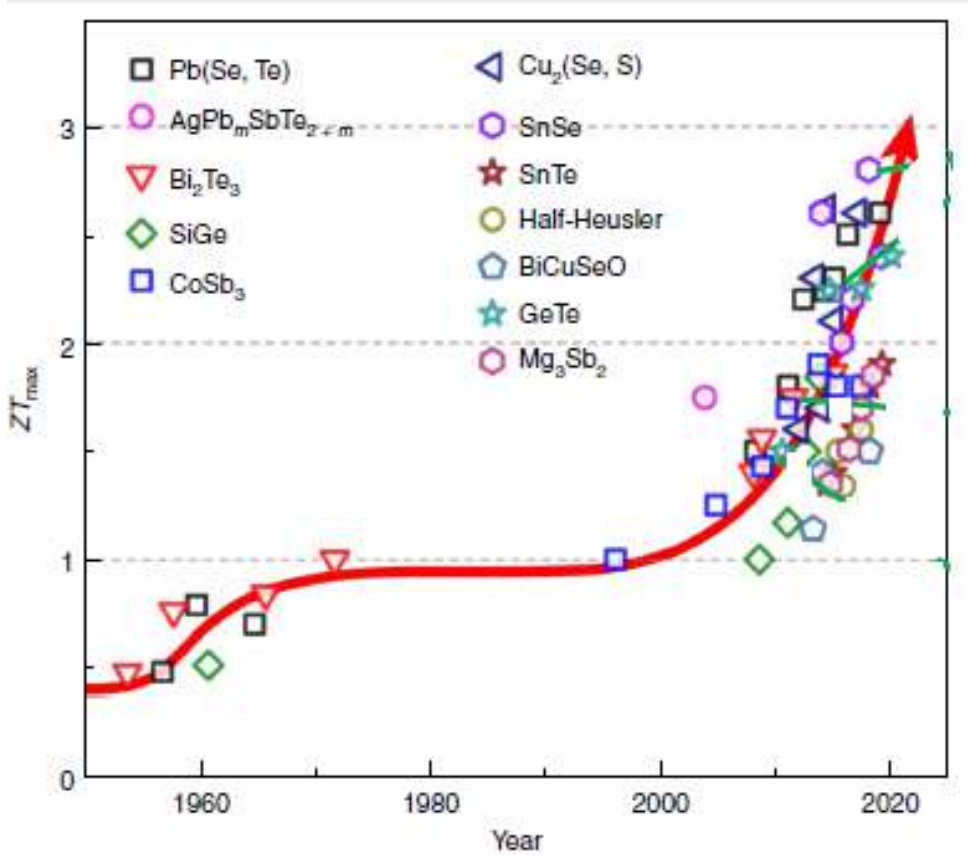

Figure 2.2: Material development [10]

2.3 Important Thermoelectric Material development in last 15 years

With the first-generation thermoelectric materials, the TEG efficiency was about 3% to 6%. Because of nanotechnology, high-efficiency materials have developed. The efficiency of devices with these high-performance materials is 12 to 15%. Based on the application thermoelectric generator can be classified as stationary application generators and mobile application generators. In Stationary applications, the source temperature is fixed and bismuth telluride or lead telluride is used as TE material. In mobile applications such as automotive vehicles, source temperature is not fixed. Because the temperature of the exhaust of an automotive vehicle is 600K to 1000k mid-temperature thermoelectric devices are suitable. Skutturudites-based materials and Half Hausler materials are promising candidates as they have mechanical strength for the fabrication of devices. But commercially available TEGs are made of Bi_2Te_3 material.

2.3.1 Telluride Based Modules

These materials were developed TEG in 1960-70 and have a conversion efficiency of 5% at a source temperature of 510^0C and sink temperature of 93^0C [39] [40]. The efficiency of nanostructured PbTe-based material is low because of high electrical contact resistance [29] [41]. Jood at al. [41] developed a P-type PbTe-MgTe material with zt=1.9 and PbTe as N-Type material with a conversion efficiency of 8.5% at $T_H = 600^0C$ & $T_c = 10^0C$. With the addition of a diffusion barrier layer using high-pressure sintering. PbTe has good thermal stability on cyclic loads below 793 K. Hazan et al [42] prepared a nanostructured $Pb_{0.953}Na_{0.04}Ge_{0.007}$ P-Type and $PbSn_{0.05}Te_{0.92}(PbS)_{0.08}$ as N-Type leg. Produced peak power of 2 watts with an efficiency of 12% for $T_H = 600^0C$ & $T_c = 10^0C$. Tellurium is a rare earth metal. Its production cost is very high hence researchers [43] [44] have used PbSe or PbS in place of PbTe. The higher melting point of Se & S will increase the operating temperature of Pb(s, Se) material and also the Vickers number. Jiang et al [45] fabricated a segmented leg with $Pb_{0.99-y}Sb_{0.012}Sn_ySe_{1-2x}Te_xS_x$ and Bi_2Te_3 as N-Type material. Sodium doped with $Bi_{2x}Sb_xTe_3$ as P-Type material. TEG was prepared with 8 uni-couple legs producing power of 3.1 w and maximum efficiency of 12.3% at a temperature difference of 500 K and the current reported is 3.5 A. Z Liu et al. [46] reported that Mg-Sb based material that has high efficiency at low temperatures. For the

fabrication of a device mechanical strength is important. PbTe has a Vickers hardness of 0.3 Gpa but doping with Na its Vickers hardness was 0.8 Gpa. PbTe sublimation was observed by Sadia et al. [47] on the hot side at 0.5 to 1.1 mm length.

2.3.2 Skutterudite-based TEG modules

Skutterudites have good mechanical properties and can work efficiently at medium temperatures [48]. Zhou et al.[49] reported for Yb-filled $CoSb_3$ the Vickers hardness of 4 Gpa and bending strength of 180 Mpa. Zhong et al.[50] fabricated 4X4 leg TEG using $Yb_yCo_4Sb_{12}$ with zt=1.5 as n-type material and $Ce_yFe_3CoSb_{12}$ as p-Type material has max $\eta = 8.4\%$. Nie et al [11] developed an 8X8 TEG device made of $CoSb_3$ as shown in Fig.2.3. The maximum efficiency reported was 9.1% and the peak power developed was 42 Kw with a temperature difference of 600 k. A segmented leg made of Bi_2Te_3 and $CoSb_3$ maximum efficiency was reported as 12% with a temperature difference of 540 K [51]. Skomedal et al.[52] performed a durability test with thermal cyclic loading failure has happened mainly on the side due to oxidation and diffusion process at the interface. Chu et al.[53] reported that Nb can be used as an electrode for TEG devices. Daniel et al.[54] reported that $CoSb_3$ & Nb junction was stable for 100 days at 848 K. Maximum efficiency was 10.4% and peak power was 4.1 W.

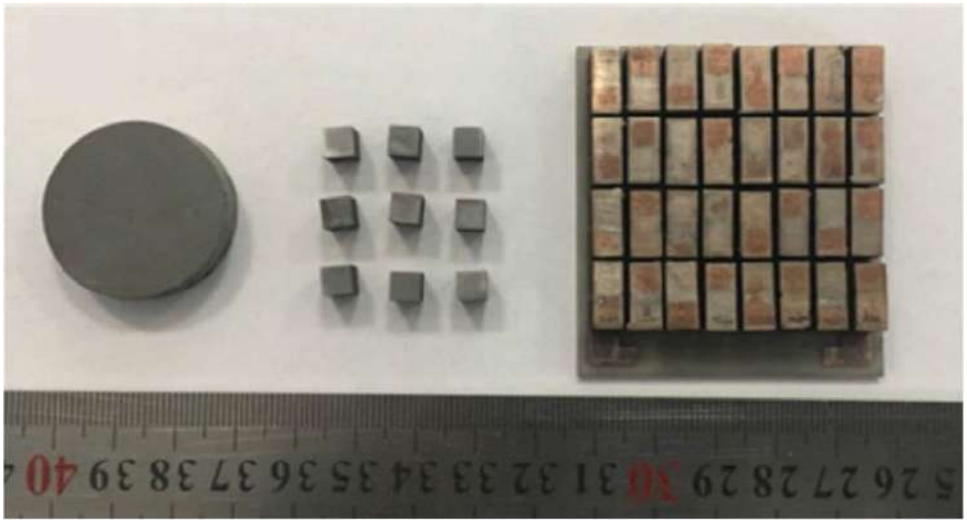

Figure 2.3: An 8x8 leg device made from $CoSb_3$ [11]

2.3.3 Half Heusler TEG modules

Half Heusler TEG is a compound of two transition or rare earth metals with P block elements. It has high mechanical strength, It is a mid-temperature TEG material with

good zt. C Fu et al. [55] fabricated a TEG device with P-Type $FeNb_{0.88}Hf_{0.12}Sb$ of zt=1.5 at 1200K and for N-Type ZrNiSn with zt=1 at 950K is used. Conversion efficiency was reported as 6.2% source temperature at 1000 K and temperature difference as 655 K.

2.4 Machine Learning Timeline

In 1943 Pitts et al. [56] were the first to build the mathematical modeling of the neural networks to predict the human brain. In 1950 Alan Turing et al. [57] reported the Turing test, It stated if a machine can convince a human being, then the machine is also a human, and it has intelligence. In 1952 Arthur Samuel [58] wrote a program for IBM that plays checkers and has the capability to improve each time it plays. In 1956 at The Dartmouth summer research project on artificial intelligence, John Mccarthy invited many scientists and developed the first concept of artificial intelligence [59]. Frank Rosenblatt developed the concept of perception, which was built to receive images as input and create output as labels and categorization [60]. In 1963 D Miche developed a MENACE program to learn and play a tic-tac-toe game [61]. In 1967 nearest neighbor algorithm was developed; pattern recognization is used to find the route for traveling salesman. In 1970 Seppo [62] developed a general method for automated differentiation This is the modern version of the backpropagation algorithm. In 1979 Kunihiko Fukushima [63] reported work on neurocognition, it is a multilayered neural network used for pattern recognition and is the backbone of a convolution neural network. In 1981 Gerald Dejong developed explanation-based learning(EBL). With this computer learns to analyze data and create rules and delete junk data. In 1996 IBM's deep blue computer, a chess-playing computer defeated Garry Kasparov. In 2006 Geoffrey Hinton 2006 used the term deep learning for algorithms that assist computers to recognize different types of objects and text.

2.5 Automotive Exhaust Thermoelectric Generator

In 1964 Tomarichio et al. [12] did experiments with air cooling as shown in Fig. 2.4 at Clarkson College of Technology. $PbTe$ was the thermoelectric material. They reported a peak power of 514 w and a voltage of 14.7 V. At a vehicle speed of 80 km/hr. In 1994 Bass et al. [64] Experimental analysis of diesel engine with the 72TEG. Mounted on an Octane-shaped heat exchanger. Assembled with fins to increase heat transfer. It

produces a maximum power of 1068 W.

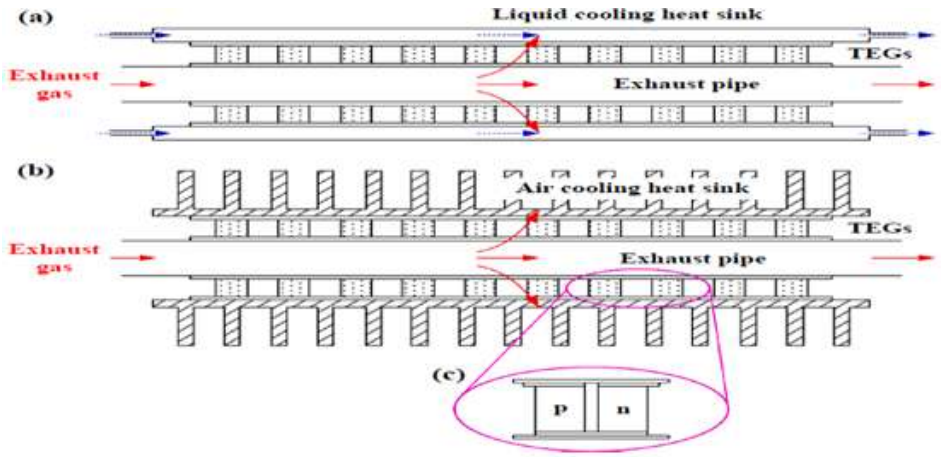

Figure 2.4: Construction of AETEG [12]

In 1998 Ikoma et al. [65] mounted 72 TEG on downstream of the catalytic converter. A 3000 cc gasoline engine is used. It is tested in hill climb mode with an exhaust gas bypass. The efficiency reported is 0.1%.

In 2002 Matsubara et al. [66] reported the use of segmented legs on 2000 cc gasoline engines. It used 10 TEG, out of which six segmented leg upstream and 4 Hi-Z TEG downstream. Efficiency is about 5-10%. Karri [67] in 2005 modeled an automotive exhaust thermoelectric generator. Reported the variation of pressure and power developed by TEG. In 2007 Thacher et al.[68] conducted experiments with wind tunnels on light-duty trucks with the gasoline engine. A rectangular heat exchanger with fins was used. 16 TEG were used, and the Heat exchanger is downstream of the catalytic converter. Engine coolant was used, and fuel economy was reported as 1% to 2%. In 2010 Wojciechowski et al. [69] reported experiments on gasoline & diesel engines. Concluded that as gasoline exhaust gas temperature is higher, AETEG is suitable for a gasoline engine.

Meisner et al.[70] conducted experiments using Skutteruditte TEG upstream and Bismuth telluride TEG on downstream. Efforts were made to maintain the uniform temperature of the heat exchanger using extended surfaces.

Mori et al.[71] reported experimental and simulation data on hybrid electric vehicles & gasoline engines. They used material having temperature TE material upstream and low-temperature TE material downstream.

Crane et al [72] fabricated an AETEG in a cylindrical shape and reduced the weight of AETEG. Steady and transient analysis of BMW X6 is reported. The fuel economy increased by 1.2%. For steady-state conditions, 605 W power is developed. For transient conditions, the power is reduced to 450 W.

Liu et al. [73] conducted experiments on diesel engines with 240 thermoelectric modules. TEG fixed upstream of the muffler. Four sections made each have 60TEG in series. These four sections are connected in series. Conducted test bench and road tests for steady and dynamic conditions.

Yu et al.[74] reported Finite volume method analysis. TEG in downstream of catalytic converter with air as cooling fluid. The maximum power was 220 W. Kim et al.[75] reported work on diesel engines. 40TEG were placed. To stabilize exhaust flow, perforated sheets were used. Analyzed pressure drop across AETEG maximum power of 119 watts reported.

Merkisz et al [76] placed 24 TEG after a two-way catalytic converter on a gasoline engine. Experiments were conducted on road conditions maximum power of 189 watts is reported. Brito et al. [77] reported a theoretical analysis of AETEG on gasoline engines. Water is on the cooling side. A variable resistance heat pipe was used, and the maximum power reported was 550 watts.

Temizer et al. [78] reported experimental and simulation analysis of a diesel engine-mounted octagonal heat exchanger between the exhaust manifold and muffler. It reported parallel connected TEG has good efficiency. Vale et al.[79] reported theoretical and experimental analysis of light and heavy-duty automotive vehicles. AETEG was downstream of DPF. The one-dimensional steady-state analysis is reported with a maximum power of 188 watts.

Ziolkowski et al. [80] conducted experiments on diesel engines with 24TEG downstream to the catalytic converter. Reported temperature distribution. The maximum efficiency is about 0.27%. Stobart et al. [81] designed two types of AETEG and simulated them. Thermoelectric properties are assumed as constant. The results are compared with experimental results with a difference of 10%.

Liu et al.[82] conducted a study of the thermoelectric generators in different locations of the exhaust system. They reported TEG located upstream of the catalytic converter and muffler has a higher surface temperature and lower back pressure. Massaguer et al. [83] conducted an experimental and numerical analysis of an AETEG. They considered power generation,back-pressure, weight, and coolant power for analysis. They reported that maximum fuel economy and maximum power don't occur at the same point. They reported maximum fuel economy values of 0.18%. Orr et al. [84] conducted experiments of TEG assisted with heat pipe. They reported TEG with heat pipe can work efficiently together. Fernandez et al. [85] compared the energy recovery potential from spark igni-

tion engines and compression ignition engines. They applied the same to diesel engines and gasoline engines. They compared electric turbogenerators with TEG and reported that electric turbogenerators have more capacity to harvest than thermoelectric generators.Orr et al. [86] conducted experiments of TEG with heat pipes. Eighth 8TEGs, the power developed was 38 w and the reduction in fuel cost was 1.57%. Nicholas et al. [87] simulated heat exchangers and compared stainless steel heat exchangers with silicon carbide heat exchangers. The reported silicon carbide heat exchanger has higher efficiency because of its high thermal conductivity. Poshekhonov et al. [88] developed a numerical model for a thermoelectric generator considering hydraulic resistance. They reported power up to 500 W for a thermoelectric generator based on germanium and lead telluride. Chi Lu et al. [89] simulated and studied the effect of heat transfer enhancement on power output. Heat transfer was enhanced using a rectangular offset strip and metal foam. Heat foam increases power but consumes pumping power. Hongliang Lu et al. [90] studied heat exchangers for automotive exhaust thermoelectric generators. They studied different configurations of heat exchangers such as 1-inlet 2-outlets, 2-inlet 2-outlets and reported pressure drop enhancement compared to the empty cavities. X.Liu et al. [91] conducted an experimental and numerical analysis of exhaust gas, heat recovery heat flow and fluid flow coupled equations are solved to obtain temperature and pressure distribution. The heat exchanger used in this study reduces resistance to exhaust heat conduction and increases heat exchanger surface temperature. X.Liu et al. [92] performed experiments on automotive exhaust thermoelectric generators and reported that heat exchangers with chaos-shaped internal structures have higher efficiency. Bo li et al. [93] simulated and studied thermoelectric generators with heat pipe technologies. Heat pipes increase heat transfer; hence power from TEG increases. Wei He et al. [94] studied heat exchanger optimization with different widths and heights for different temperatures. They reported for exhaust gas temperatures of 300^0C to 600^0C, the optimum height of the heat exchanger is 0.004 m. A height of 0.004 m and a length of 0.5 m to 0.8 m are recommended. Bai, Shengqiang et al. [95] designed six different heat exchangers as shown in Fig. 2.5 and performed CFD analysis. They reported serial plate structure has a maximum heat transfer of 1737w. It produced a pressure drop of 9.7 kpa in the suburban drive cycle. The inclined plate and empty cavity structure had a pressure drop of 80 kpa.

Energy harvesting attracts many researchers as it has wider applications in MEMS and the Internet of Things . More than 90% of primary energy is first converted to heat

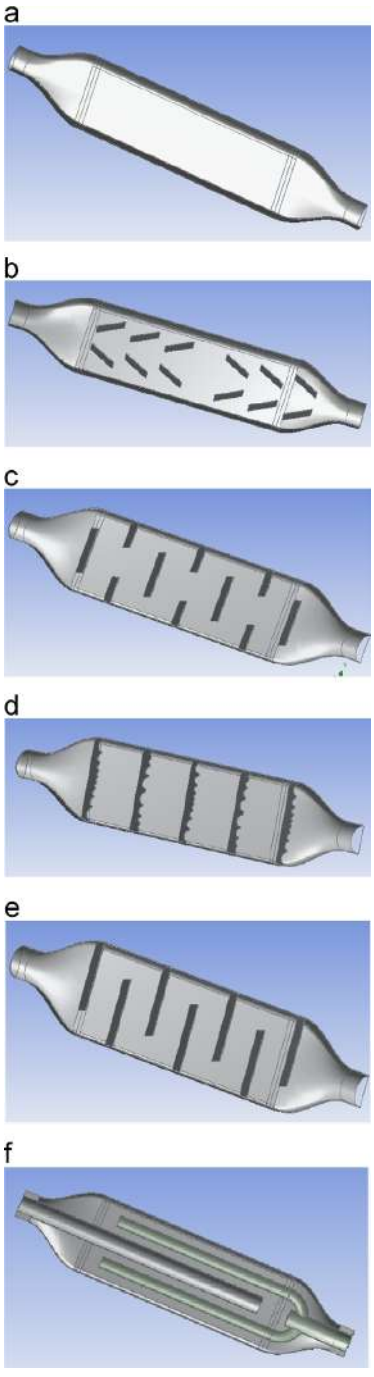

Figure 2.5: Six internal structures a) Empty cavity b) Inclined Plate c) Parallel plate structure d) Separate plate with holes e) Series plate structure f) Pipe structure

before converting to electricity. The energy available in fuel is highly ordered, but the energy associated with heat is disordered. Overall, end energy is 12% of the source [96]. In automotive vehicles, about 40% of heat energy is lost in exhaust gases [67]. If we utilize that heat collectively, it can potentially increase the efficiency of the automotive vehicle. One of the earliest documented research on TEG can trace back to 1964 when an experimental rig with air cooling was constructed, and some tests were conducted by Tomarchio [12] at Clarkson College of Technology. Lead telluride was selected as the thermoelectric material. Results showed that a maximum power of 514 W with a voltage of 14.7 V was obtained for a vehicle speed of 80 km/h, which could furnish sufficient power to the electrical load of an automobile. The decent results promote the research and development of AETEGs to a large extent. [64] reported an experimental analysis of diesel engines with the 72TEG. They were mounted on an Octane-shaped heat exchanger and assembled with fins to increase heat transfer. It produces a maximum power of 1068 watts. [65] mounted 72 TEG downstream of the catalytic converter. A 3000cc gasoline engine is used. It is tested in hill climb mode with an exhaust gas bypass. The efficiency reported is 0.1%. [82] studied temperature distribution and backpressure analysis of AETEG. Different heat exchanger designs were proposed.

[83] did an analysis of AETEG fuel economy considering weight, back pressure, and coolant pumping work and reported a fuel economy of 0.18%. [97] analyzed energy recovery potential for diesel engines using 20 TEG. Peak efficiency was reported as 3%. Biodiesel is also used for the study; it shows there is an increase in NO_x with bio-diesel. Performance of oxide-based TEG is reported with energy and exergy analysis by [98]. [99] reported a heat pipe-assisted thermoelectric generator with 36TEG. It produced a maximum open circuit voltage of 81.09V .[100] simulated AETEG and analyzed power and stress by the multi-physics coupling method. [101] performed an experimental study on AETEG for an onboard vehicle. Results show that using a dimple, the power output increases by 173% compared to without a dimple. [89] modeled using metal foam plates to increase heat transfer. It increased power output but caused a high-pressure drop, reducing net power output. The internal topology of the heat exchanger is studied by [102], which suggests that cylindrical grooves could enhance the heat transfer coefficient and increase efficiency with low back pressure. [103] built a numerical model in FORTRAN and reported the optimal length and width of the heat exchanger. CFD simulation of folded heat exchangers for uniform temperature distribution is written by [104]. Transient behavior of automotive thermoelectric generators is reported for New

European Driving Cycle(NEDC) by [105]. It shows the performance of AETEG in the transient condition is low compared to the steady state.

Each leg is made of more than one material in a segmented leg. [66] reported using segmented leg on 2000cc gasoline engine. It used 10 TEG, six segmented legs upstream, and 4 Hi-Z TEG downstream of the catalytic converter. Efficiency is about 5-10%. In 2007 [68] conducted experiments with wind tunnels on a light-duty truck with a gasoline engine. A rectangular heat exchanger with fins was used. 16 TEG were used, and the Heat exchanger is downstream of the catalytic converter. Engine coolant was used on the cold side, and fuel economy was reported as 1% to 2%. [69] reported experiments on gasoline & diesel engines. As gasoline exhaust gas temperature is higher, AETEG is suitable for a gasoline engine. [70] conducted experiments using Skutteruditte TEG upstream and Bismuth telluride TEG downstream of the catalytic converter. Efforts were made to maintain the uniform temperature of the heat exchanger using extended surfaces. [71] reported experimental and simulation data on hybrid electric vehicles & gasoline engines. They used high-temperature TE material upstream and low-temperature TE material downstream.

The performance of AETEG depends on the properties of TEG material [106], the geometry of TEG [107] and heat exchanger design [108]. A thermoelectric material should have high electrical conductivity, thermal resistivity, and Seebeck coefficient. These three terms are combined and defined in a term called the figure of merit [18] zt. If zt is high, it is considered a good thermoelectric material. The mathematical model for commercial Bi_2Te_3 TEG 12706 is reported by [109] [22].

Figure of merit of thermoelectric material is high for only a short temperature range [5]. Different sections of the TEG leg with different materials based on the performance at that temperate performance can be increased. The temperature of the leg in an AETEG varies from 200^0C to 600^0C from sink to source. A segmented leg is a better choice to improve the efficiency of AETEG. During combining two materials to form a segmented leg, a term compatibility factor is defined [110]. The compatibility factor signifies the ability of the charge carrier to transfer from one segment to another. Two materials with different compatibility factors cannot be combined to form an efficient TEG. Thermal analysis of segmented thermoelectric generator is reported by [111] its shows that efficiency increases by 11%. Segmented TEG is modeled in commercial software by [112] and reported efficiency of 17% to 20%.

Artificial neural networks are a part of machine learning. Machine learning is a set

of techniques to make computers better at doing things that humans (traditionally) can do better [113]. Machine learning involves making machines learn things as humans do. A neural network includes input and hidden layers called neurons and output layers. Weights are assigned from one layer to another. In each neuron, the summation of weights is calculated with bias. The summation of weights with bias is calculated. The activation function is specified. If the activation function calculated is higher than the specified activation value, a neuron gets activated, and output is sent. Mean square error is calculated. The error is propagated by the backpropagation algorithm [114]. [115] used a deep neural network to predict the performance of the TEG device. Training data was taken from the FEM simulation method. DNN results were validated with experimental results. Optimization was done, and a 182% power increase was reported. [116] reported an ANN model. It used 5000 data for training, compared with FEM results. It reports ANN model requires less CPU time compared to the FEM model. Niu et al. [117] conducted experiments on a thermoelectric generator with a parallel flow heat exchanger. Glycol and water as the working fluids. They reported the effect of the mass flow rate of hot fluid, and cold fluid on power and efficiency.

Literature review suggests that both TEG and heat exchanger play a vital role in optimizing power. Most of the study is a simulation or on the test bench. Few reports are available on the artificial neural network models of AETEG. Several experimental works have been reported on AETEG. A significant number of them have used single-leg AETEG. There is potential to use segmented legs to increase efficiency. Therefore, in this work, we compare experimental results with numerical and ANN results and apply segmented leg considering compatibility factors. The current model uses constant material properties called effective material properties for analysis of AETEG and temperature-dependent properties for Uni-couple and segmented leg analysis. Equivalent material properties are calculated by experiments for commercially available thermoelectric generators. For commercial TEG, the manufacturer doesn't provide material properties. They provide a set of parameters such as maximum current voltage and power; using these parameters, effective material properties are calculated [118].

2.5.1 Components of Automotive Exhaust Thermoelectric Generator

An Automotive Exhaust Thermoelectric Generator has three main components.

1. Hot side heat exchanger.
2. Cold side heat exchange.
3. Thermoelectric Generator.
4. Power extraction unit.

Hot side heat exchanger

This heat exchanger extracts heat from the hot side. A hot-side heat exchanger needs to be designed such that the surface temperature of the heat exchanger reaches the exhaust gas temperature. This is possible if the heat transfer coefficient $h(w/m^2K)$ is high. The heat transfer coefficient is directly proportional to the temperature of exhaust gases and velocity. Wang et al [119] reported that with an increase in heat transfer coefficient power og TEG increases. Lesage et al. [13] studied different insertions as shown in Fig 2.6 in heat exchangers to create turbulence and increase the heat transfer coefficient. Jaideep Pandit et al [120] studied the effect of pin fins geometry on hot side of the heat exchanger. It suggests diamond-shaped pin fins have higher efficiency and it reports that as the duct size reduces heat transfer coefficient increases. X.Liu et al. [92] performed experiments on automotive exhaust thermoelectric generators and reported that heat exchangers with chaos-shaped internal structures have higher efficiency. Niu et al.[121] reported a 3-dimensional simulation model on the exhaust-based thermoelectric generator. It reports the use of bafflers in the exhaust channels. Bafflers increase the heat transfer coefficient but it decreases the wall temperature downstream of bafflers. The baffler angle should be large to increase efficiency. A single baffler angle is not suitable for all flow rates.

Pressure drop in heat exchanger is an important parameter to study as heat exchanger is placed in the exhaust system of an automotive vehicle. Liu et al.[82] conducted a study of the thermoelectric generators in different locations of the exhaust system. They reported TEG located upstream of the catalytic converter and muffler has a higher surface temperature and lower back pressure. [89] modeled using metal foam plates to increase heat transfer. It increased power output but caused a high-pressure drop, reducing net power output. The internal topology of the heat exchanger is studied by [102], which suggests that cylindrical grooves could enhance the heat transfer coefficient and increase efficiency with low back pressure.

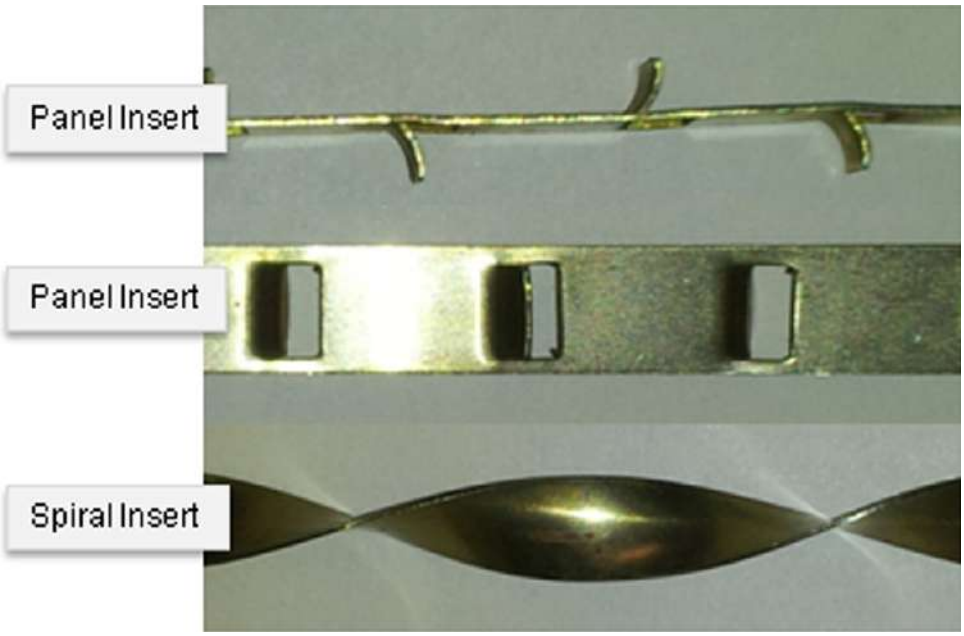

Figure 2.6: Insertions [13]

Cold side heat exchanger

Cold-side heat exchangers should have a minimum thermal resistance. If cooling is not done both sides of the thermoelectric generator reach the same temperature and power output reduces. Hendricks et al. [122] reported that the thermal resistance on the hot side should be 10 to 30 times more than the thermal resistance on the cold side. Most of the research is on water, air, or engine coolant as cold fluid.

Thermoelectric Generator

A thermoelectric generator is a solid-state device. It directly converts heat to electricity without any moving parts. The performance of thermoelectric material is based on the material property called $zt = \frac{\alpha^2\sigma}{\kappa}$ A good thermoelectric material should have a high Seebeck coefficient and electrical conductivity but low thermal conductivity. Most of the thermoelectric materials research is based to reduce thermal conductivity. Thermal conductivity has two parts one is the Lattice part of thermal conductivity other is the electronics part, the lattice part of thermal conductivity can be decreased with some techniques [22]. With nanotechnology, a high figure of merit materials can be produced by nano inclusion [23]. [24] reported Tin selenide p-type thermoelectric material of zt 2.6 and [25] Shang et al. reported n-Type material of zt 2.8 in bulk thermoelectrics.

Power extraction unit

The power output from the thermoelectric generator needs an extraction unit. To get maximum output power, load resistance should match the internal resistance. For this purpose maximum power point tracking method(MPPT) is used. TEGs are connected in series to get more voltage and are connected in parallel to get more current [123]. Based on the requirement TEGs are connected.

2.6 Summary from literature review

From the review, some features are summarized, and the assessment is made:

Sl.No	Key Points	Description
1.	Research Scope	Automotive exhaust Thermoelectric generators (AETEGs) have been simulated and studied for two-wheelers and heavy vehicles. Most studies are conducted on test benches, with only a few reporting actual road tests.[101] [124] [125] [126]
2.	Factors Explored	Studies have focused on the effect of different thermoelectric materials, heat exchanger design, working fluid on the cold side, strategies to enhance heat transfer coefficient, and conversion efficiency.[127] [128] [129] [130]
3.	TEG Materials	Commercially available TEGs mainly use Bismuth telluride (Bi2Te3). However, due to temperature limitations, modifications such as bypassing exhaust gases or using high-temperature materials like Skutterudites, Half-Heusler, and SiGe have been reported. Some studies also utilize segmented legs or use different materials upstream and downstream of the exhaust system [109] [131] [132] [133]
4.	Placement of TEG on Exhaust System	Most studies place TEGs downstream of the catalytic converter to avoid interference with its performance. Some propose integrating AETEG and the catalytic converter in the rear of the exhaust heat exchanger to utilize the reaction heat and improve temperature distribution. [134] [135] [136] [137]

Continued on next page

(Continued)

5.	Design of Exhaust Heat Exchangers	To enhance heat transfer and reduce back pressure, various exhaust heat exchanger structures have been designed, including modified shapes like rectangular, octagonal, and hexagonal exhaust pipes. Heat pipes and vortex generators have also been utilized as heat transfer enhancement structures. [138] [139] [140] [141] [142]
6.	Working Fluid	While early studies used air as the cooling medium, later studies employed water or engine coolant for better heat transfer. However, most studies fail to consider the power loss associated with transmitting water or coolant. [143] [144] [145] [146]
7.	Power Output and Efficiency	Many studies report power output and efficiency without considering parasitic losses. These losses include the power consumed by an electric pump and increased exhaust back pressure due to the TEG. Some researchers have proposed the concept of net power, which subtracts the power loss associated with parasitic losses from the produced power, leading to negative power outputs in some cases. [147]
8.	Vehicle Types	A wide range of vehicles, including light-duty trucks, heavy-duty trucks, passenger cars, and hybrid electric vehicles (HEVs), have been studied for AETEG applications. [66] [100] [103]
9.	Dynamic Road Tests	While most studies are based on bench tests, only a few have conducted actual dynamic tests on the road. [148] [149] [150]
10.	Fuel Economy Improvement	The literature reports the power output, efficiency, and fuel economy improvement achieved by incorporating TEGs into vehicles. The effects of thermoelectric material, mounting position, weight, configuration, and connections on these performance parameters are discussed in various studies. [83] [71] [9]

Continued on next page

(Continued)

11.	Cost Analysis	Comprehensive cost analysis on AETEGs, including the contributions of components, manufacturing, operating, and maintenance costs, has been lacking in most studies. Cost reduction strategies and feasible directions to reduce overall costs are not adequately explored.
12.	Space Constraints	The space required for AETEGs and associated auxiliary devices (heat exchangers, accumulators, pipelines) has not received enough attention in the literature. Limited chassis space in vehicles like passenger cars poses a challenge for the direct implementation of AETEGs.
13.	Transient Operation	Most studies have focused on steady-state operation, while real driving conditions involve variations in exhaust temperature and mass flow rate. Transient operation poses challenges in terms of operating points and the risk of high-temperature damage to AETEGs. Investigations under transient states are essential for practical applications. [105]

2.7 Research Gaps

Based on the literature review, the research gaps identified are as follows:

Comprehensive Performance Evaluations: Although there have been experimental, numerical, and mathematical modeling studies on automotive exhaust thermoelectric generators (AETEGs), there is a need for comprehensive performance evaluations. This includes analyzing the power output, efficiency, and considering various factors such as thermoelectric material properties, design of heat exchangers, working fluid selection, and strategies to enhance heat transfer coefficient and power output. In this work, we aim to address this gap by conducting thorough performance evaluations of AETEGs.

Exploration of Alternative Materials: Most commercially available thermoelectric generators (TEGs) are made of Bismuth telluride (BiTe), which has limitations when mounted downstream of the exhaust system due to its medium-temperature characteristics. To overcome this limitation, we explore alternative materials such as Skutterudites, which have shown promise in improving AETEG performance. Additionally, the use of segmented thermoelectric generators is investigated as a strategy to further enhance AETEG efficiency.

Design and Fabrication of Heat Exchangers: The efficiency of AETEGs is significantly influenced by the design and performance of heat exchangers. In this research, we focus on designing and fabricating two heat exchangers to optimize AETEG performance. The performance evaluation of the AETEG system with the newly designed heat exchangers is an important aspect of this work.

By addressing these research gaps, we aim to contribute to the understanding and improvement of AETEGs by conducting comprehensive performance evaluations, exploring alternative thermoelectric materials, and optimizing heat exchanger design and fabrication.

Chapter 3

Research Methodology

3.1 Introduction

This chapter focuses on the theoretical and numerical analysis of a thermoelectric generator (TEG), specifically the use of bismuth telluride (Bi_2Te_3) as the thermoelectric material. The chapter begins with analysis of 12P-N pair TEG further by introducing the commercially available TEG made of bismuth telluride and provides an inside view of the thermoelectric module (TEC 12706). The same module is then simulated using the Finite Element Method (FEM) and a mathematical model.

The theoretical model of a TEG is presented, describing the conversion of thermal energy into electrical energy based on the temperature difference between the hot and cold sides of the thermoelectric materials. Equations are provided to describe the heat flow at the hot and cold sides, electric power generated by the thermocouple, electric current equation, and the thermal efficiency of the TEG. The chapter also presents equations for output power, thermal efficiency, maximum conversion efficiency, optimum current, maximum power, and maximum power efficiency in terms of load resistance.

Assumptions made for the analysis of the TEG include the independence of transport properties on temperature, negligible heat loss due to convection and radiation, negligible contact resistance, and neglecting the Thomson effect.

The chapter then moves on to the theoretical modeling and numerical modeling of an automotive exhaust gas thermoelectric generator (AETEG). The governing equations for the heat exchanger and the TEG are explained. The heat exchanger equations include conservation of mass, momentum, and energy, while the TEG equations include the general TEG equation and its source term components.

The chapter concludes with the performance investigation and validation of both

the TEG and the AETEG. Power versus load resistance for different scenarios and leg lengths are analyzed, along with the variation of power with temperature difference. The experimental results for the AETEG are compared with the theoretical and numerical results, showing a good agreement with a small deviation attributed to heat losses and assumptions made during the analysis.

Overall, this chapter provides a comprehensive analysis of both a TEG and an AETEG, incorporating theoretical models, numerical simulations, and validations, to evaluate their performance and efficiency.

3.2 Theoretical and Numerical Analysis of Thermoelectric Generator

Commercially available thermoelectric generators are made of bismuth telluride. This section includes the Theoretical and Numerical Analysis of Thermoelectric Generator. A thermoelectric module TEC 12706 is shown in fig. 3.1. Its ceramic cover is removed and the inside view is as shown in Fig. 3.2. It consists of P and N-type semiconductors. The same with same dimensions are simulated with the FEM method and mathematical model.

3.2.1 Theoretical model

A thermoelectric generator (TEG) is a device that converts thermal energy into electrical energy. It operates based on the temperature difference between two dissimilar materials, known as the n-type and p-type junctions. The following equations describe the operation and efficiency of a TEG [23]:

$$\dot{Q}_h = \alpha T_h I - \frac{1}{2} I^2 R + K(T_h - T_c) \tag{3.1}$$

$$\dot{Q}_c = \alpha T_c I + \frac{1}{2} I^2 R + K(T_h - T_c) \tag{3.2}$$

$$P_{\text{out}} = \dot{Q}_h - \dot{Q}_c \tag{3.3}$$

$$P_{\text{out}} = \frac{\alpha I(T_h - T_c) - \frac{1}{2} I^2 R}{2} \tag{3.4}$$

$$I = \frac{\alpha(T_h - T_c)}{R_L + R} \tag{3.5}$$

$$\eta_{\text{th}} = \frac{P_{\text{out}}}{\dot{Q}_h} = \frac{I^2 R_L}{\alpha T_h I - \frac{1}{2} I^2 R + K(T_h - T_c)} \tag{3.6}$$

$$P_{\text{out}} = \frac{\alpha}{2} \left(\frac{T_c}{T_h}\right)^2 \left[\left(\frac{T_c}{T_h}\right)^{-1} - 1\right] \frac{R_L}{R} \left(R + \frac{R_L}{2}\right) \tag{3.7}$$

$$\eta_{\text{th}} = \frac{\left(1 - \frac{T_c}{T_h}\right)\left(1 + \sqrt{1 + Z\overline{T}_c}\right) - 1}{2\left(1 - \frac{T_c}{T_h}\right) + 4\frac{T_c}{T_h}\sqrt{1 + Z\overline{T}_c}} \tag{3.8}$$

$$\eta_{\text{mc}} = \left(1 - \frac{T_c}{T_h}\right)\sqrt{1 + Z\overline{T}_c} - 1 + \frac{T_c}{T_h} \tag{3.9}$$

$$I_{mp} = \frac{\alpha \Delta T}{2R}, \quad P_{\max} = \frac{\alpha}{2\Delta T}\frac{1}{4R}, \quad \eta_{\text{mp}} = \left(1 - \frac{T_c}{T_h}\right)\left(2 - \frac{1}{2}\left(1 - \frac{T_c}{T_h}\right) + 4\frac{T_c}{T_h}\sqrt{1 + Z\overline{T}_c}\right) \tag{3.10}$$

where:

$\dot{Q}_h$ and $\dot{Q}_c$ are the heat flows at the hot and cold sides, respectively.

P_{out} is the electric power generated by the TEG.

T_h and T_c are the temperatures at the hot and cold sides, respectively.

α is the Seebeck coefficient.

I is the electric current.

R is the internal resistance.

K is the thermal conductivity.

R_L is the load resistance.

Z is the figure of merit.

$\overline{T}_c$ is the average temperature between the hot and cold sides.

following assumptions are made for the analysis of TEG.

Figure 3.1: Commercially available TEM

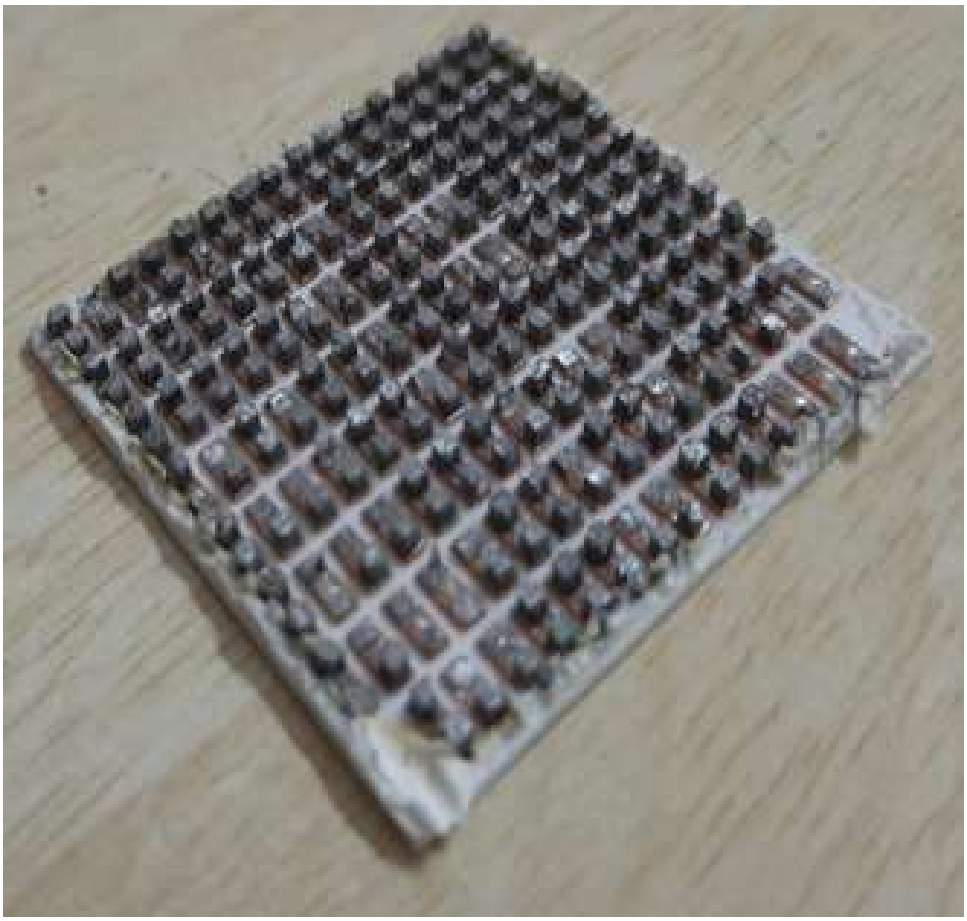

Figure 3.2: commercial TEG inside view

1. Transport properties don't depend on temperature.

2. Heat loss due to convection and radiation is negligible

3. Contact resistance is negligible

4. Thomson effect is negligible

The boundary conditions used for analysis of thermoelectric generator are.The source temperature is assumed as $T_h = 300^oC$.The sink temperature is assumed as $T_c = 30^oC$ Figure 3.3 shows different types of heat distributions in an element of TEG.
The following equations for theoretical modeling are as follows.

Heat input to the element

$$\dot{Q_{in}} = \alpha T_h I - \frac{1}{2} I^2 R + \kappa (T_h - T_c) \tag{3.11}$$

Heat output from the element

$$\dot{Q_{out}} = \alpha T_c I - \frac{1}{2} I^2 R + \kappa(T_h - T_c) \tag{3.12}$$

Power produced by Thermoelectric generator is calculated as

$$P_{out} = \dot{Q_{in}} - \dot{Q_{out}} = \alpha I \Delta T - I^2 R \tag{3.13}$$

Efficiency is calculated as

$$\eta = \frac{power}{Heatinput} \tag{3.14}$$

performance evaluation is reported in the section 3.4.1.

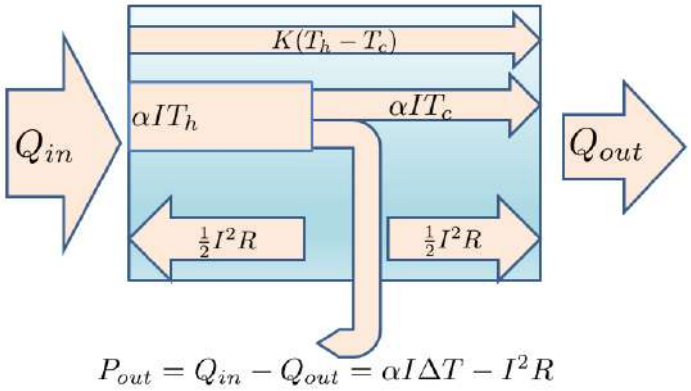

Figure 3.3: Different Heat Contributions in TEG

3.2.2 Numerical Analysis

Ansys Workbench is used for numerical simulation. Modeling of commercial TEG is done in ANSYS design modeler. The model is shown in fig. 3.4. Meshing is done in Ansys Mesh the details of the mesh are in Tabel. 3.1. Following points are considered during meshing.

1. Element size: The element size should be small enough to capture the important features of the TEG, such as the size of the thermoelectric legs and the heat source. However, the element size should not be too small, as this can lead to a large number of elements and a long computational time.

2. Mesh quality: The mesh quality should be high in order to ensure accurate results. This means that the elements should be as close to regular as possible, with low

skewness and orthogonality.

3. Mesh density: The mesh density should be higher in areas where the temperature gradients are steep, such as the junctions between the thermoelectric legs. This will help to capture the heat transfer accurately.

The minimum element size is 0.1mm , the hexahedral mesh are used.The skewness is 0.7,The orthogonality is 0.9. Under relaxation factor is 0.75. Figure 3.6 shows the temperature distribution. In the numerical analysis of a thermoelectric generator (TEG) using ANSYS thermal electric, the Finite Element Analysis (FEA) method is employed. The governing equations for the TEG are solved using the FEA method in ANSYS thermal electric.

The main equation used in the analysis is the general TEG equation, which is based on the conservation of energy. The equation takes into account the thermal conductivity, temperature distribution, and the source term in the TEG [151]. It can be expressed mathematically as:

$$\mathrm{div}(k\mathrm{grad}(T)) + \dot{S}_T = 0 \tag{3.15}$$

In this equation, k represents the thermal conductivity, T represents the temperature, and $\dot{S}_T$ represents the source term in the TEG. The source term $\dot{S}_T$ includes contributions from different components of the TEG. It can be further divided into three components: the source component of the P-Type leg ($\dot{S}_{TP}$), the source component of the N-Type leg ($\dot{S}_{TN}$), and the source component of the copper ($\dot{S}_{TC}$).

The source component of the P-Type leg is given by the equation:

$$\dot{S}_{TP} = \frac{J^2}{\sigma_p} + \alpha_p J T_p \tag{3.16}$$

Here, J represents the current density, σ_p represents the electrical conductivity of the P-Type leg, α_p represents the Seebeck coefficient of the P-Type leg, and T_p represents the temperature of the P-Type leg.

Similarly, the source component of the N-Type leg can be expressed as:

$$\dot{S}_{TN} = \frac{J^2}{\sigma_n} + \alpha_n J T_n \tag{3.17}$$

In this equation, σ_n represents the electrical conductivity of the N-Type leg, α_n represents the Seebeck coefficient of the N-Type leg, and T_n represents the temperature of

the N-Type leg.

Finally, the source component of the copper can be represented by the equation:

$$\dot{S}_{TC} = \frac{J^2}{\sigma_{\text{cop}}} \tag{3.18}$$

Here, σ_{cop} represents the electrical conductivity of the copper.

These equations, along with appropriate boundary conditions and material properties, are solved using the finite element method in ANSYS thermal electric. The FEA method divides the TEG into small elements, allowing for the numerical solution of the governing equations. By solving these equations, the temperature distribution and other characteristics of the TEG can be analyzed and evaluated.

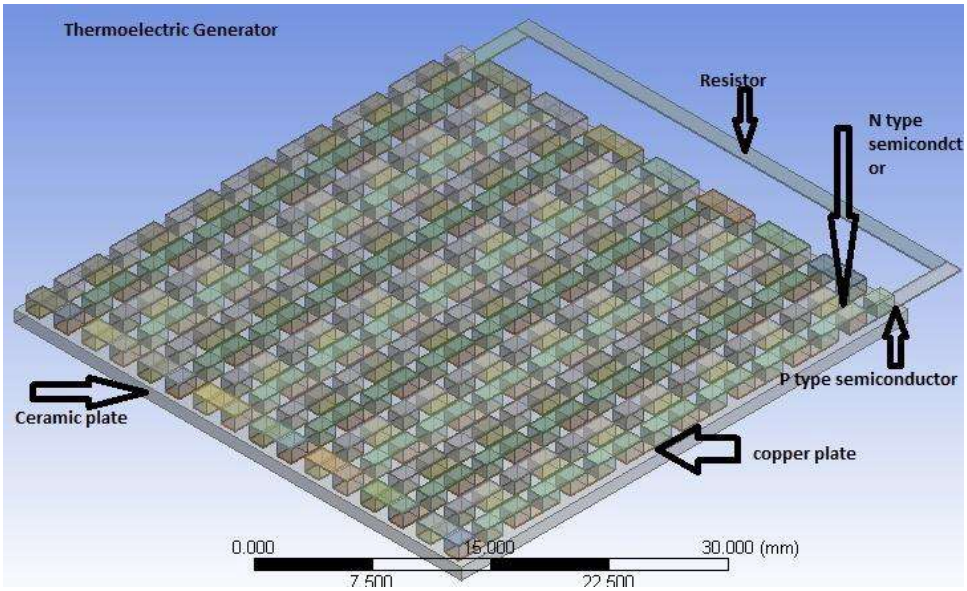

Figure 3.4: Model of Commercial TEG

Table 3.1: Mesh Details

Nodes	251524

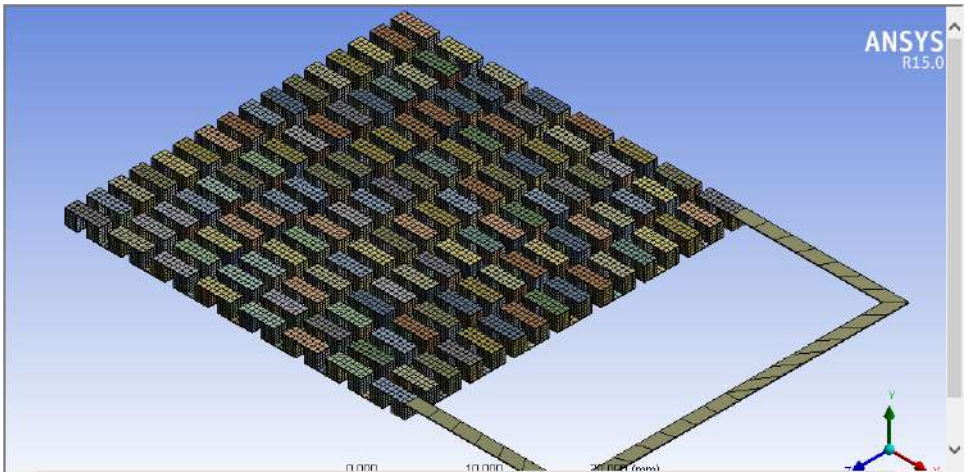

Figure 3.5: Meshed component of TEM

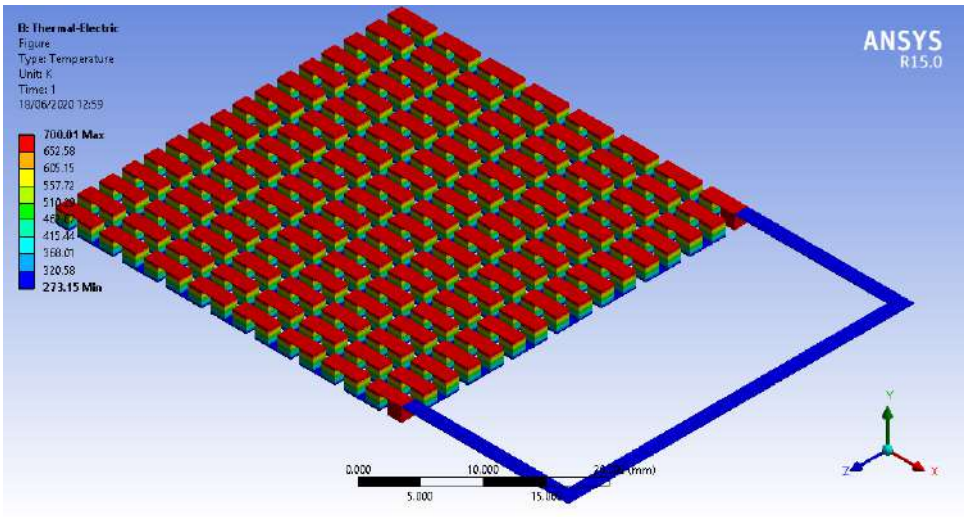

Figure 3.6: Temperature profile

3.3 Theoretical and Numerical Modeling of AETEG

3.3.1 Theoretical Modeling of AETEG

Theoretical modeling for an automotive exhaust gas thermoelectric generator explanations and equations:

1. Heat Flux Calculation: The first step in modeling an exhaust gas thermoelectric generator is to calculate the heat flux ($\dot{Q}_{\text{inlet}}$) from the exhaust gases to the TEG module. The heat flux can be determined using the following equation:

$$\dot{Q}_{\text{inlet}} = \dot{m}_{\text{exhaust}} \cdot C_{p_{\text{exhaust}}} \cdot (T_{\text{inlet}} - T_{\text{exhaust}}) \tag{3.19}$$

where:

$\dot{m}_{\text{exhaust}}$ is the mass flow rate of the exhaust gases (in kg/s),

$C_{p_{\text{exhaust}}}$ is the specific heat capacity of the exhaust gases (in J/(kg·K)),

T_{inlet} is the temperature of the exhaust gas at the TEG inlet (in Kelvin), and

T_{exhaust} is the temperature of the exhaust gases at TEG outlet (in Kelvin).

2. Temperature Distribution: To model the temperature distribution along the TEG module, we consider the heat flux and thermal resistances. Assuming uniform temperature distribution within each TEG material pair, the temperature difference across each pair (ΔT_{pair}) can be calculated using the following equation:

$$\Delta T_{\text{pair}} = \frac{\dot{Q}_{\text{inlet}}}{N \cdot A_{\text{leg}} \cdot k_{\text{leg}}} \tag{3.20}$$

where:

N is the number of thermoelectric material pairs in the TEG module,

A_{leg} is the cross-sectional area of a single leg of the TEG (in m^2),

k_{leg} is the thermal conductivity of a single leg of the TEG (in W/(m·K)).

3. Electrical Output Power: The electrical power output (P_{out}) of the TEG module can be determined by considering the temperature difference (ΔT_{pair}) and the internal electrical resistance (R_{internal}) of the TEG. The equation for electrical output power is given by:

$$P_{\text{out}} = N \cdot \left(\frac{\Delta T_{\text{pair}}}{R_{\text{internal}}} \right)^2 \tag{3.21}$$

The equation can be derived from the Seebeck effect, which states that a voltage is generated across a thermoelectric material when there is a temperature difference across it. The magnitude of the voltage is proportional to the temperature difference and the Seebeck coefficient of the material.

The internal electrical resistance of the TEG module is due to the resistance of the materials used in the module and the contact resistance between the materials. The internal resistance limits the amount of electrical power that can be generated by the TEG module. The internal resistance can be given as.

$$R_{\text{internal}} = \frac{L_{\text{total}}}{A_{\text{leg}}} \cdot \frac{1}{\sigma_{\text{leg}}} \tag{3.22}$$

where:

R_{internal} is the internal electrical resistance of the TEG module,

L_{total} is the total length of the TEG module,

A_{leg} is the cross-sectional area of a single thermoelectric leg,

σ_{leg} is the electrical conductivity of the thermoelectric leg material.

4. Overall Efficiency: The overall efficiency (η) of the TEG system can be calculated as the ratio of electrical output power to the heat input:

$$\eta = \frac{P_{\text{out}}}{\dot{Q}_{\text{inlet}}} \tag{3.23}$$

5. Figure of Merit: The figure of merit (ZT) is an important parameter in thermoelectric materials and represents their performance. It can be calculated using the Seebeck coefficient (S), electrical conductivity (σ), and thermal conductivity (k) of the thermoelectric material:

$$ZT = \frac{S^2 \cdot \sigma \cdot T}{k} \tag{3.24}$$

where:

S is the Seebeck coefficient of the thermoelectric material (in V/K),

σ is the electrical conductivity of the thermoelectric material (in S/m),

T is the average temperature across the thermoelectric material (in Kelvin), and

k is the thermal conductivity of the thermoelectric material (in W/(m·K)).

These equations provide a comprehensive theoretical modeling approach for an automotive exhaust gas thermoelectric generator. These equations are used for theoretical analysis of AETEG and the results are discussed in section 3.4.2.

3.3.2 Numerical Modeling of AETEG

Theory used in the numerical analysis of an automotive exhaust gas thermoelectric generator (TEG) with a heat exchanger, using ANSYS. In ANSYS, this includes fluid flow analysis in heat exchanger and thermoelectric equations for thermoelectric generator. The details are as follows.

Heat Exchanger Equations Heat Exchanger Equations:

The heat exchanger in the TEG system is modeled using the following equations:

a) Conservation of Mass: The conservation of mass equation describes the fluid flow in the heat exchanger and is given by:

$$\text{div}(\mathbf{V}) = 0 \tag{3.25}$$

where: - $\mathbf{V}$ is the fluid velocity.

b) Conservation of Momentum: The conservation of momentum equation accounts for the forces acting on the fluid and is given by:

$$\text{div}(\mathbf{VV}) + \frac{1}{\rho}\nabla P + \text{div}(\mu\nabla\mathbf{V}) = 0 \tag{3.26}$$

where:

ρ is the fluid density,

P is the pressure,

μ is the dynamic viscosity.

c) Conservation of Energy: The conservation of energy equation represents the heat transfer in the heat exchanger and is given by:

$$\text{div}(k\nabla T) = 0 \tag{3.27}$$

where:

k is the thermal conductivity,

T is the temperature.

These equations are solved using the Finite Volume Method (FVM) in ANSYS Fluent, which discretizes the domain into small control volumes and numerically solves the governing equations.

Thermoelectric Generator Equations

The TEG equations account for the heat transfer, electrical behavior, and performance of the TEG. The equations include:

a) General TEG Equation: The general TEG equation represents the conservation of energy in the TEG system and is given by:

$$\text{div}(k\nabla T) + \dot{S}_T = 0 \tag{3.28}$$

where:

k is the thermal conductivity,

T is the temperature,

$\dot{S}_T$ is the source term in the TEG equation.

b) Source Term Components: The source term $\dot{S}_T$ in the TEG equation consists of several components that account for different heat sources and effects. These components include:

Peltier Effect Component: The Peltier effect component represents the heat generation or absorption at the junctions of the TEG due to the Peltier effect. It is given by:

$$\dot{S}_P = -\alpha JT \tag{3.29}$$

where:

α is the Seebeck coefficient,

J is the current density, and

T is the temperature.

Joule Heating Component: The Joule heating component accounts for the heat generated within the TEG due to the electrical resistance of the material. It is given by:

$$\dot{S}_J = \frac{J^2}{\sigma} \tag{3.30}$$

where:

J is the current density,

σ is the electrical conductivity.

Heat Conduction Component: The heat conduction component represents the transfer of heat within the TEG due to thermal conductivity. It is given by:

$$\dot{S}_C = \text{div}(k\nabla T) \tag{3.31}$$

where:

k is the thermal conductivity,

T is the temperature.

These equations, along with the appropriate boundary conditions and material properties, are solved using the Finite Element Method (FEM) in ANSYS Thermal Electric to analyze the behavior and performance of the automotive exhaust gas TEG. The following is a summary of the steps involved in the numerical modeling:

1. The conservation of mass, momentum, and energy equations are solved for the heat exchanger using the FVM in ANSYS Fluent.

2. The temperature field is calculated from the heat exchanger equations.

3. The source term components are calculated from the temperature field.

4. The TEG equations are solved for the heat generation and electrical behavior of the TEG using the FEM in ANSYS Thermal Electric.

5. The process is repeated until the temperature field converges.

Figure 3.7 illustrates an AETEG model implemented in ANSYS. The simulation was conducted, and the outcomes are analyzed in section 3.4.1.

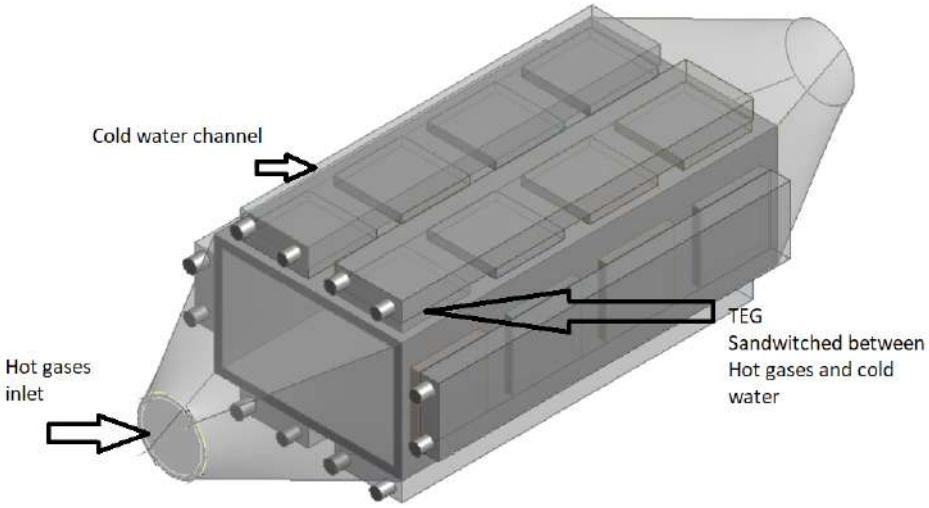

Figure 3.7: AETEG model in ansys on test bench

Numerical Model Validation

Results of the numerical model are validated by results reported by [117].A heat exchanger with 600mm length and cross-section of 40mmx8mm with four layers. Each layer has 14TEG made of Bi_2Te_3 is simulated similarly to the one reported by Niu et al. [117]. Present numerical model results are compared with Niu et al. [117] results as shown in Fig. 3.8. Hot side fluid temperature is $T_h = 90^0C$ & $T_c = 30^0C$. A glycol water mixture of 60:40 is used as working fluid for both hot and cold sides. The hot fluid volume flow rate is $Q_h = 0.4m^3/hr$. Cold fluid volume flow rate is $Q_c = 0.3m^3/hr$. The power output from the present and from the literature are comparable as shown in Fig. 3.8. This validated numerical model is used to simulate the experimental model and is reported in sec 5.2.1.

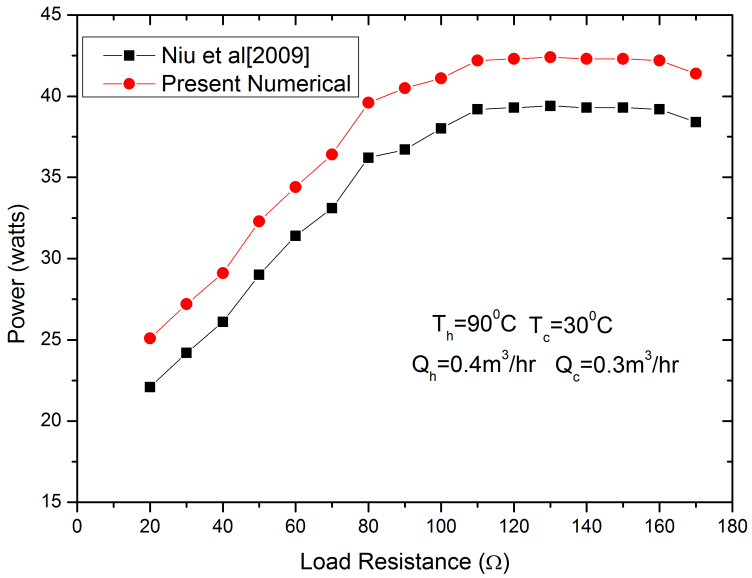

Figure 3.8: Numerical results compared with niu et al

3.4 Performance Investigation and Validation of TEG and AETEG(TEG Mounted on Hot air Blower)

3.4.1 Performance investigation and validation of TEG

Analysis of 12P-N Pair TEG

Initially a 12 P-N pair TEG is analyzed initially theoretically and numerically with the model peoposed in the section 3.2.The model of 12pair TEG is done in ANSYS and the mesh of 12p-n pair TEG is shown in figure 3.9. Constant material properties are used in this simulation and are tabulated in the table 3.2. Only in this section effective material properties are not used for simulation.

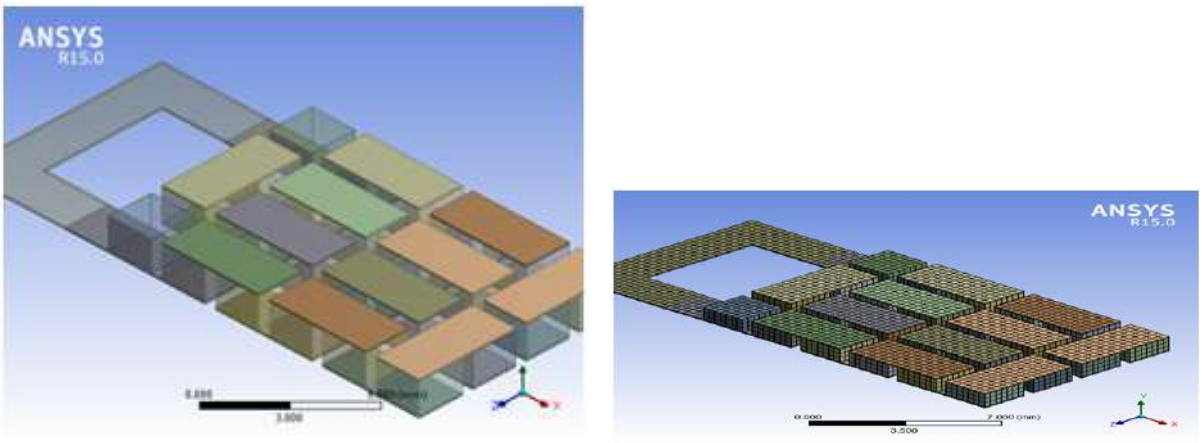

(a) 12 pair TEG module (b) Mesh 12 pair TEG

Figure 3.9: TEG with 12 P-N Pair

Table 3.2: Properties of material used for simulation

Geometry	Value	Units
P type		
· Thermal Cross section area	2 mm^2	mm^2
· Length	Varies from 0.1 mm to 1.7 mm	mm
· Seebeck coefficient	160	µV/C
· Electrical resistivity	1.27e-5	ohm m
N type		
· Thermal Cross section area	2 mm*2 mm	mm^2
· Length	Varies from 0.1 mm to 1.7 mm	mm
· Seebeck coefficient	-160	µV/C
· Electrical resistivity	1.27e-5	ohm m
Load Resistance		
· Cross section area	0.1 mm*2 mm	mm^2
· Electrical resistivity	Varies accordingly	-
· Electrical length	19 mm	mm

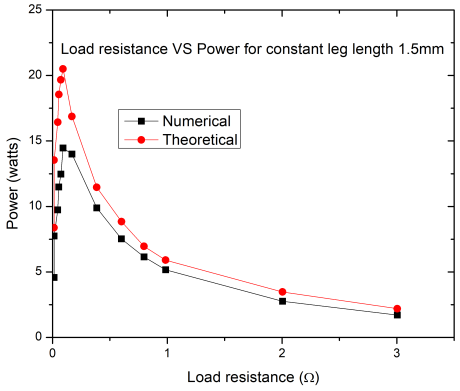

Figure 3.10: Load resistance VS Power for constant leg length 1.5mm

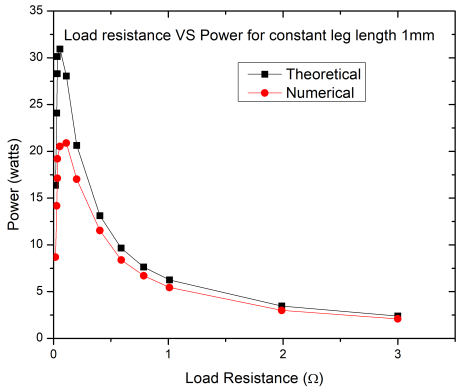

Figure 3.11: load versus power for 1mm

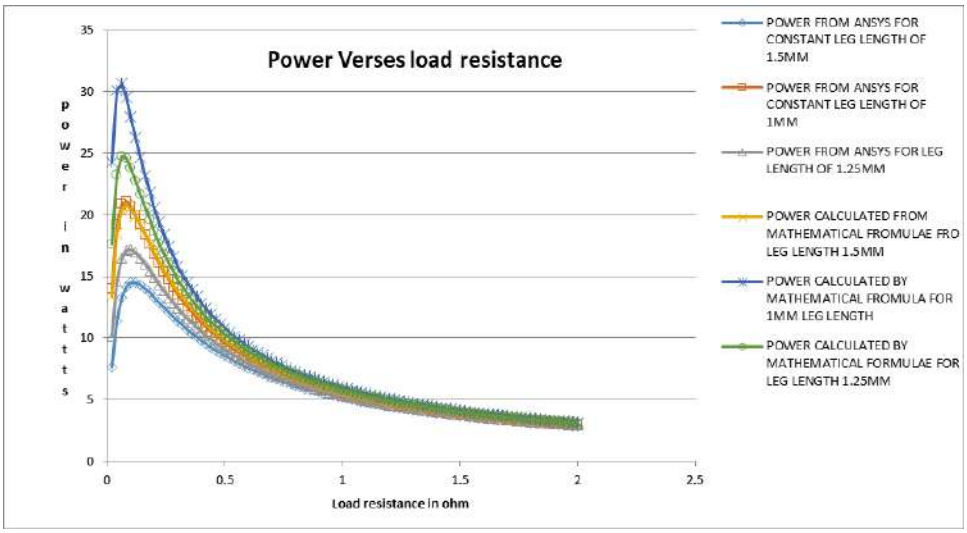

Figure 3.12: Power versus load resistance 12pair TEG

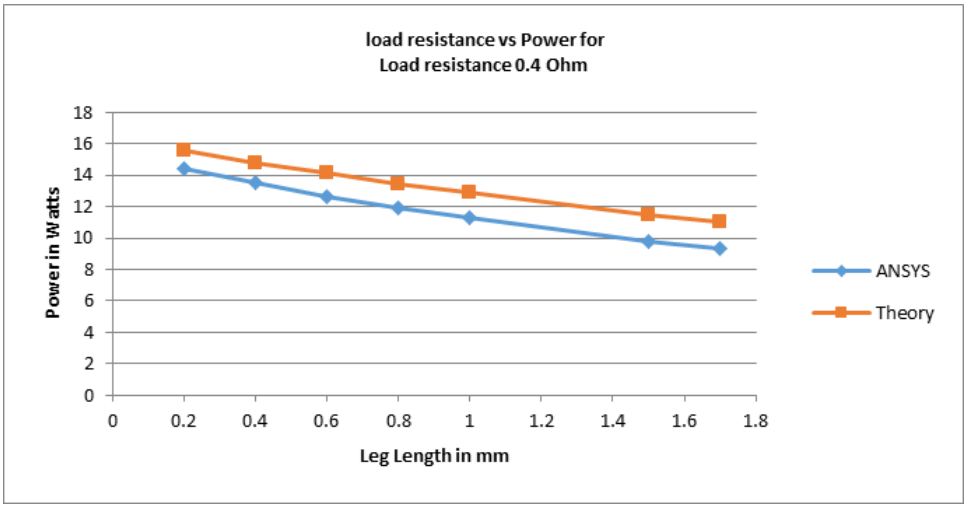

Figure 3.13: power versus length of leg 12 pair

Grid Independence Test

In a simulation using ANSYS to optimize a number of elements a grid independence test is necessary. In the present work, the grid independence test is done on single P-N pair thermoelectric generator. The hot side temperature is 700^0C and the cold side temperature is 300^0C. From Fig.3.14 it is observed that as the number of elements increases more than 500 the results will not change. But with the increase in element numbers computing time increases. Hence the optimum element number is 500.

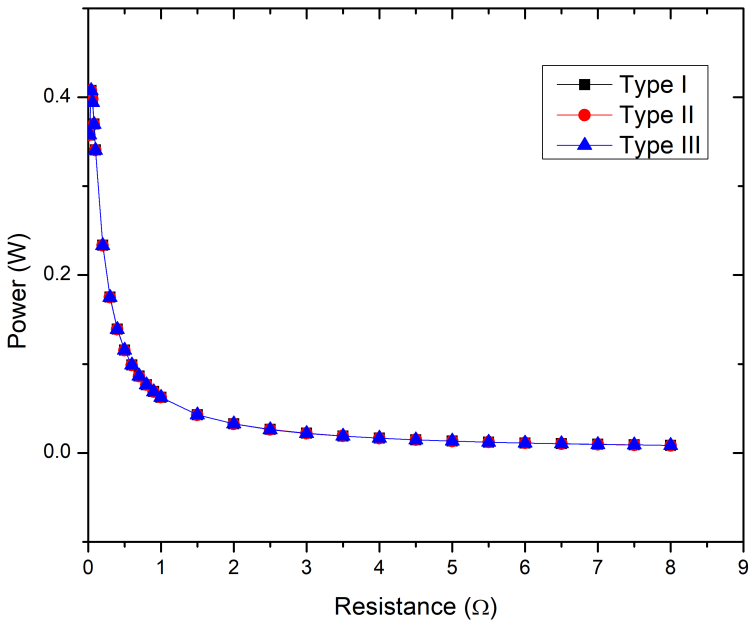

Figure 3.14: Grid independence test

Table 3.3: Details of Grid

Particulars	Type-I	Type-II	Type-III
Elements	500	3296	2500

Analysis of 127 PN Pair Bismuth Telluride TEG

Based on the theoretical and numerical models for a thermoelectric generator, the source temperature is assumed to be $T_h = 300°C$, while the sink temperature is assumed to be $T_c = 30°C$. This simulation use the properties tabulated in section 3.2. The relationship between power and load resistance for various load resistances is depicted in Figure 3.15. Both the mathematical modeling results and numerical simulation results exhibit a high level of agreement.

As the load resistance increases, the power initially increases until it reaches its maximum when the load resistance equals the internal resistance. At this peak power point, the power measures $20watts$, attributed to electrical resonance. Subsequently, as the load resistance continues to increase, the power progressively decreases.

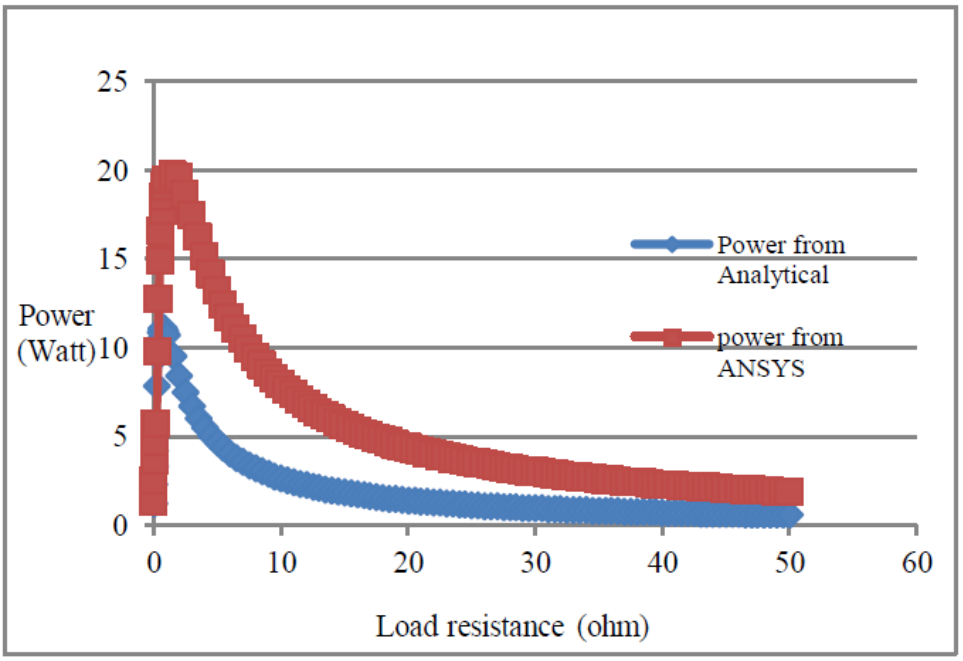

Figure 3.15: Power versus load resistance Bi2te3

Figure 3.16 illustrates the relationship between power and load resistance for different leg lengths. It is evident from the figure that as the leg length decreases, the power generated by the thermoelectric generator increases. Moreover, Figure 3.17 demonstrates the variation of power with temperature difference. As the temperature difference increases, the power produced by the TEG also increases.

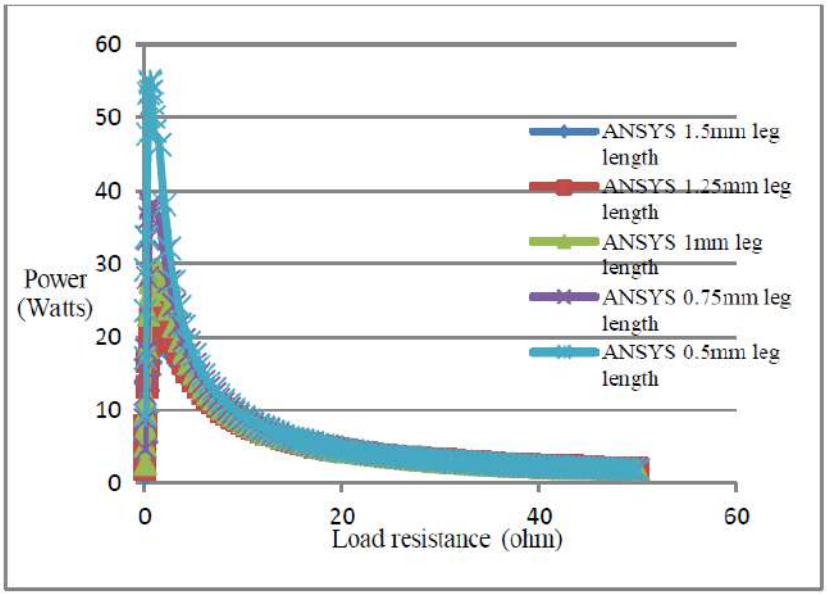

Figure 3.16: Power versus load resistance for different leg length

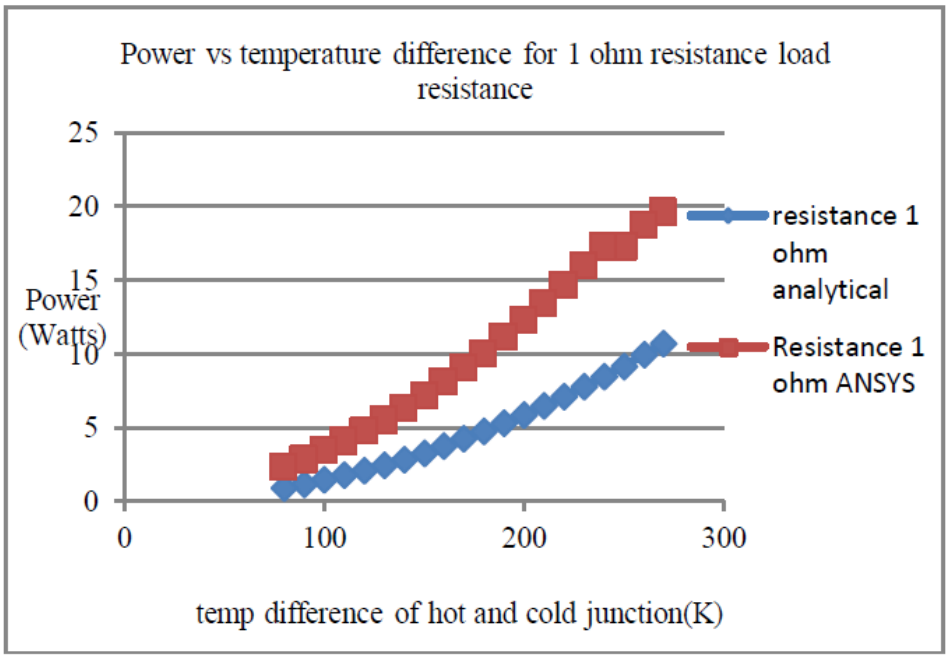

Figure 3.17: Power vs temperature difference

3.4.2 Performance Investigation and validation of AETEG(TEG Mounted on Hot air Blower)

Based on the analysis of the thermoelectric generator on the test bench with a hot air blower, Figure 3.18 demonstrates that at a load resistance of 81 Ω, the power generated is 67 watts, with an average hot-side temperature of $300°C$ and an average cold-side temperature of $30°C$. The mass flow rate of hot gases is $m_{hi} = 0.5$ g/s, and the cold-side mass flow rate is $Q_c = 0.1$ ltr/s. The theoretical and numerical simulation results are compared, and they exhibit close similarity. A detailed experimental study of this is reported in section 4.8.

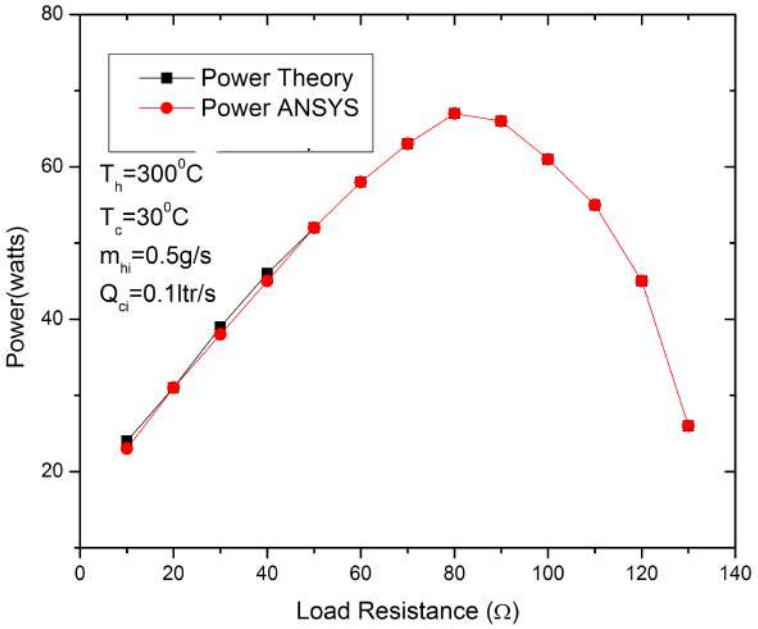

Figure 3.18: Power verses load resistance validation

3.5 Results

For analysis of 12P-N pair TEG. The hot side temperature is assumed as 427C and the cold side temperature is assumed as 27C. From figure 3.10 it is observed that. The peak power produced by 12pair TEG is 21 watts calculated by a mathematical model for 1.5mm leg length. For 1mm leg length TEG from fig. 3.11 the peak power produced from the mathematical model is 31 watts. Power versus load resistance for different leg lengths is shown in fig. 3.12. It is observed that as the length of the leg decreases power increases. A graph of power versus the length of the leg is shown in fig. 3.13. It is observed that as the length of the leg decreases power increases.

The performance investigation and validation of the Thermoelectric Generator (TEG) revealed promising results. The power generated by the TEG was analyzed in relation to load resistance, leg length, and temperature difference. Figure 3.15 displayed the power-load resistance relationship, indicating an initial increase in power until reaching a maximum at the peak power point. At this point, a power of 20 watts was achieved due to electrical resonance. Further increasing the load resistance resulted in a gradual decline in power. Additionally, it was observed from Figure 3.16 that reducing the leg length increased the power output of the TEG. Furthermore, Figure 3.17 illustrated the positive correlation between power production and temperature difference. As the temperature difference increased, the power generated by the TEG also increased.

Moving on to the Advanced Exhaust Thermoelectric Generator (AETEG), its performance was evaluated on a test bench with a hot air blower. Figure 3.18 showcased the power-load resistance relationship, highlighting a power output of 67 watts at a load resistance of 81 Ω. The AETEG operated with an average hot-side temperature of $300°C$ and an average cold-side temperature of $30°C$. The mass flow rate of hot gases was 0.5 g/s, while the cold-side mass flow rate was 0.1 ltr/s. Comparing theoretical and numerical simulation results, a strong resemblance was observed, validating the accuracy of the AETEG model.

Overall, the results obtained from both TEG and AETEG investigations demonstrate the potential and reliability of thermoelectric generators in converting temperature gradients into electrical power.

3.6 Conclusion

Theoretical and numerical modeling of TEG and AETEG can be used for performance investigation and validation of the TEG and AETEG revealed promising results. The power generated by the TEG was analyzed in relation to load resistance, leg length, and temperature difference. For a hot side temperature $T_h = 300^0C$ and cold side temperature $T_h = 30^0C$ the peak power produced is 20 watts. The results showed an initial increase in power until reaching a maximum at the peak power point, attributed to electrical resonance. Further increasing the load resistance resulted in a gradual decline in power. Reducing the leg length increased the power output of the TEG, while increasing the temperature difference also led to higher power generation.

The Automotive Exhaust Thermoelectric Generator (AETEG) was evaluated on a test bench with a hot air blower. The power-load resistance relationship demonstrated a theoretical and numerical power output of 67 watts at a load resistance of 81 Ω. The AETEG operated with an average hot-side temperature of $300°C$ and an average cold-side temperature of $30°C$. The comparison between theoretical and numerical simulation results showed close similarity, validating the accuracy of the AETEG model.

Chapter 4

Design Optimization and modeling of Thermoelectric Generator

4.1 Introduction

This chapter focuses on the characterization and performance analysis of Thermoelectric Generators (TEGs). TEGs are devices that convert heat energy into electrical energy using the Seebeck effect. The chapter begins with the characterization of TEGs, including the measurement of transport properties such as electrical conductivity, thermal conductivity, and Seebeck coefficient.

The section presents the experimental setup used to measure temperature-dependent transport properties. A thermoelectric module is sandwiched between two copper blocks, one heated and the other cooled using liquid nitrogen. The Seebeck coefficient is calculated from the open circuit voltage, and the electrical resistivity is determined from the voltage-current relationship. The thermal conductivity is evaluated by measuring heat transfer from the hot side to the cold side.

The subsequent section discusses the experimental analysis of commercially available TEG models, including Marlow, TEC12706, and TEC SP 27145. A detailed characterization is conducted using a well-designed experimental setup, which includes a heating element, PID controller, liquid nitrogen cooling, and instrumentation for electrical and temperature measurements. LabVIEW software is utilized for data acquisition and analysis.

The performance parameters of TEG modules are evaluated, including current, voltage, power, and efficiency. Experimental results are compared with analytical and sim-

ulation results, demonstrating the effectiveness of the characterization and performance analysis.

Furthermore, the chapter explores the experimental analysis of a single-leg TEG made of Indium-filled CoSb3. The preparation procedure for the thermoelectric material is described, followed by the testing setup and measurements of open circuit voltage. The limitations and challenges associated with measuring low voltage outputs are addressed.

Mathematical modeling and simulation techniques are employed to analyze the performance of multi-leg TEGs. The finite element method (FEM) is utilized to simulate the temperature profile and evaluate power output. The effects of leg geometry, cross-section area, and leg length on TEG performance are studied and compared through simulations.

Further the chapter investigates the performance evaluation and optimization of single P-N pair TEGs. The influence of various leg shapes, cross-section areas, and temperatures on power output and thermal stresses is analyzed using numerical simulations. The results provide insights into the design and optimization of TEGs for efficient energy conversion. The concept of segmented leg is studied to increase power output from a thermoelectric generator. Section 4.8 reports Thermoelectric Generator with a Heat exchanger mounted on a hot air blower. 24 TEGs are connected in series.

Overall, this chapter provides a comprehensive analysis of TEG characterization, performance evaluation, and optimization techniques, offering valuable insights for the development of efficient thermoelectric energy conversion systems.

4.2 Characterization of TEG

In this section, the characterization of a Thermoelectric Generator (TEG) is outlined, with a focus on assessing its transport properties, namely electrical conductivity, thermal conductivity, and Seebeck coefficient. To achieve this, a experimental technique is employed to calculate equivalent material properties and reported in section 4.2.1. Additionally, theoretical methods are utilized to determine the effective material properties reported in section 4.2.2.

4.2.1 Equivalent Material Properties

These are temperature-dependent transport properties. These include the effect of losses and contact resistance. These are calculated with experiments. The experimental setup for characterization is shown in fig. 4.1. The commercially available thermoelectric

module is sandwiched between two copper blocks; one side is heated with a heater, and another is cooled using liquid nitrogen. Using thermocouples, four temperatures are measured, two on the hot side and two on the cold side, as shown in Fig. 4.1.

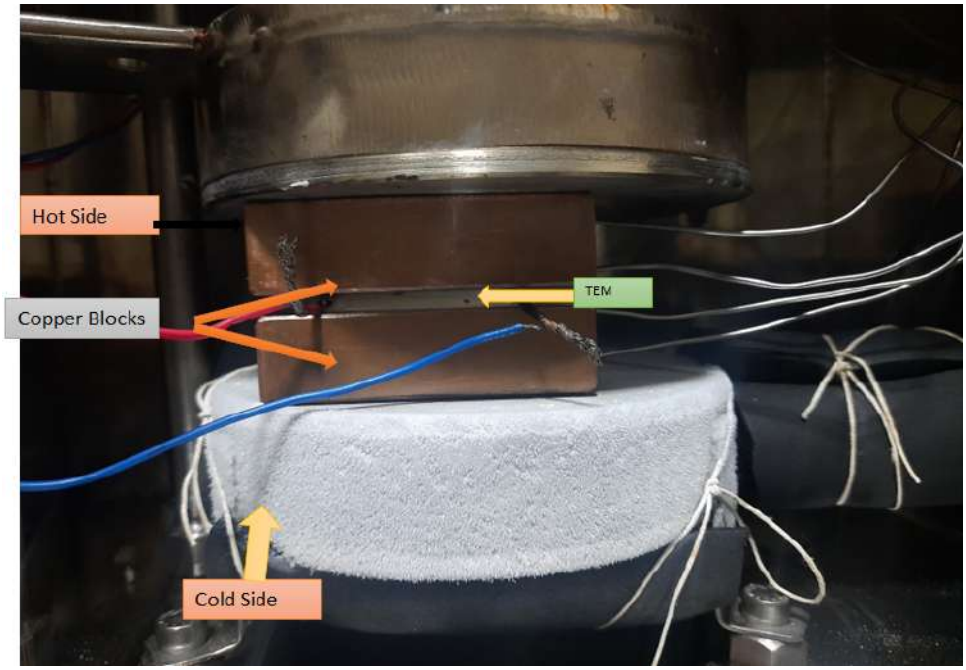

Figure 4.1: Equivalent material property set up (IISC Banglore)

Equivalent Seebeck coefficient

Seebeck coefficient is calculated from open circuit voltage. A plot of open circuit voltage versus hot and cold side temperature is shown in Fig.4.2. The formula to calculate the equivalent Seebeck coefficient is in Eqn. 4.1. This is taken for mean temperature $(T_h + T_c)/2$. Seebeck coefficient versus temperature is plotted as shown in Fig.4.3. For this material as temperature increases Seebeck coefficient increases.

$$S = \frac{V_{open}}{T_h - T_c} \tag{4.1}$$

Equivalent Electrical Resistivity

A graph of voltage versus current is plotted by measuring the closed circuit voltage. Electrical resistance is calculated by Eqn. 4.2. For the fixed temperature difference between the hot side and cold side temperature, a plot of current and voltage is plotted as shown in Fig. 4.4. The slope of the curve is internal resistance. Figure. 4.5 shows the equivalent electrical resistance for different temperatures. As temperature increases the electrical resistivity of the material increases.

$$\frac{1}{\sigma_p} + \frac{1}{\sigma_n} = \frac{R_{in} A_{leg}}{N h_{leg}} \tag{4.2}$$

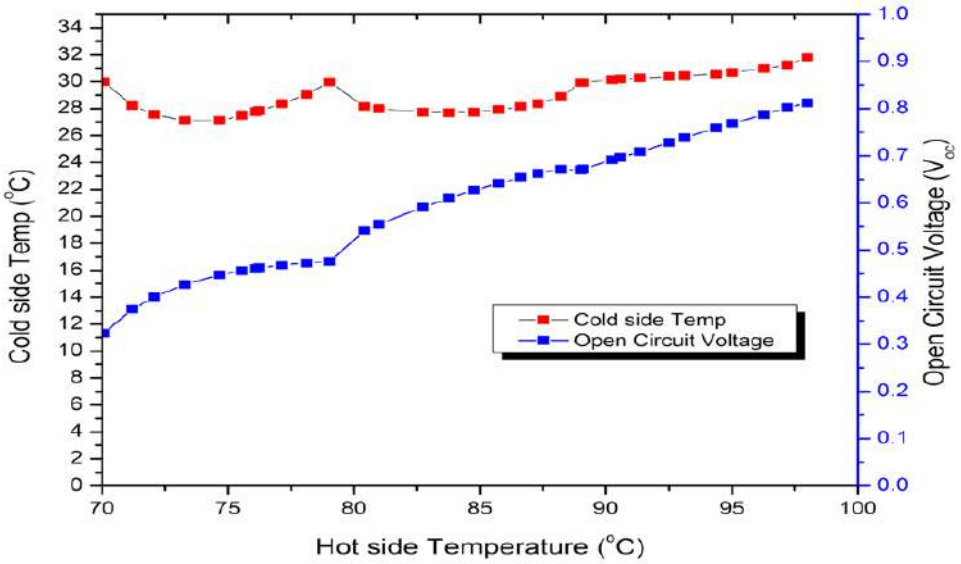

Figure 4.2: Open circuit voltage versus hot and cold side temperatures

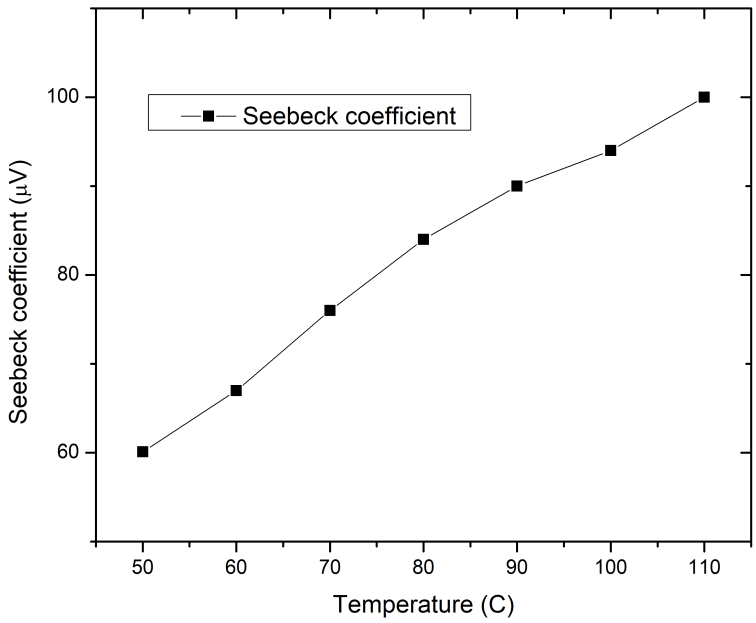

Figure 4.3: Seebeck coefficient for equivalent properties

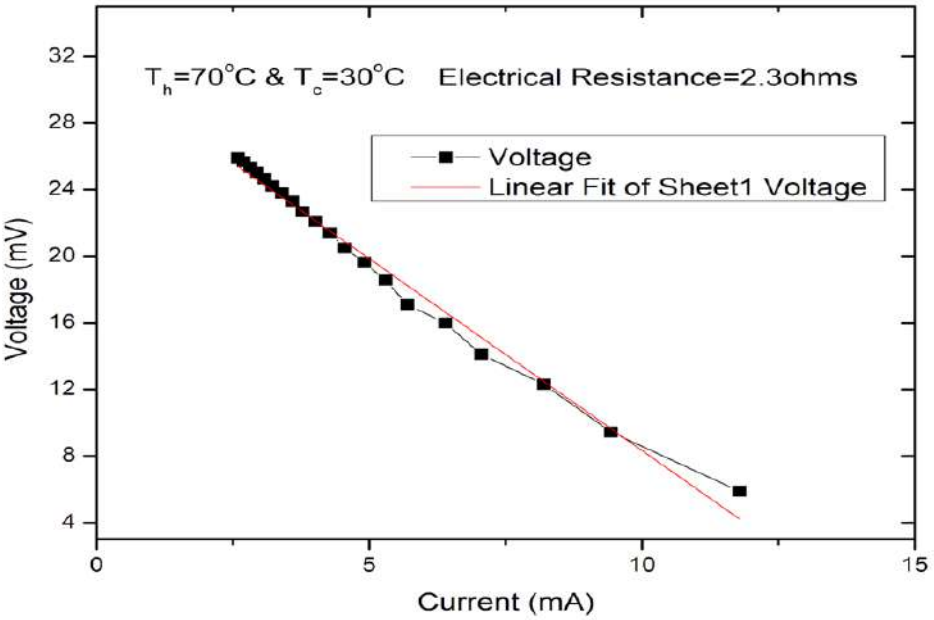

Figure 4.4: Internal Resistance

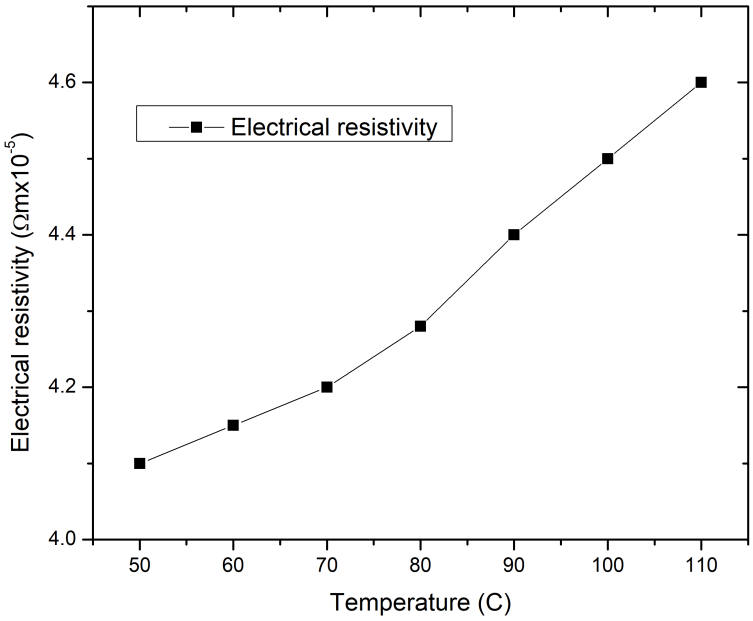

Figure 4.5: Electrical resistivity for equivalent properties

$$Q = \frac{\kappa_{cu} A(T_1 - T_2)}{L} \tag{4.3}$$

$$Heat\ Flux\ q = \frac{\kappa_{cu}(T_1 - T_2)}{L} = \frac{T_2 - T_3}{R_{in} + 2R_{alumina}} \tag{4.4}$$

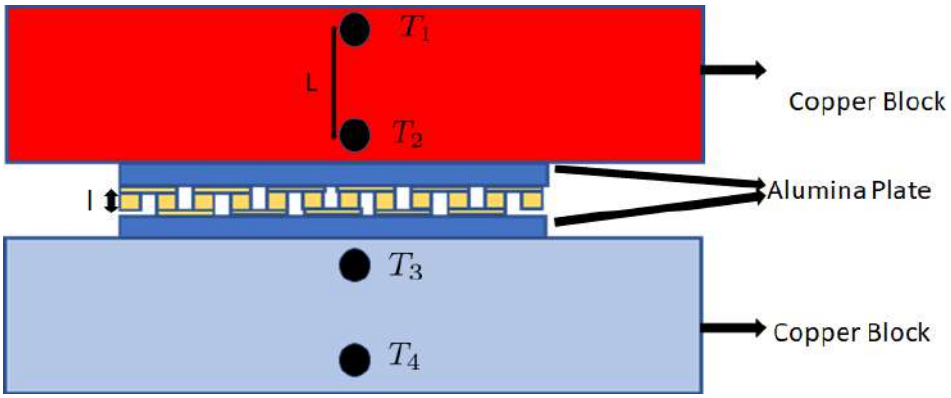

Figure 4.6: Equivalent thermal conductivity Evaluation setup

$$R_{in} = \frac{l}{\kappa_{in}} \tag{4.5}$$

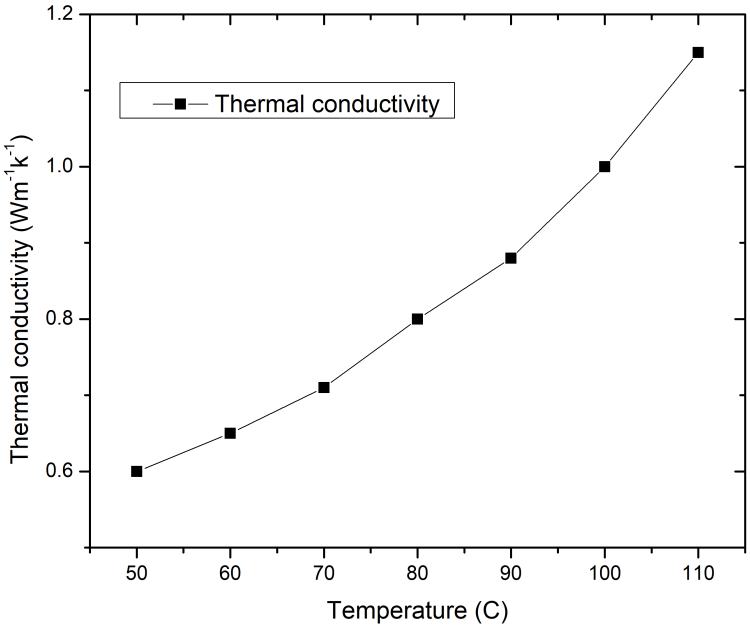

Figure 4.7: Equvilent thermal conductivity

Equivalent Thermal Conductivity Equivalent Thermal Conductivity of TEG is calculated by measuring heat flux across the TEG using equation 4.4. The setup for evaluation is shown in Fig. 4.6. From Fig 4.7 it is observed that as the temperature increases equivalent thermal conductivity increases.

4.2.2 Effective material properties

Effective matrial properties are temperature independent properties. The manufacturer of TEG doesn't not provide the properties of TEG materials. They provide a set of performance curve containing maximum parameters such as maximum current,voltage,power and efficiency as tabulated in tabel 4.1. Using these parameters effective material properties are calculated theologically. Lofee [18] was a pioneer in thermoelectrics. He proposed the constant material properties method. It used average properties of different temperatures. The following equations are used for analysis of effective material properties.

Table 4.1: Data of TEGs provided by munufacturer

Specification	TEC 12706	Marlow	TEC SP27145	Hi-Z 97
Hot Side Temp (^{o}C)	27 - 50	25 - 50	25 - 50	25 - 250
Q_{max} (Watts)	61.4 - 66.7	63 - 69	65.3 - 69.3	47 - 53
Delta Tmax (^{o}C)	70 - 79	60	60 - 65	200
I_{max} (Amps)	6.4	0.2	6.1	0.71 - 0.79
V_{max} (Volts)	14.4 - 16.4	7	13.8 - 14.2	5.7 - 6.3
Cross Section Area (mm^2)	1.25	1.5	1.25	1.25
Leg Length	1.25	1.25	1.25	1.75
Number of Thermocouples	127	241	127	97
Module Resistance (Ohms)	2 - 2.4	4.2 - 4.8	2.5 - 2.9	3.8 - 4.2

Current is calculated as

$$I = \alpha \frac{T_h - T_c}{R_L + R_i} \tag{4.6}$$

Where R_L is load resistance and R_i is internal resistance

Voltage is calculated as

$$V = n\alpha(\frac{R_L}{R_i})(\frac{T_h - T_c}{\frac{R_L}{R_i} + 1}) \tag{4.7}$$

Power can be calculated as

$$P = \frac{n\alpha^2(T_h - T_c)^2}{R_i} \frac{\frac{R_L}{R_i}}{(1 + \frac{R_L}{R_i})^2} \tag{4.8}$$

Efficiency can be calculated as

$$\eta_{th} = \frac{1 - (\frac{T_c}{T_h})\frac{R_l}{R_i}}{(1 - \frac{R_L}{R_i}) - \frac{1}{2}(1 - \frac{T_c}{T_h})\frac{(1+\frac{R_L}{R_i})^2 \frac{T_h}{T_c}}{ZT_c}} \tag{4.9}$$

ZT_c is called the dimensional figure of merit

The efficiency of the thermoelectric module is maximum for

$$\frac{R_L}{R_i} = \sqrt{1 + zT_m} \tag{4.10}$$

T_m is the mean temperature. Maximum power is produced when $R_L = R_i$. The maximum current is produced when loading resistance $R_L = 0$. Therefore

$$I_{max} = \frac{\alpha(T_h - T_c)}{R_i} \tag{4.11}$$

Maximum voltage can be obtained as.

$$V_{max} = n\alpha(T_h - T_c) \tag{4.12}$$

Maximum power can be obtained as

$$P_{max} = \frac{n\alpha^2(T_h - T_c)^2}{4R_i} \tag{4.13}$$

From maximum properties, effective material properties are calculated with the following equations. α^* is effective seebeck coefficient, ρ^* is effective electrical resistivity, k^* is effective thermal conductivity.

$$\alpha^* = \frac{2(Q_c)_{max}}{nI_max(T_h - \Delta T_max)} \tag{4.14}$$

$$\rho^* = \frac{\alpha^*(T_h - \Delta T_{max})\frac{A}{l}}{I_{max}} \tag{4.15}$$

$$Z^* = \frac{2\Delta T_{max}}{(T_h - \Delta T_{max})^2} \tag{4.16}$$

$$k^* = \frac{(\alpha^*)^2}{\rho^* Z^*} \tag{4.17}$$

Calculated Effective material properties calculated are tabulated in Table 4.2.

Table 4.2: Effective Properties TEG material

Material	Thermal conductivity (w/mk)	Seebeck Coefficient (mV/k)	Electrical Resistivity (Ohm.cm)	Youngs modulus (Gpa)	Poision Ratio	CTE (/K)	Specific heat (j/kgk)
Hz-2 TEG							
N-Type	1.62	-0.167	0.00153	45	0.22	$1.6* 10^{-}5$	154
P-Type	1.62	0.167	0.00153	0.22	$1.6 * 10^{-}5$	154	
Copper	385		$1.68 * 10^{-}8$	120			385
Resistor			Varies				
TEC12706							
N-Type	1.83	-0.120	0.00130				
P-Type	1.83	0.120	0.00130				
TEC SP27145							
N-Type	2.1	-0.103	0.00121				
P-Type	2.1	0.103	0.00121				
Marlow							
N-Type	1.84	-0.213	0.00168				
P-Type	1.84	0.213	0.00168				

4.2.3 Results

Effective material properties are calculated by theoretical calculations using the data provided by the manufacturer as discussed in section 4.2.2. As effective material properties are temperature independent and can hence it will be easy to do theoretical and

numerical modeling of TEG and it give similar results for performance evaluation compared to experimental results as reported in section 4.3. The maximum deviation of power for theoretical and numerical model compared to experimental value is 13% and 12% respectively as shown inthe Fig 4.11. Hence for present work theoretical and numerical modeling are done using effective material properties.

4.3 Experimental Analysis of Commercially available thermoelectric generator

The performance evaluation of different commercially available Thermoelectric Generators (TEG) models, specifically Marlow, TEC12706, and TEC SP 27145, involved conducting a detailed characterization using a well-designed experimental setup. The setup, as depicted in the schematic diagram shown in Figure 4.8, allowed for precise measurements and analysis of the TEG devices.

To initiate the experiments, a heating element with a power output of 500 watts was employed to heat one side of the TEG. This heating element provided the necessary thermal energy to generate a temperature gradient across the device. The temperature of the hot side was accurately regulated and controlled using a select 544 PID controller. The PID controller ensured that the desired temperature was maintained consistently throughout the experiments.

On the opposite side of the TEG, cooling was achieved by liquid nitrogen. Liquid nitrogen is a commonly used cryogenic cooling medium due to its low temperature and efficient heat transfer properties. By subjecting the cold side of the TEG to liquid nitrogen cooling, a substantial temperature difference was established across the device, contributing to the thermoelectric effect and the generation of electricity.

To measure the electrical parameters, such as voltage and current, a Keithley 3700A System Switch Multimeter is utilized. The Keithley 3706-S 32-Channel Switch Module is a modular switching unit designed to be used as part of the Keithley 3700A series mainframe system. The mainframe serves as the central control unit for the entire measurement system, and the 3706-S module is one of the many available plug-in modules that can be integrated into the mainframe. The measurement capacities are in table 4.3. Based on the requirements resolutions can be changed. It provided the necessary means to monitor the electrical behavior of the TEG devices under varying conditions.

Measurement	Range	Accuracy	Resolution
Voltage (DC)	100 nV to 300 V	±0.002% of reading ±2 counts	1 nV
Voltage (AC)	1 μV to 300 V	±0.02% of reading ±2 counts	1 μV
Current (DC)	1 nA to 3 A	±0.002% of reading ±2 counts	1 nA
Current (AC)	10 μA to 3 A	±0.02% of reading ±2 counts	10 μA
K-type temperature	-200°C to 1372°C	±0.5°C	0.1°C

Table 4.3: Keithley 3700A System Switch Multimeter

The voltage measured ranged from 0.001volts to 2 volts. Uncertainty is measured with this formula :

Relative uncertainty

To calculate the uncertainty for a DC voltage measurement of 2 volts, we use the accuracy and resolution specifications provided in the table4.3:

Using the formula for relative uncertainty:

$$\text{Relative Uncertainty}(\%) = \left(\frac{\text{Absolute Error}}{\text{Measured Value}}\right) \times 100\%$$

we can proceed with the calculations:

1. Calculate the Absolute Error:

$$\text{Absolute Error} = \text{Accuracy} \times \text{Measured Value} + \text{Resolution}$$

$$\text{Absolute Error} = \left(\frac{0.002}{100} \times 2\right) + 0.000001$$

$$\text{Absolute Error} = 0.00004 + 0.000001$$

$$\text{Absolute Error} = 0.000041 \text{ volts}$$

2. Calculate the Relative Uncertainty:

$$\text{Relative Uncertainty}(\%) = \left(\frac{0.000041 \text{ volts}}{2 \text{ volts}}\right) \times 100\%$$

$$\text{Relative Uncertainty}(\%) = 0.00205\%$$

Therefore, the uncertainty for a DC voltage measurement of 2 volts is approximately 0.00205%. Similarly, the relative uncertainty for a DC voltage measurement of 0.0001 volts is approximately 0.001002%.

The uncertainties are tabulate in table

Voltage	Relative uncertainty
0.0001 V	0.001002%
2V	0.00205%

Table 4.4: Uncertainty for DC Voltage Measurements

In addition to electrical measurements, K-type thermocouples were strategically placed

at various points within the setup to measure temperature differentials accurately. K-type thermocouples are specifically designed to measure temperature variations and provide reliable readings in a wide temperature range. These thermocouples ensured precise temperature measurements, allowing to evaluate the thermal performance of the TEG devices.

To facilitate data acquisition, analysis, and control of the experimental setup, LabVIEW software was employed. LabVIEW is a popular programming environment that enables efficient interfacing with instruments and sensors, providing a comprehensive platform for data collection, analysis, and visualization. It streamlined the experimental process and enabled to effectively manage and interpret the collected data.

Figure 4.9 provides a picture representation of the actual experimental setup used for the characterization of the TEG devices. The setup, incorporating the heating element, PID controller, liquid nitrogen cooling, Keithley multimeter, thermocouples, and LabVIEW software, offered a controlled and controlled environment for evaluating the performance of the different TEG models. It allowed for precise measurements of electrical and thermal properties, contributing to a comprehensive analysis of the TEG.

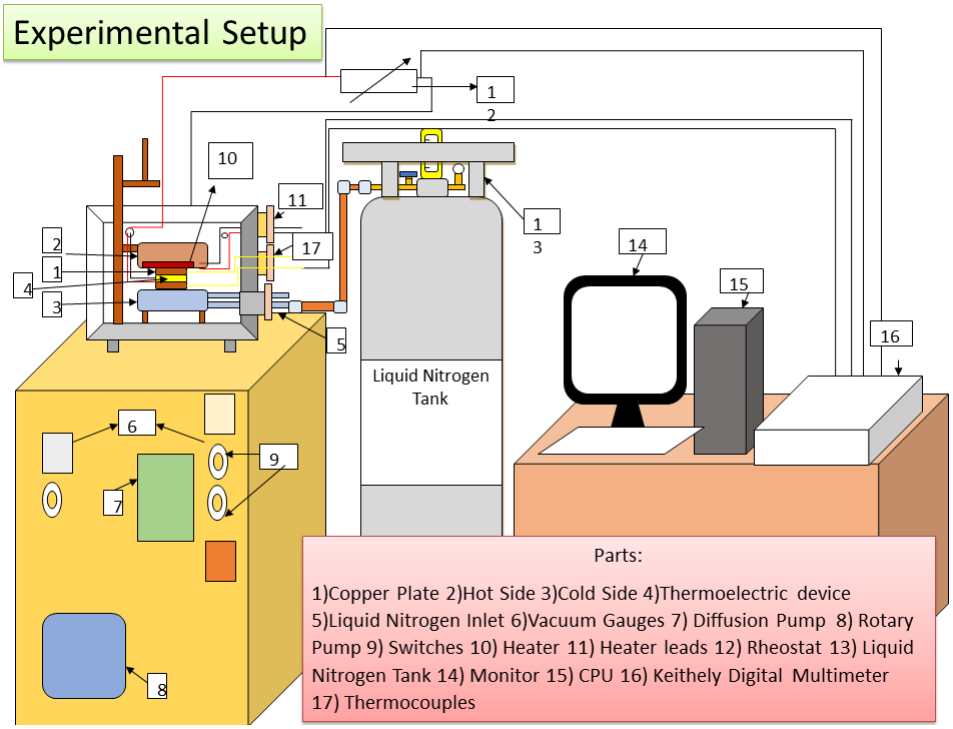

Figure 4.8: TEG Device testing setup(IISC Bangalore)

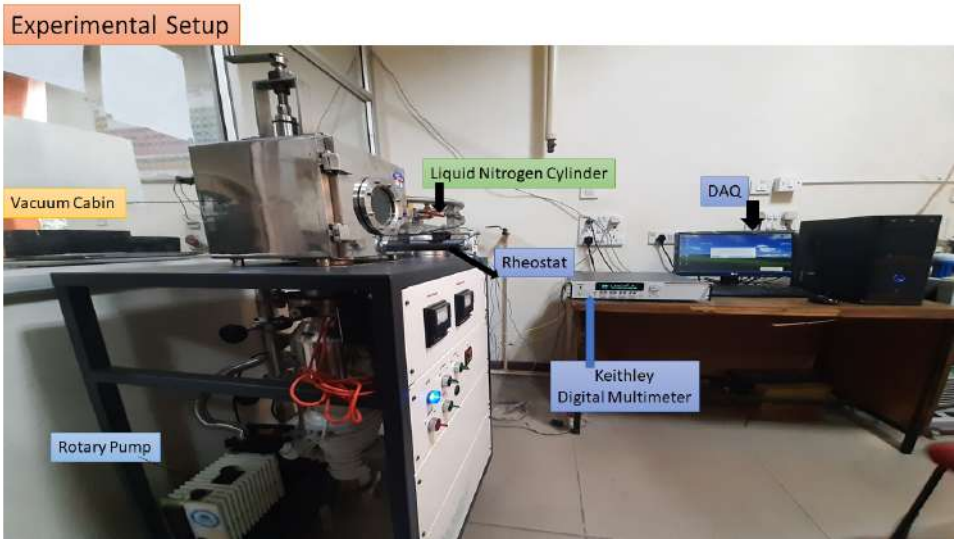

Figure 4.9: Picture of expt setup(IISC Bangalore)

4.3.1 Performance Parameters of TEG module

In this section the performance of three commercially available thermoelectric generators are calculated. The current is calculated as in equation 4.18. Voltage, Power & efficiency are calculated as in Eqn. 4.19,4.20, 4.21 respectively. ZTc is called the dimensional figure of merit.

$$I = \alpha \frac{T_h - T_c}{R_L + R_i} \tag{4.18}$$

$$V = n\alpha(\frac{R_L}{R_i})(\frac{T_h - T_c}{\frac{R_L}{R_i} + 1}) \tag{4.19}$$

$$P = \frac{n\alpha^2 (T_h - T_c)^2}{R_i} \frac{\frac{R_L}{R_i}}{(1 + \frac{R_L}{R_i})^2} \tag{4.20}$$

$$\eta_{th} = \frac{1 - \frac{(T_c)}{T_h})\frac{R_l}{R_i}}{(1 - \frac{R_L}{R_i}) - \frac{1}{2}(1 - \frac{T_c}{T_h})\frac{(1+\frac{R_L}{R_i})^2 \frac{T_h}{T_c}}{ZT_c}} \frac{R_L}{R_i} = \sqrt{1 + zT_m} \tag{4.21}$$

4.3.2 Repeatability Analysis

This section reports the repeatability of experiments conducted to measure the voltage across a circuit at different load resistances. The experimental setup is shown in the figure 4.8.

The table 4.5 has the data on voltage measurements in circuit load resistance experiments for three trails. The Repeatability Analysis involves utilizing the standard deviation method to assess the consistency and precision of the experimental results. The standard deviation method is a statistical tool used to quantify the dispersion or spread

of data points around the mean value, providing valuable insights into the repeatability of the measurements.

Table 4.5: Voltages for different trails

Load ResistanceΩ	Th	Tc	Voltage Trail 1	Voltage Trail 2	Voltage Trail 3
0.5	70	30	0.255273	0.260378	0.252951
1	70	30	0.365084	0.372768	0.356959
1.5	70	30	0.483124	0.491579	0.489856
2	70	30	0.561158	0.568904	0.573659
2.5	70	30	0.631187	0.620345	0.619212
3	70	30	0.669339	0.684314	0.657174
3.5	70	30	0.726160	0.738791	0.740272
4	70	30	0.784764	0.769341	0.763189
4.5	70	30	0.814389	0.792229	0.826693
5	70	30	0.841620	0.852879	0.856945
5.5	70	30	0.870583	0.850405	0.893635
6	70	30	0.899589	0.884704	0.881536
6.5	70	30	0.921505	0.908634	0.928467
7	70	30	0.934401	0.948037	0.943973
7.5	70	30	0.959812	0.967047	0.948588
8	70	30	0.965233	0.981682	0.974977

To perform the Repeatability Analysis using the standard deviation method, first the mean voltage and standard deviation are calculated for each load resistance, considering three voltage trials for each resistance. The formulas for calculating the mean and sample standard deviation are as follows:

1. Mean Voltage ($\bar{x}$) for a load resistance:

$$\bar{x} = \frac{\sum_{i=1}^{n} x_i}{n}$$

2. Sample Standard Deviation (s) for a load resistance:

$$s = \sqrt{\frac{\sum_{i=1}^{n}(x_i - \bar{x})^2}{n-1}}$$

Where: x_i represents each individual voltage trial value for a specific load resistance. $\bar{x}$ is the mean voltage for that load resistance.
n is the number of voltage trials (3 in this case).

Figure 4.6 shows mean voltage and standard deviation calculated for each load resistance. The standard deviation is low implying higher repeatability and precision in the experiment's results. Figure 4.10 represents the standard deviation, for different mean

voltages at different load resistance.

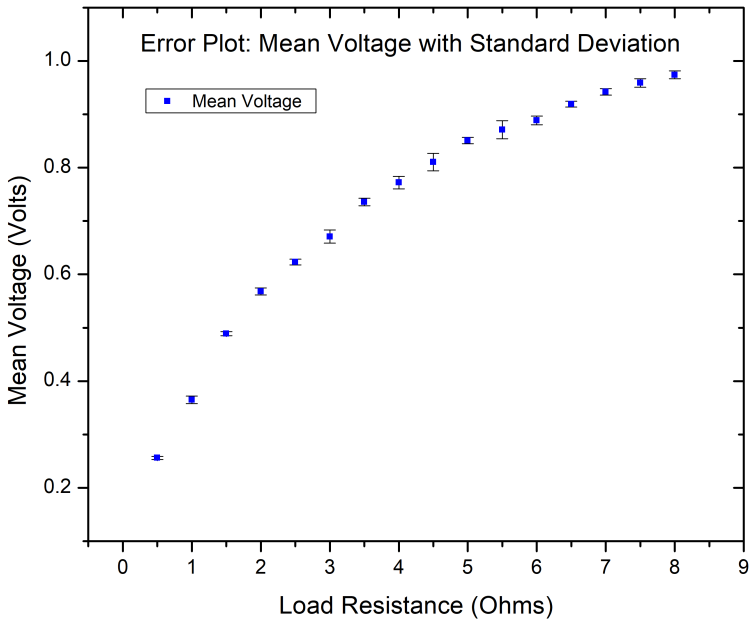

Figure 4.10: Error plot: Mean Voltage with Standar deviation

Table 4.6: Repeatability Analysis of Voltage Measurements

Load Resistance (Ohms)	Mean Voltage	Standard Deviation
0.5	0.256201	0.003015
1	0.364937	0.007059
1.5	0.488853	0.003879
2	0.567907	0.006547
2.5	0.623248	0.005457
3	0.670942	0.012062
3.5	0.735741	0.006922
4	0.772098	0.011873
4.5	0.810437	0.016434
5	0.850815	0.006181
5.5	0.871208	0.016915
6	0.888609	0.008174
6.5	0.919202	0.005378
7	0.942137	0.006136
7.5	0.958816	0.007875
8	0.973964	0.007591

4.3.3 Results

The hot side temperature is maintained at 70C, and the cold side temperature is maintained at 30C. Variation of power with load resistance for TEG 12706 is shown in Fig. 4.11. Experimental results shows the peak power produced is 168 milliwatts at a load resistance of 2.4Ω. Power increases as load resistance increases and reaches the maximum when the load resistance is equal to internal resistance. This is due to electrical impedance matching. Further power decreases. For the same boundary, condition simulation is done in ANSYS using effective material properties. Analytical simulation is also done and analytical and simulation results are compared with the experimental. The results are comparable. The maximum deviation of power for theoretical and numerical model compared to experimental value is 13% and 12% respectively as shown in the Fig 4.11. The deviation is due to the use of effective material properties at peak power, further deviation has decreased. Experimental performance analysis of commercially available Marlow 241-1.4-1.2 TEG is done. Figure 4.12 shows open circuit voltage versus hot side temperature for different cold side temperatures. It shows that open circuit voltage depends on the temperature difference between the hot and cold sides. Figure 4.13 shows Variation of voltage with current is linear, and power with current is parabolic. Figure 4.14 shows the power variation with the load resistance; the curve is parabolic. Figure 4.15 shows the variation of power with hot side temperature for two (SP27145 &

TEG12706) commercially available TEGs; it is observed that power output is directly proportional to hot side temperature. For constant cold side temperature.

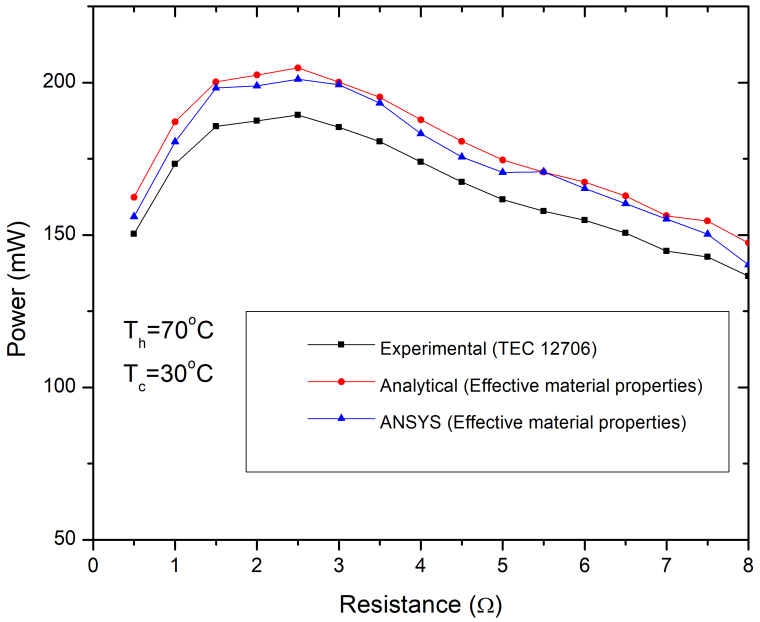

Figure 4.11: Results of 12706 experimental TEG

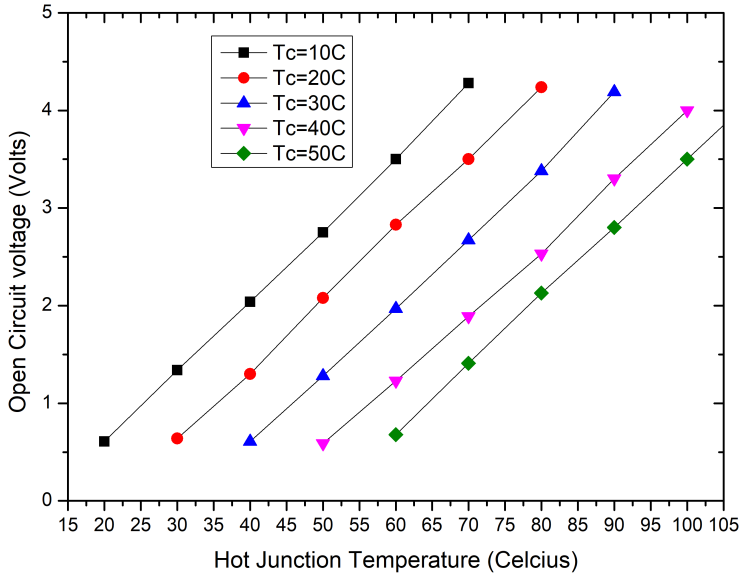

Figure 4.12: Open circuit voltage of marlow thermoelectric generator

From the table 4.7, we can observe a comparison of three different Thermoelectric Generators (TEGs) based on their performance characteristics.

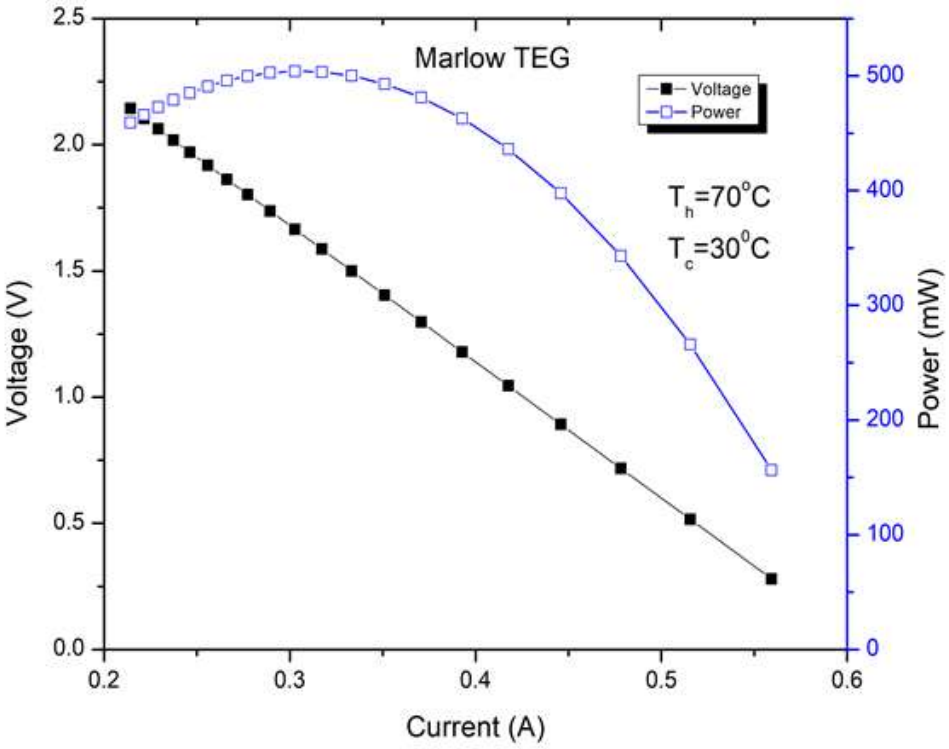

Figure 4.13: Morlow current verses voltage

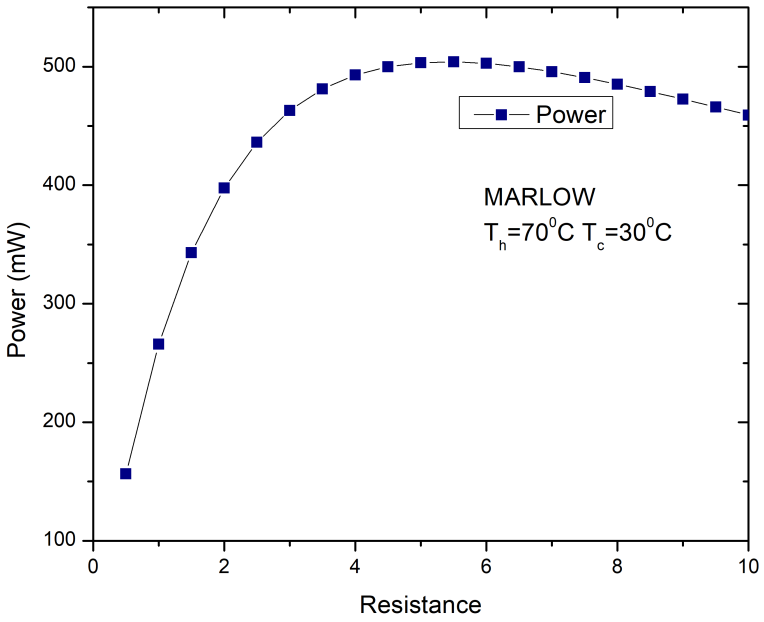

Figure 4.14: Marlow power verses load resistance

Table 4.7: Comparison of TEG Performance

Delta T	Power	Type of TEG	Hot Side	Cold Side
50	485mW	MARLOW	70	30
50	115mW	SP27145	70	30
50	168mW	TEG12706	70	30

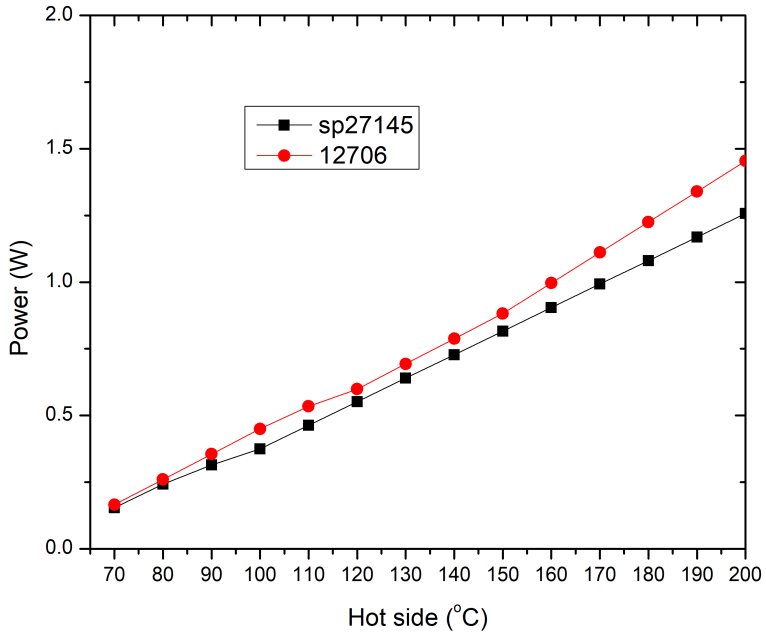

Figure 4.15: Power verses temperature for different TEG

1. Power Output: The TEG with the highest power output is the MARLOW TEG, generating 485mW of power. The other two TEGs, SP27145 and TEG12706, produce lower power outputs.

2. Type of TEG: The table lists three different types of TEGs - MARLOW, SP27145, and TEG12706. Each TEG has its own unique design and specifications.

3. Temperature Difference (Delta T): All three TEGs operate with the same temperature difference of 50 degrees Celsius between the Hot and Cold sides. This indicates that the comparison focuses on the TEGs' efficiency and performance rather than the temperature gradient.

In summary, the MARLOW TEG demonstrates the highest power output among the three TEGs, while the other two TEGs generate lower power outputs.

4.4 Experimental Analysis of Single Leg $CoSb_3$ Thermoelectric Generator

A single leg TEG made of $CoSb_3$ is tested. A single leg TEG made of In filled $CoSb_3$ is taken. The procedure for In filled $CoSb_3$ reported in Mallik et al. [152]. The flow diagram for the preparation of the thermoelectric material leg is shown in Fig. 4.16. A stoichiometric mixture of different elements is prepared. It is sealed in a quartz tube under vacuum pressure. Then the material is melted in an induction furnace. Heat treatment is carried out in the furnace. The ingot is taken and powdered in a ball mill machine with a vacuum hot press sintering technique. The powdered sample is converted into a circular pellet.

With low-speed diamond cutting, These pellets are cut to the required cross-section leg as shown in Fig.4.18a. A uni-couple TEG holder made of copper is fabricated as shown in the model Fig.4.17. A single leg made of $CoSb_3$ is placed inside the uni-couple holder and is insulated. Single-leg teg is tested with the heating on one side with a heater and cooling on another side with liquid nitrogen, as shown in fig. 4.18d. A low internal resistance wire is soldered to the uni-couple leg as shown in fig. 4.18c.

4.4.1 Results

Open circuit voltage is measured, and a plot of open circuit voltage versus hot side temperature is as shown in fig. 4.19. Open circuit voltage is very low, about 7 mv at a temperature difference of 50 C. Low voltage is due to electric contact resistance between leads to measure voltage and the TEG leg. There is a metal-semiconductor junction due to band bending there is low voltage output.

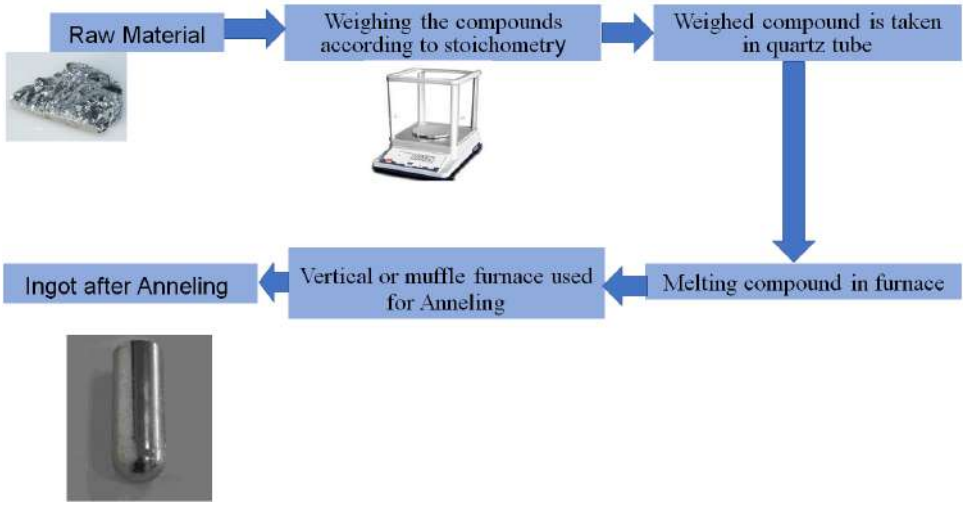

Figure 4.16: Procedure for sample preparation

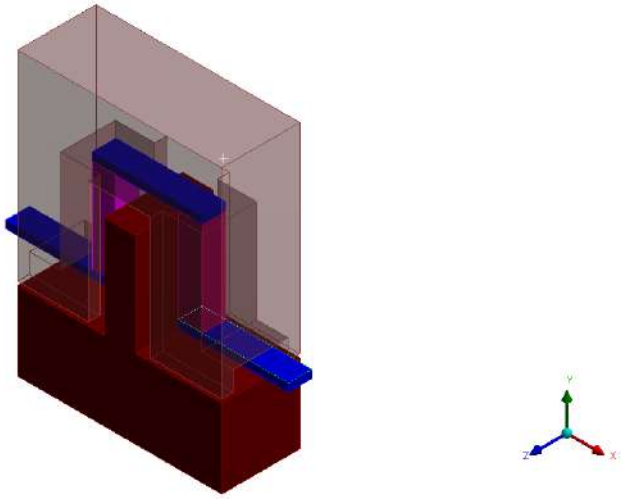

Figure 4.17: Uni couple TEG holder complete

(a) Cutting of single leg

(b) single leg

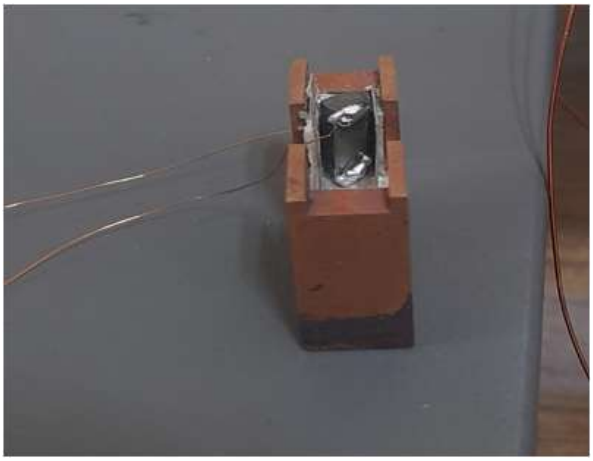

(c) Single Leg soldered in testing device

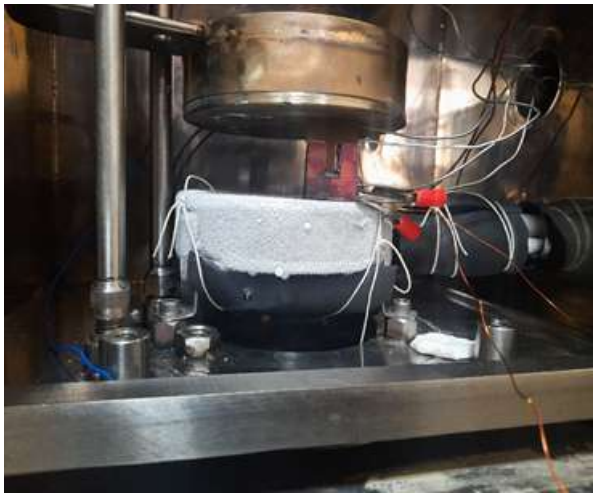

(d) Single leg testing setup

Figure 4.18: Single LEG TEG Characterization

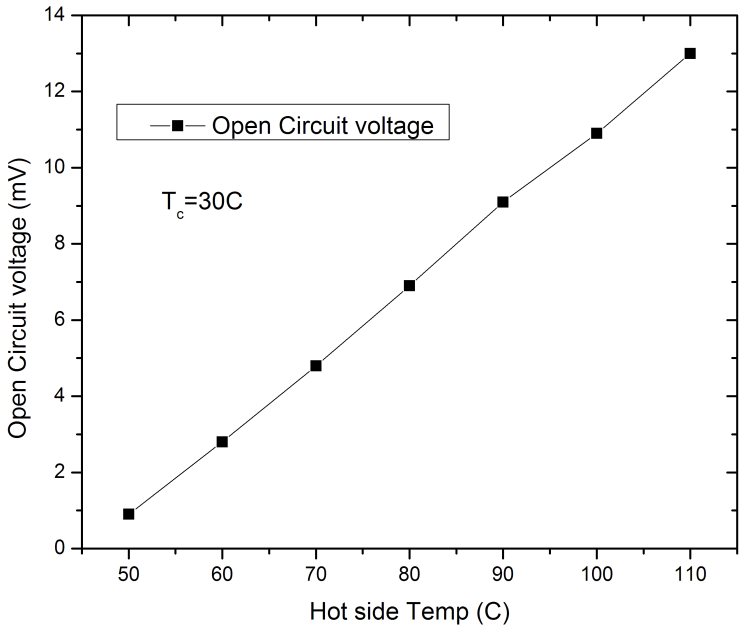

Figure 4.19: Open circuit voltage for Skutturides

4.5 Design Optimization of Thermoelectric Generator

4.5.1 Methodology

A Hi-Z thermoelectric generator consisting of 97 P-N pairs is simulated using the finite element method(FEM). Commercially available software ANSYS is used for simulation. Mathematical modeling is done using effective material properties as explained in section 4.2.2. Simulation of Hi-Z Thermoelectric generator is done for square and circular-shaped thermoelectric generators.

4.5.2 Simulation Modeling and performance evaluation of of Thermoelectric Generator for HiZ-2 TEG

A thermoelectric generator is simulated using commercial software ANSYS thermal electric. It uses the finite element method[FEM]. In 1943 [153] Courant was the first to propose the finite element method. In 1996 Lau et al. [154] were the first to use the finite element method in thermoelectrics. The finite element method is suitable for a wide range of solid mechanics problems. It is also used for fluid mechanics and heat transfer problems. The present work thermal-electric coupled analysis is done. Several commercial software such as ANSYS, and COMSOL can solve these equations effectively.

In the present work a commercial HiZ-2 Thermoelectric module is modeled in ANSYS design modeler as shown in Fig.4.20a it consists of 97 P-N pair semiconductors. To study the effect of shape. A similar cross-section area circular leg is also simulated as shown in Fig.4.20b. Meshing is done in ANSYS mesh with coarse meshing. For checking the performance of meshing a grid independence test is done and is reported in section 3.4.1.

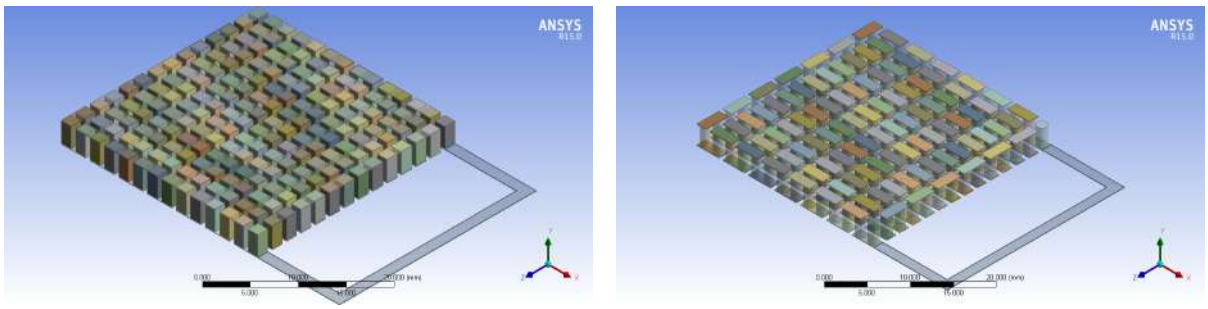

(a) Square leg TEG [155] (b) circular leg TEG

Figure 4.20: TEG of different leg shapes

4.5.3 Performance analysis of HiZ-2 TEG

A Hi-Z thermoelectric generator consists of 97- P-N pairs. This TEG is simulated in ANSYS with effective material properties. The temperature profile of square and circular TEG are shown in Fig. 4.21. The hot side boundary condition is 230^0 cold side 30^0C. Analytical results are obtained with equations as reported in section 3.2.1. The simulation results and analytical results are compared with experimental results from lee et al. [156] and the graph of hot junction temperature with power is shown in Fig. 4.22. It is observed that the results of the experimental, simulation, and analytical are well in agreement. Figure 4.23 shows the performance curves. The variation of power with current is shown in Fig.4.23a and it is parabolic. Figure 4.23b shows the linear variation of current with voltage.

To study the effect of the shape of the leg of the thermoelectric generator. The shape of the leg is varied from a standard square shape to a circular shape. For the same boundary condition of a hot side, the temperature is 250C and the cold side temperature is 50C. The simulation results experimental results and analytical results are compared and a graph of power with hot side temperature is shown in Fig. 4.24. The C/s area of the square leg is $2mm^2$ and the circular leg is $1.6mm^2$. The square leg has low internal resistance and is suitable for low load resistance. Circular has high internal resistance hence it is suitable for high load resistance.

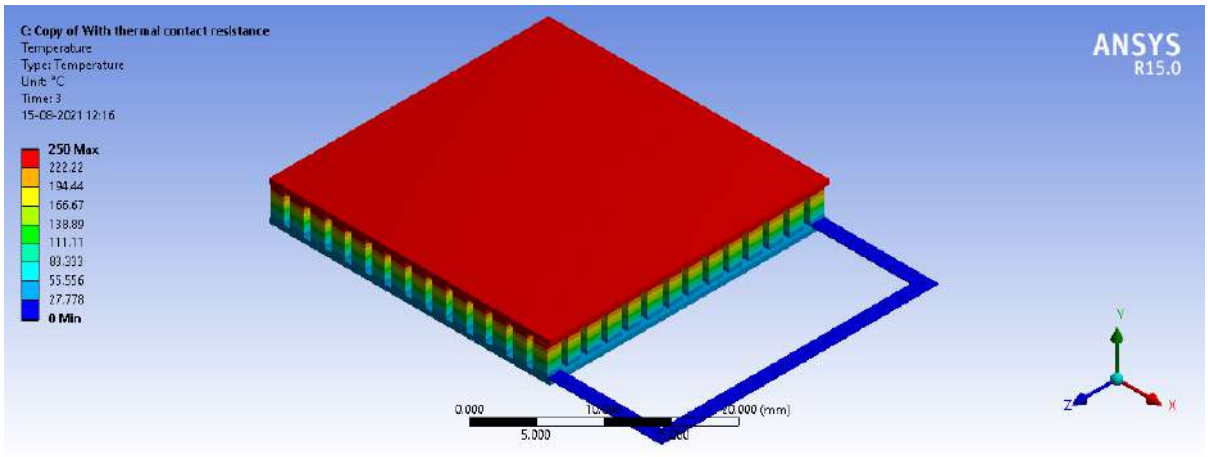

(a) Temperature distribution of HiZ-2

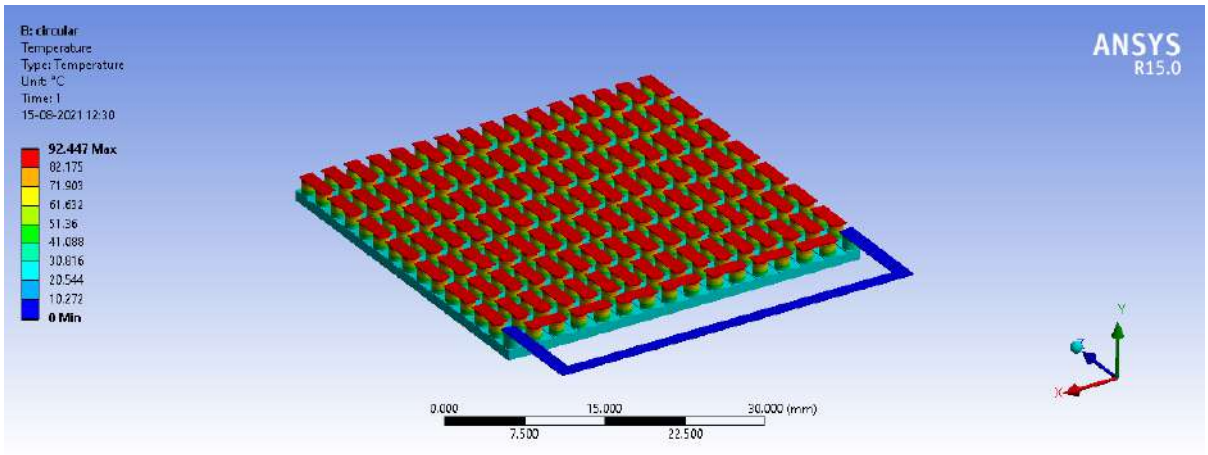

(b) circular leg TEG Temperature distribution

Figure 4.21: Temperature profile of square and circular TEG

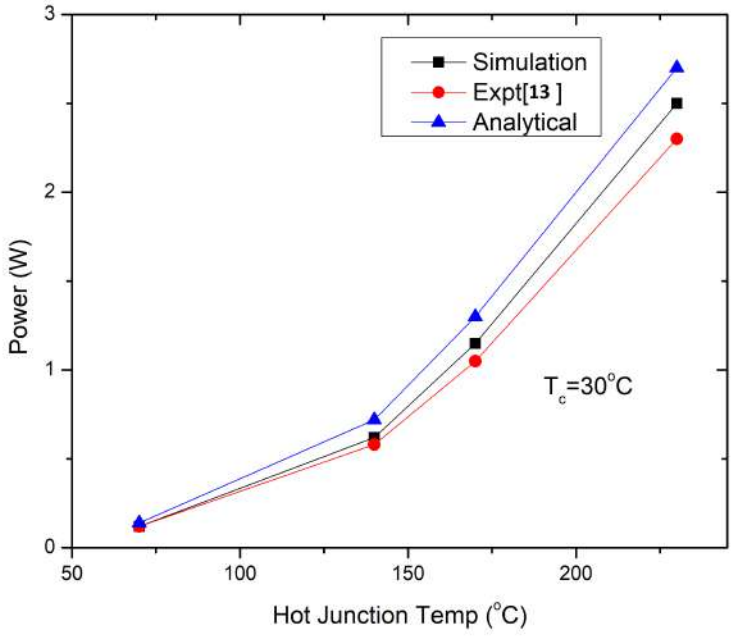

Figure 4.22: Power Verses Hot junction temperature

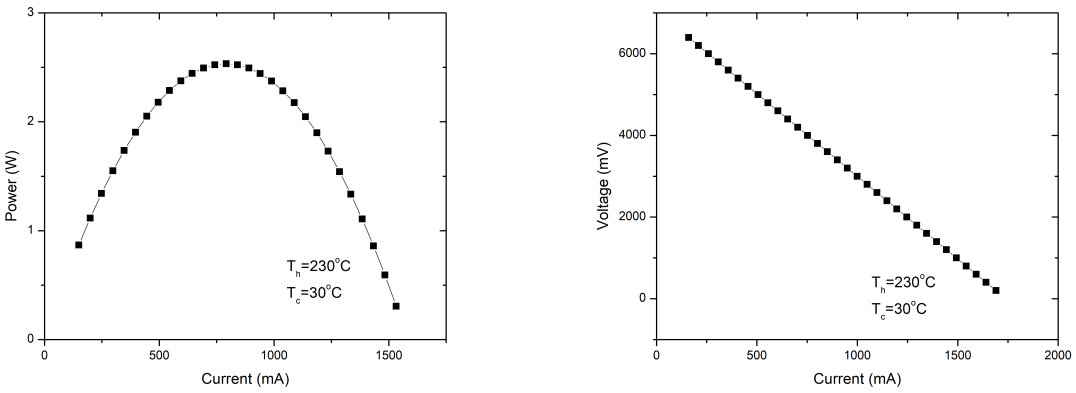

(a) variation of power with current (b) variation of voltage with current

Figure 4.23: Performance analysis of 97 P-N Pair TEG(HiZ-2)

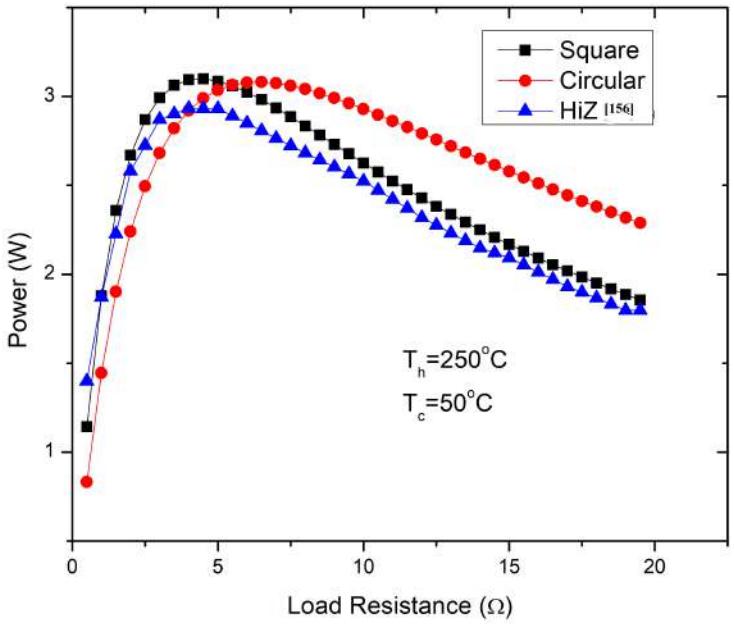

Figure 4.24: Effect of load resistance on power

4.6 Study of the effect of Geometry of Thermoelectric generator

Figure 4.25 shows different geometries of a thermoelectric generator. The hot junction temperature $T_h = 700^oC$ and The cold junction temperature $T_h = 30^oC$. square cross-section leg is converted to circular with the same cross-section area. From Fig Fig. 4.26 it is observed that there is no change in power output. Because thermoelectric transport properties don't depend on temperature. The cascaded thermoelectric generator has

produced low power but if different materials are used at different stages cascaded has good potential. The "Cone-up" TEG consistently demonstrates the highest power output compared to other shapes across different load resistances. It is a strong candidate for applications prioritizing maximum power generation.

With the increase in cross-section area more heat enters into the element but this will create difficulty in maintaining the temperature difference between the hot and cold sides. To reduce heat transfer a new design is proposed as shown in Fig. 4.25f. This produced more power than a cone and trapezoid-shaped TEG as shown in Fig. 4.26. A combination of square and trapezoid produces less power than square or circular TEG. P-type larger TEG produced the least power. Trapezoid-shaped TEG has higher efficiency compared to others as shown in Fig.4.27. But the power produced is not higher. This analysis provides valuable insights for designing and selecting TEG shapes tailored to different application needs.

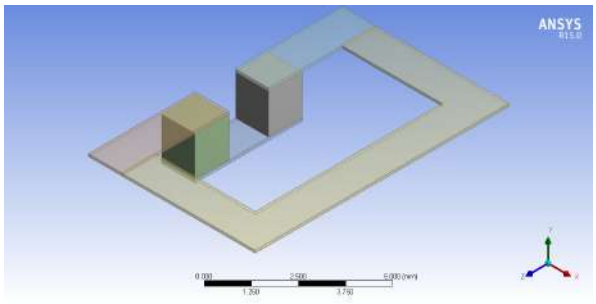

(a) Single PN junction Square leg

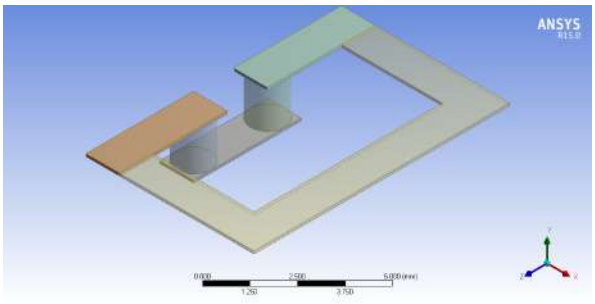

(b) Single PN junction circular leg

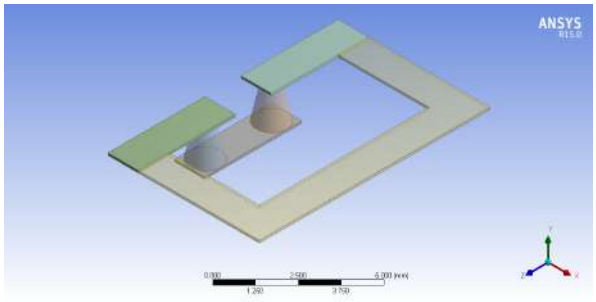

(c) Single PN junction cone up leg

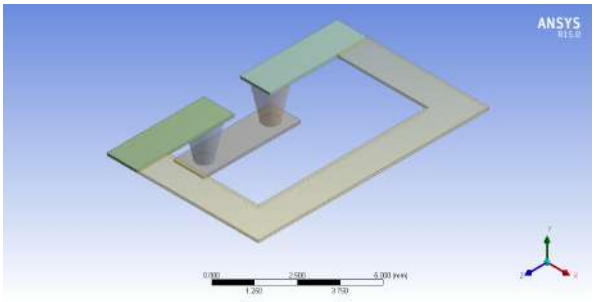

(d) Single PN junction cone down leg

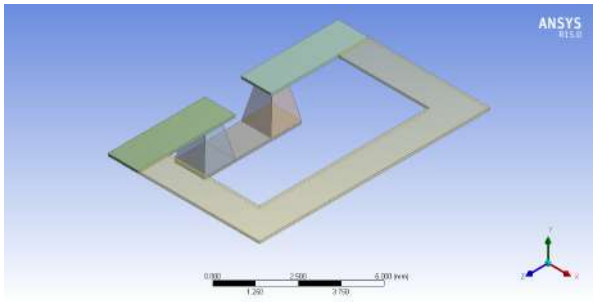

(e) Pyramid up(Trapezoid)

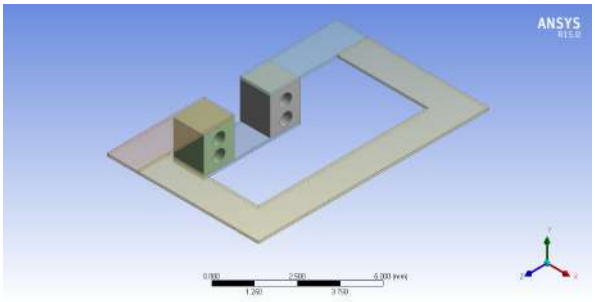

(f) New shape

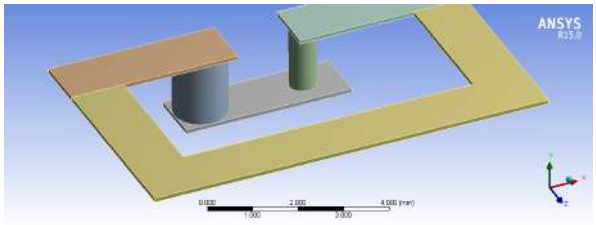

(g) P Larger

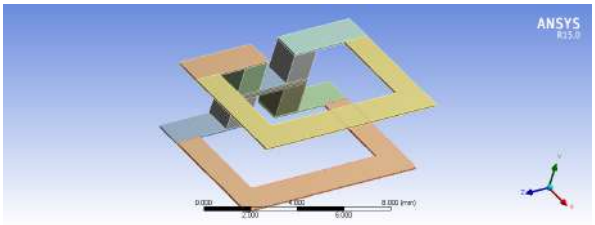

(h) Cascaded

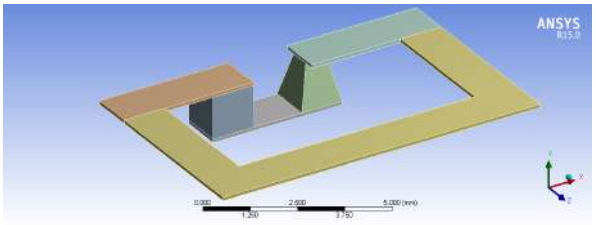

(i) Square trapezoid

Figure 4.25: Different shapes of uni-couple thermoelectric generator

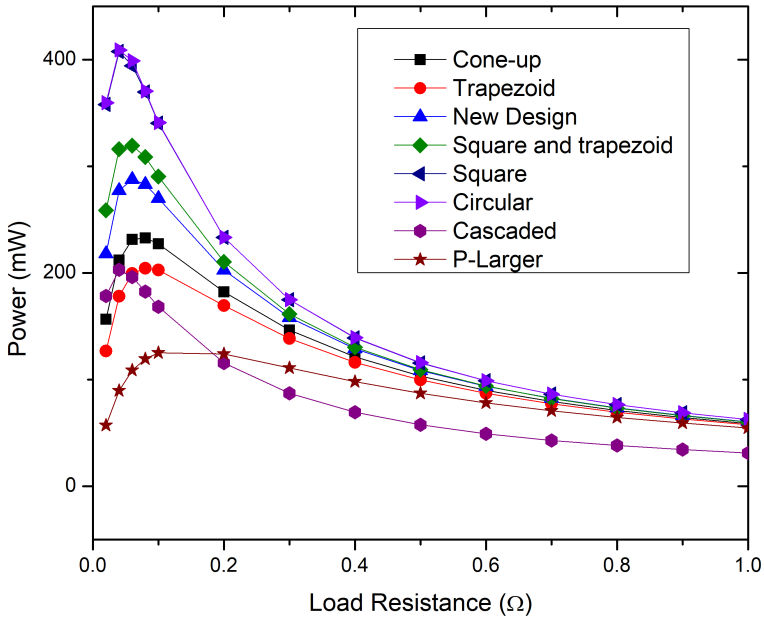

Figure 4.26: Effect of load resistance on power for uni-couple TEG

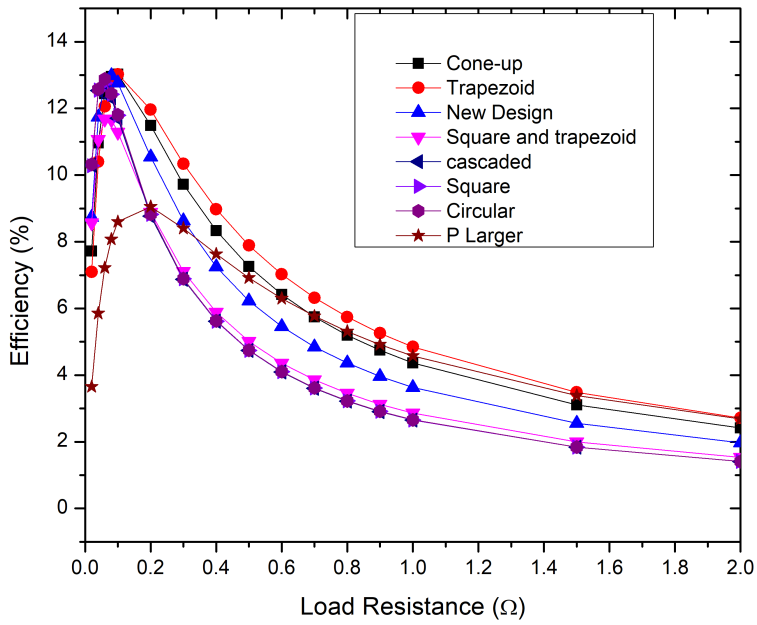

Figure 4.27: Variation of efficiency with load resistance for uni-couple TEG

Effect of C/S area of leg

A cone-shaped single P-N pair leg of cone up is simulated in ANSYS. Two top cone diameters one of 0.6mm diameter and another of 0.8mm diameter. It is observed from Fig. 4.28 as top cross-section area increases power output increases. Because more heat enters into the element as the cross-section area increases.

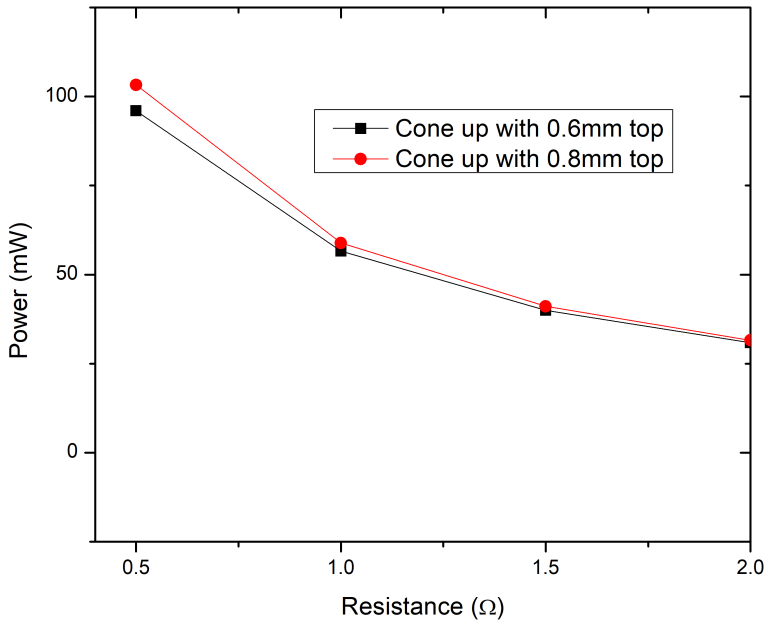

Figure 4.28: Effect of C/S area of leg

From Fig.4.29 it is observed that there is no change in power by changing the pyramid up to pyramid down and cone up to down.

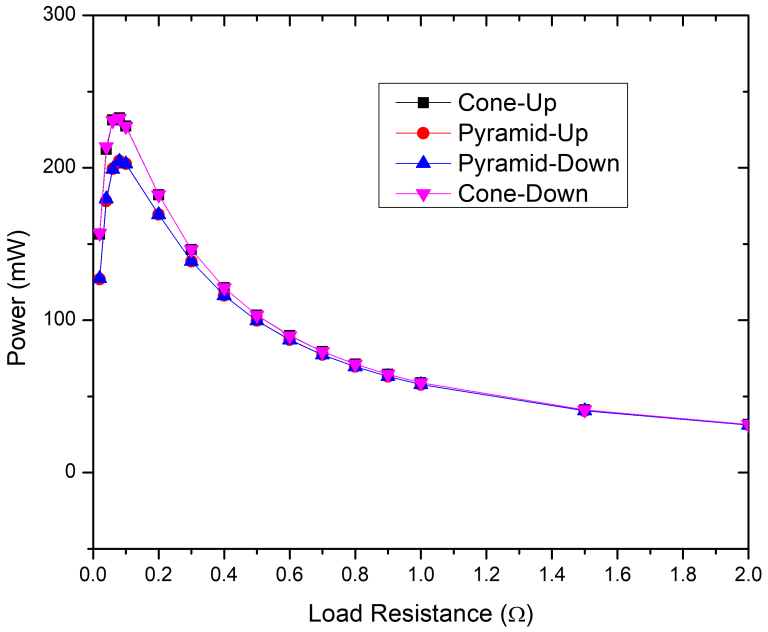

Figure 4.29: Performance analysis of Cone, pyramid Up & Down TEG

Thermal Stress Analysis on TEG leg

In a thermoelectric generator thermal stresses are developed due to the coefficient of linear expansion. Because of exposure to high temperatures, is an important parameter for the design of a thermoelectric generator. For the present study of thermal stresses hot side temperature is 500^0C and the cold side temperature is 30^0C. Figure 4.30a shows the effect of length on maximum von mises stress. It is observed that as the length of the leg decreases Von mises stress increases. From Fig. 4.30b It is observed that the pyramid shape has maximum von mises stress of 795 MPa, the square has 755Mpa and the circular has 710Mpa. Pyramid has the highest stress and circular has the least stress. From Fig. 4.30c it is observed that as hot side temperature increases von Mises stress increases. From Fig 4.30d it is observed that the circular cross-section has the least von mises stress.

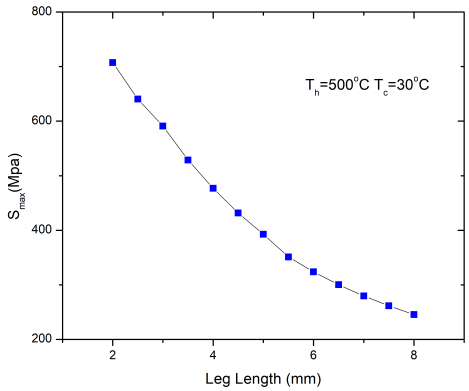

(a) Variation of max von Mises stress with the length of leg

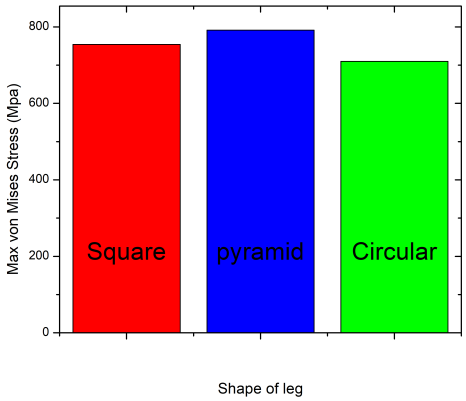

(b) Thermal stress for different shapes

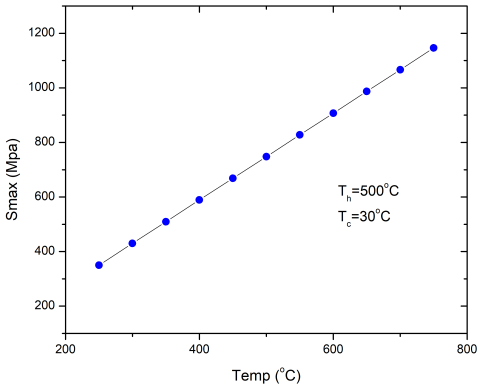

(c) Variation of Max von Mises stress with temperature

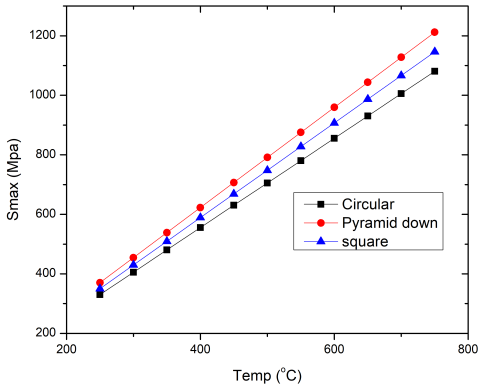

(d) Variation of Max von Mises stress with temperature for different shapes

Figure 4.30: Thermal Stress Analysis

Effect of Hot and Cold side Temperature

A single P-N pair TEG is simulated with a constant temperature difference of 630C as shown in Fig. 4.31. Cold side temperature is increased from 0C to 50C the variation in power is 0.75mw. With increasing the hot side temperature from 700C to 750C the variation in power is 0.58mw. The variation in cold side temperature has more effect on performance than the hot side.

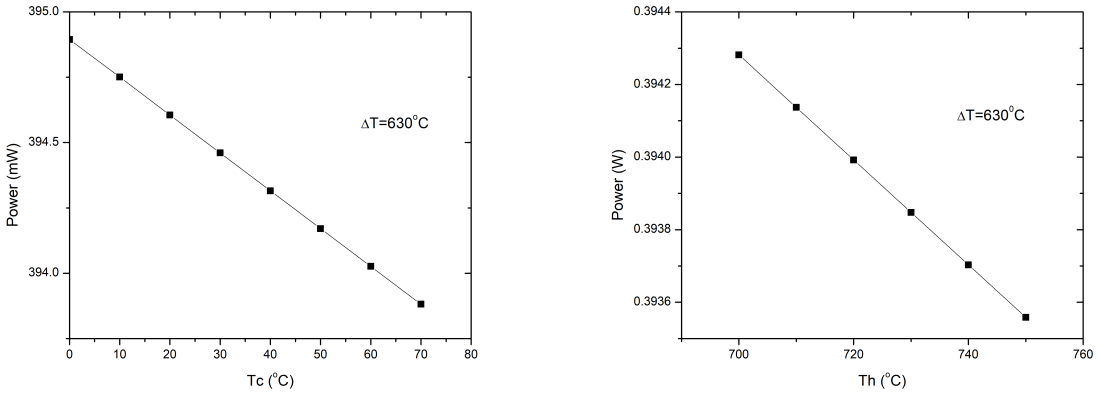

(a) Variation of power with cold junction temperature

(b) Variation of power with hot junction temperature

Figure 4.31: Effect of Hot and cold Junction Temperature

Effect of Leg Length

From Fig. 4.32 it is observed that as the length of the leg decreases power produced increases. But it will be difficult to maintain temperature difference for a small length.

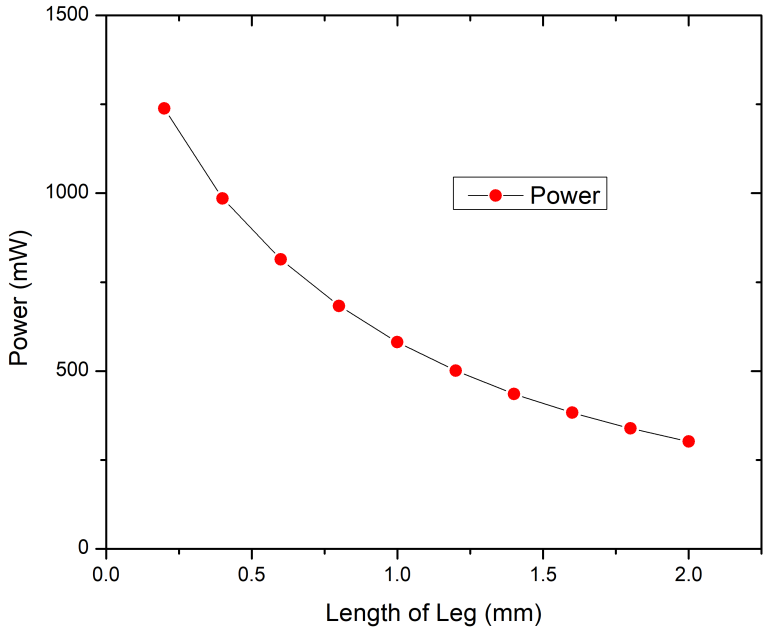

Figure 4.32: Effect of leg length on power

4.7 Segmented Leg

Thermoelectric material zt is high for a small temperature range. The temperature of the leg of the thermoelectric generator varies from 200^0C to 600^0C. Based on the temperature of the leg, different materials are used for different lengths, called a segmented leg. While doing a segmented leg, a term compatibility factor is considered. The compatibility factor is calculated by Eqn.4.22. Materials with compatibility factor differences of more than two cannot be combined to form segmented legs to get high efficiency. The compatibility factor for different materials is plotted in Fig.4.34

$$s = \frac{\sqrt{1+zt}-1}{\alpha T} \tag{4.22}$$

Two P-Type materials, one reported by [157] is skutterudites based with zt>1.3; it is a high-temperature TE material. The second, reported by [158] is nanostructured bismuth telluride-based TE material; its zt is high at low temperatures. Two N-Type materials, one reported by [159] is high-temperature SiGe-based TE material. Another reported by [160] is Bismuth-thulium co-doped chalcogenide is low-temperature TE material. With these materials, segmented legs are simulated. Uni-couple TEG is analyzed considering

it is made entirely of Bi_2Te_3, $CoSb_3$ & segmented leg. Figure 4.33a shows the Uni-couple TEG of a single material. Figure 4.33b shows a segmented leg. Temperature-dependent transport properties are taken from respective literature for segmented leg for corresponding material [157] [158] [159] [160]. The hot side temperature is 900K cold side temperature is 400K.

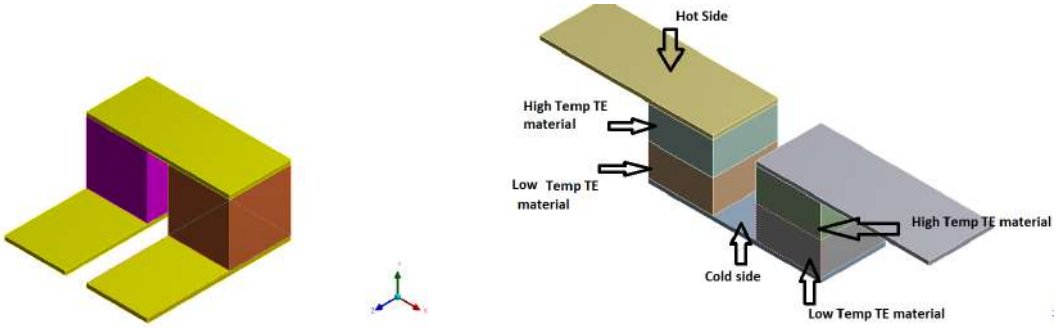

(a) Singleleg (b) Segmented TEG

Figure 4.33: Uni-couple TEG

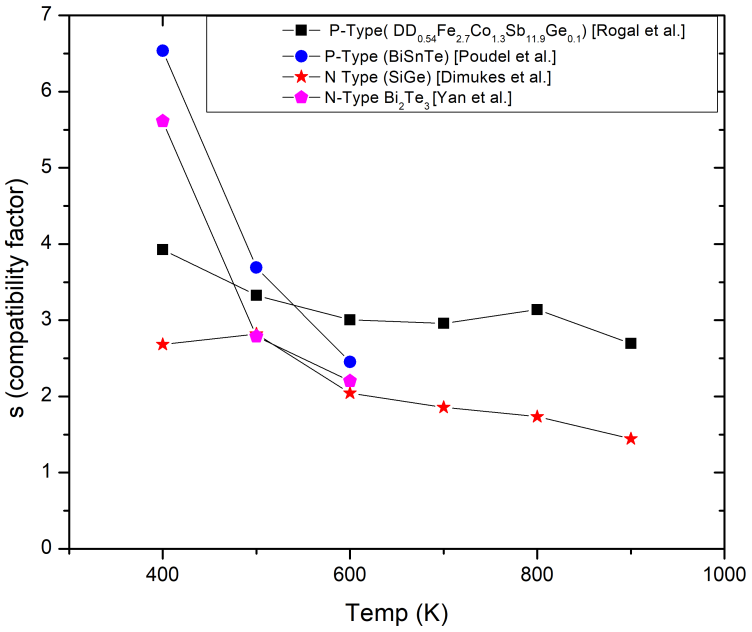

Figure 4.34: Compatibility factor

4.7.1 Results

Open circuit voltage is V_{open} is an indicator of the amount of power a TEG can produce. Figure 4.35shows the comparison of output voltage for uni-couple TEG. The results show that Bismuth Telluride (Bi_2Te3) produces the least voltage of 70mV, as

its zt is low at high temperatures. But the temperature of exhaust gases varies from 250^0C to 750^0C. Hence Bismuth Telluride (Bi_2Te3) is not suitable for direct AETEG application. The TEG made of Skutterudite $CoSb_3$ produces 170mV voltage as its zt is high at medium temperature. Skutterudite $CoSb_3$ zt is low at low temperatures. When these two materials are segmented & a leg is formed and analyzed. It shows an increase in power of 14.7% compared to the Skutterudite $CoSb_3$ leg. There is a 178% increase compared to the single Bi_2Te3 leg.

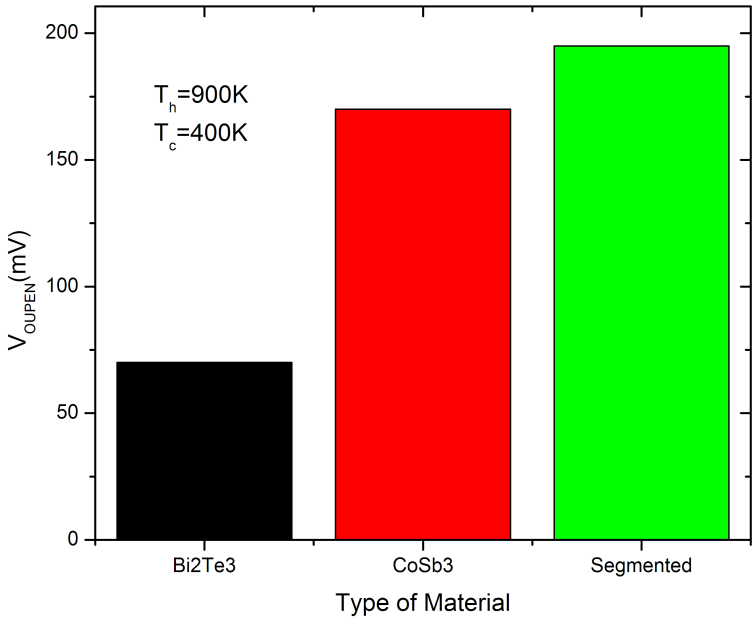

Figure 4.35: Segmented and single leg open circuit voltage

4.8 Analysis of Thermoelectric Generator with Heat exchanger mounted on hot air blower

4.8.1 Heat sink to cool the cold side of TEG

In this study we used aluminum alloy block measuring 40 x 200 x 12mm. It is available in market mostly used to cool CPU. It boasts a smooth, polished surface and incorporates an innovative M-shaped flow channel design. The pagoda nozzle, featuring a minimum outer diameter of 7mm, facilitates easy connection to water pipes with inner diameters ranging from 7mm to 8mm. The dimensions are shown in Fig.4.36. Flow pattern and nozzle parameters are shown in Fig.4.37.

Heat Transfer The heat transfer rate from the hot component to the coolant is given by:

$$Q_{\text{heat}} = \dot{m} \cdot C \cdot \Delta T \tag{4.23}$$

Where:

- Q_{heat}: Heat transfer rate (in watts, W)
- $\dot{m}$: Mass flow rate of the coolant (in kilograms per second, kg/s)
- C: Specific heat capacity of the coolant (in joules per kilogram per degree Celsius, J/kg°C)
- ΔT: Temperature difference between the hot component and the coolant (in degrees Celsius, °C)

Flow Rate

The flow rate of the coolant through the heat sink is determined by the cross-sectional area of the flow channel and the velocity of the coolant. Formulas used are:

$$Q_{\text{flow}} = A_{\text{channel}} \cdot v \tag{4.24}$$

Where:

- Q_{flow}: Flow rate of coolant (in cubic meters per second, m^3/s)
- A_{channel}: Cross-sectional area of the flow channel (in square meters, m^2)
- v: Velocity of the coolant flow (in meters per second, m/s)

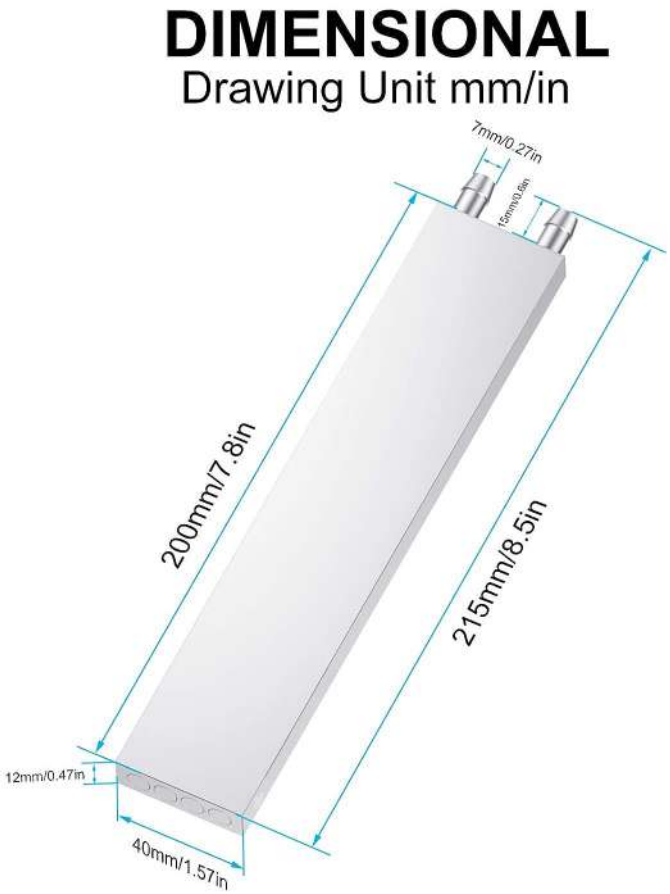

Figure 4.36: Heat sink[14]

Reynolds number

The Reynolds number (Re) is essential for determining the flow regime (laminar, transitional, or turbulent). It's calculated as:

$$\mathrm{Re} = \frac{\rho \cdot v \cdot D_h}{\mu} \tag{4.25}$$

Where:

- Re: Reynolds number (dimensionless)
- ρ: Density of the coolant (in kilograms per cubic meter, kg/m^3)
- v: Velocity of the coolant flow (in meters per second, m/s)
- D_h: Hydraulic diameter (in meters, m)
- μ: Dynamic viscosity of the coolant (in pascal-seconds, Pa·s)

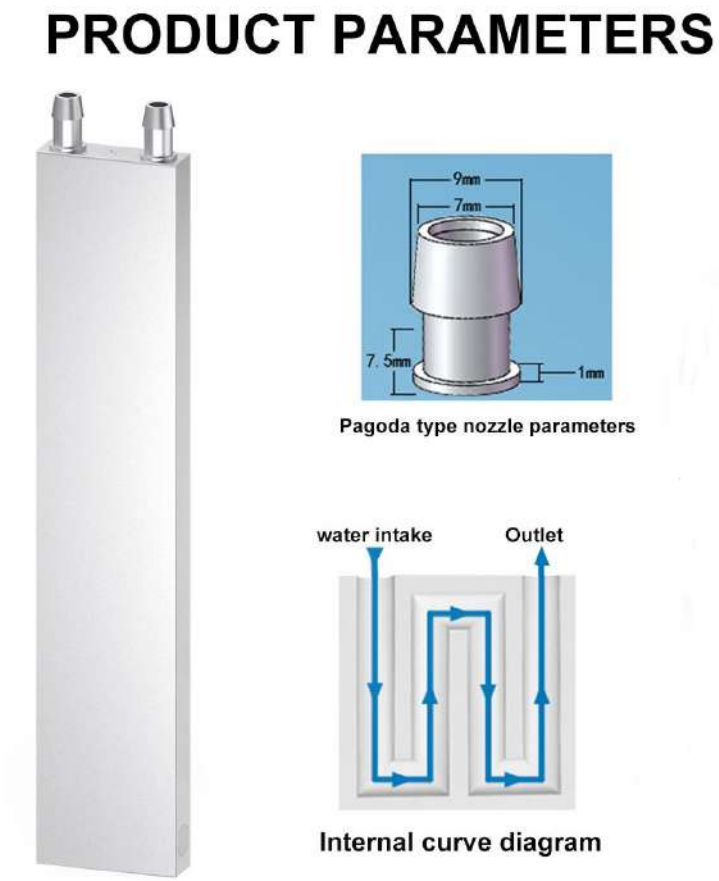

Figure 4.37: heatsink dimensions[14]

4.8.2 Methodology

In this study six heat sinks are used to cool the cold side of TEG and 24 Commercially available TEGs are fixed on a heat exchanger. A hot air blower with a controlled temperature and mass flow rate blows hot air on the hot side, and on the cold side, water is made to flow, as shown in fig. 4.38. Figure 4.39 shows an infrared thermal camera. An infrared thermal imager and infrared temperature indicator are used to measure the surface temperature of the heat exchanger, as shown in fig. 4.40 and Fig. 4.41. The thermal image of the hot side heat exchanger without TEGs captured by the IR thermal imager is shown in Fig. 4.43.

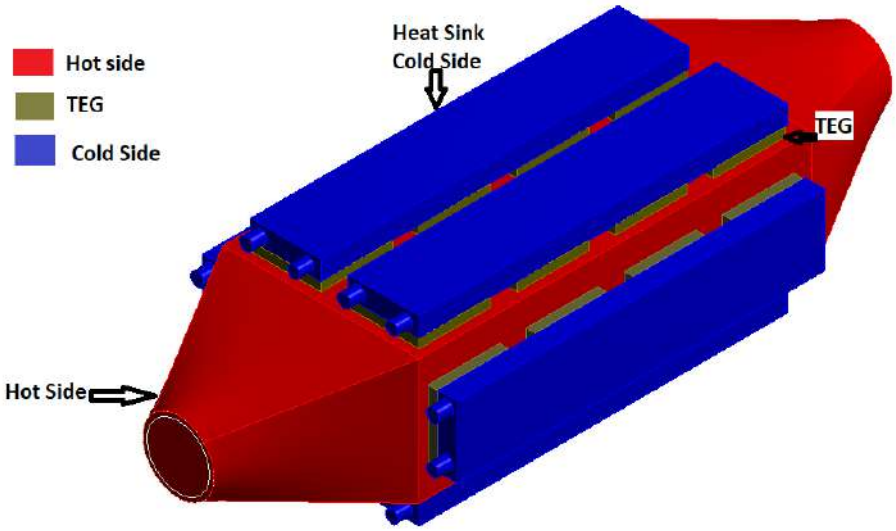

Figure 4.38: AETEG heat exchanger for hot air blower

Figure 4.39: Fluke infrared camera

24 TEGs are connected in series. The thermoelectric generators are sandwiched between hot and cold sides as shown in the Fig 4.42. The thermal image of heat exchanger

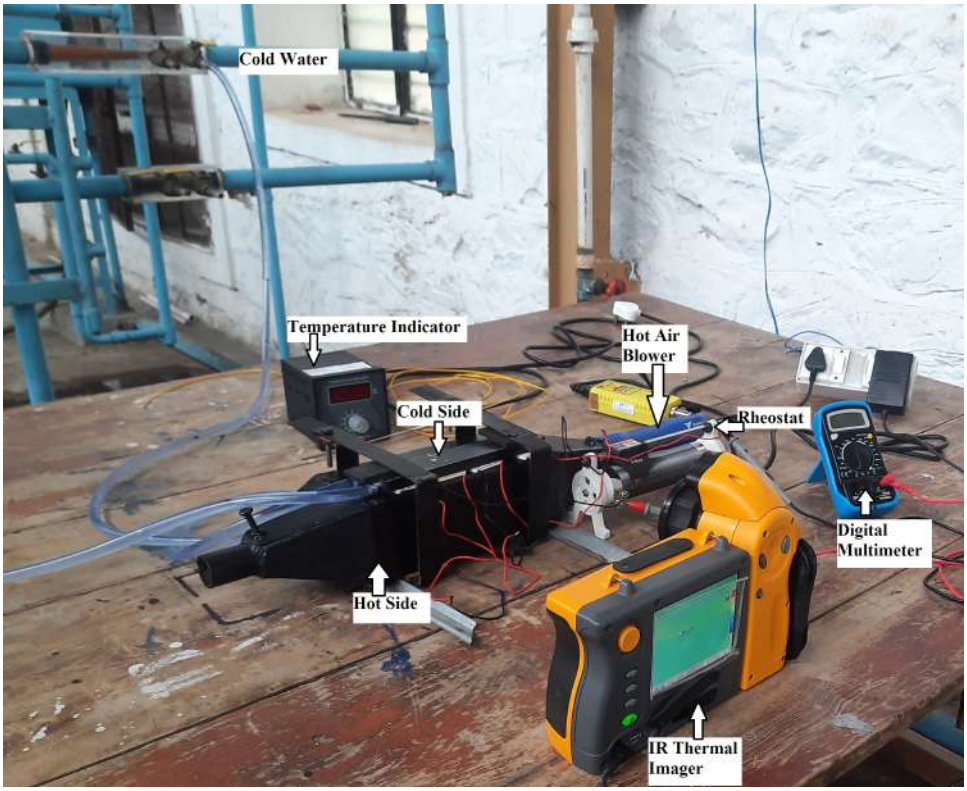

Figure 4.40: AETEG with hot air blower and IR camera

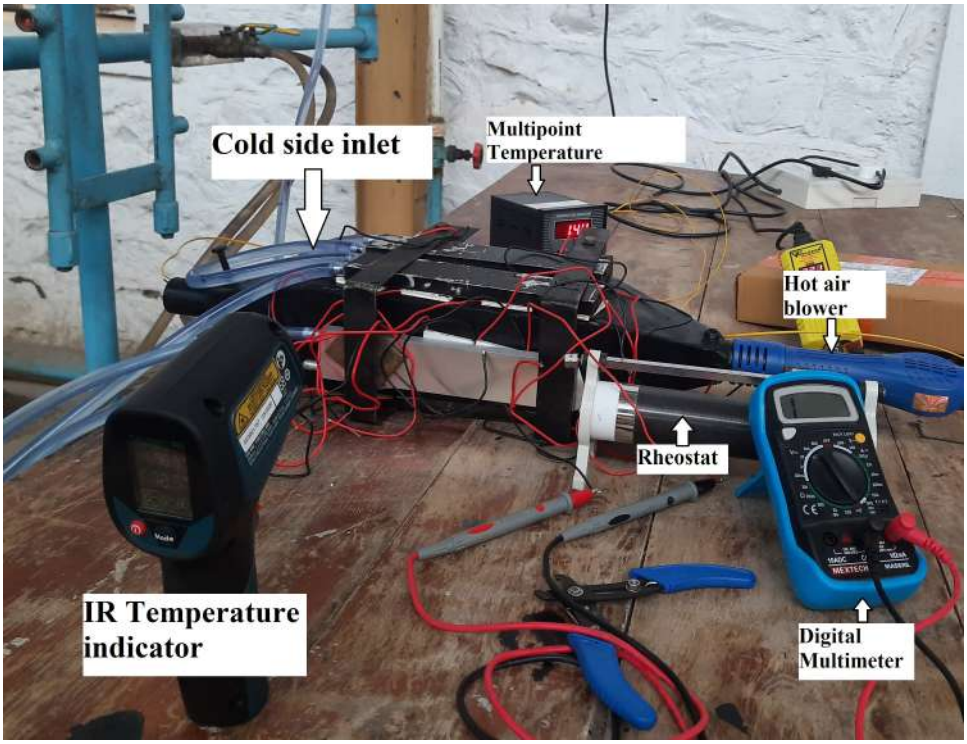

Figure 4.41: AETEG Expt setup with infrared temperature indicator gun

without TEG module is shown in Fig 4.43. For different load resistance, voltage is measured, and power is calculated. Parameters such as mass flow rate of hot fluid, cold fluid hot and cold side temperatures are measured. Numerical simulation of the heat exchangers is done using commercial software ANSYS. Theoretical analysis of TEG is done using effective material properties. The results are compared.

Figure 4.42: Heat Exchanger for hot air blower

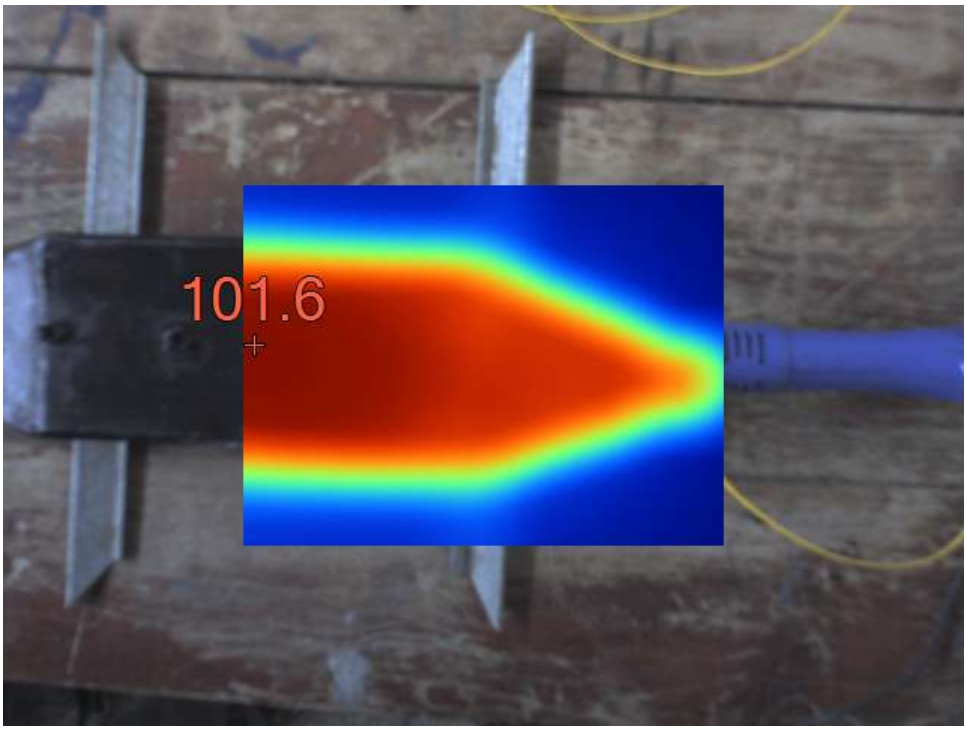

Figure 4.43: Thermal image of heat exchanger

4.8.3 Results and discussion

From the analysis of the thermoelectric generator on the test bench with hot air blower. It is observed from fig. 4.44 that at a load resistance of 81 Ω experimental power produced is 59 watts for hot side average temperature of 300^0C and cold side average temperature of 30^0C. The mass flow rate of hot gases is $m_{hi} = 0.5$g/s. The cold side mass flow rate is $Q_{0.1}$ltr/s. The theoretical and numerical simulation results are compared with experimental results. Theoretical and numerical results are almost similar with a deviation of 11.94%. There is a small deviation in experimental results due to heat losses and the assumption of equivalent material properties. Figure 4.45 shows that as the hot side temperature increases, the power produced by the thermoelectric generator increases. The simulation results are shown in Fig. 4.46. It shows for constant hot side temperature as cold side temperature decreases, power produced increases. Figure 4.47 shows the variation of power with the mass flow rate of cold fluid. Hot side cold side temperatures are constant. The mass flow rate of the hot side is also constant. As the mass flow rate of cold fluid increases, the power produced increases. Figure 4.48 shows the power versus the mass rate of hot fluid for the constant cold fluid flow rate of $Qci = 0.1$ltr/s. As the mass flow rate of hot fluid increases, the power produced increases.

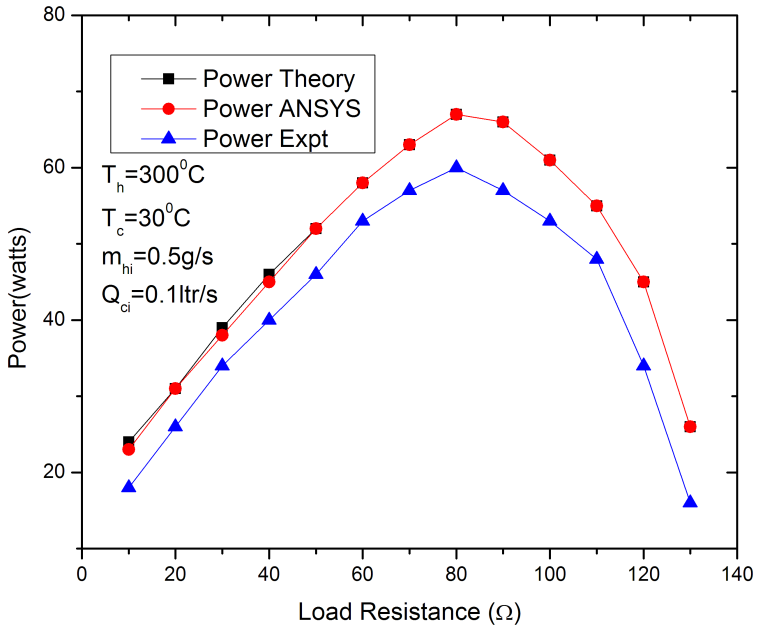

Figure 4.44: Power verses load resistance for AETEG with hot air blower

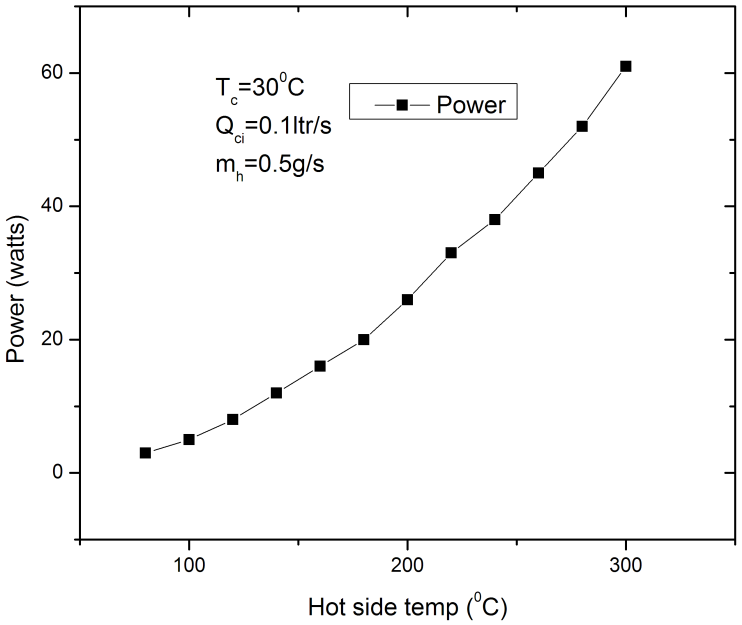

Figure 4.45: Power versus Hot side temperature

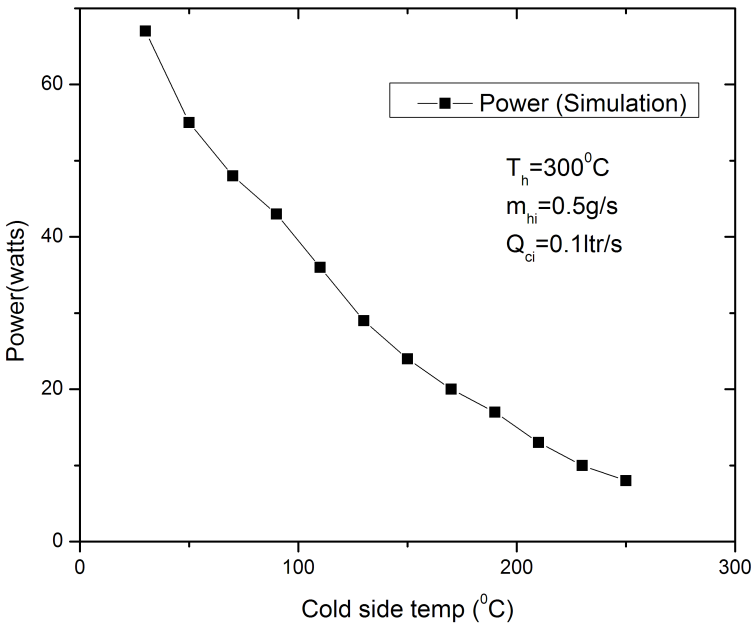

Figure 4.46: Power versus cold side temperature

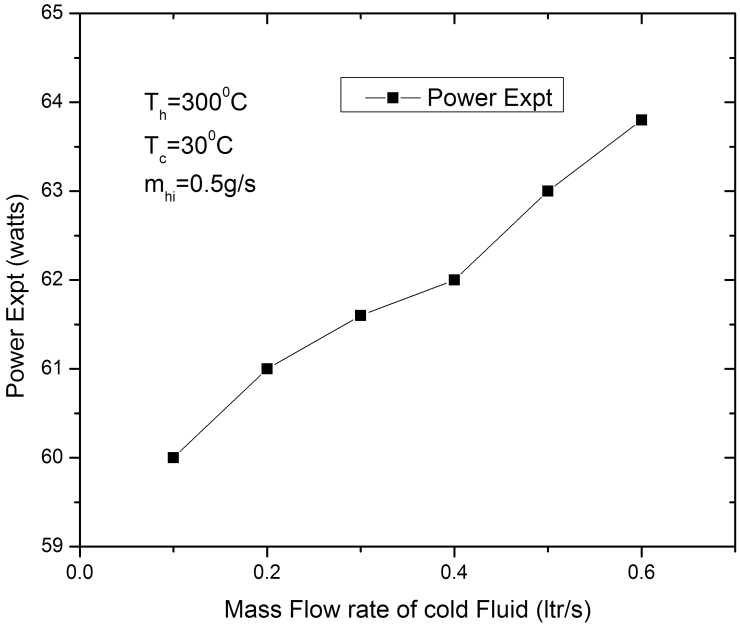

Figure 4.47: Power versus mass flow rate of cold fluid

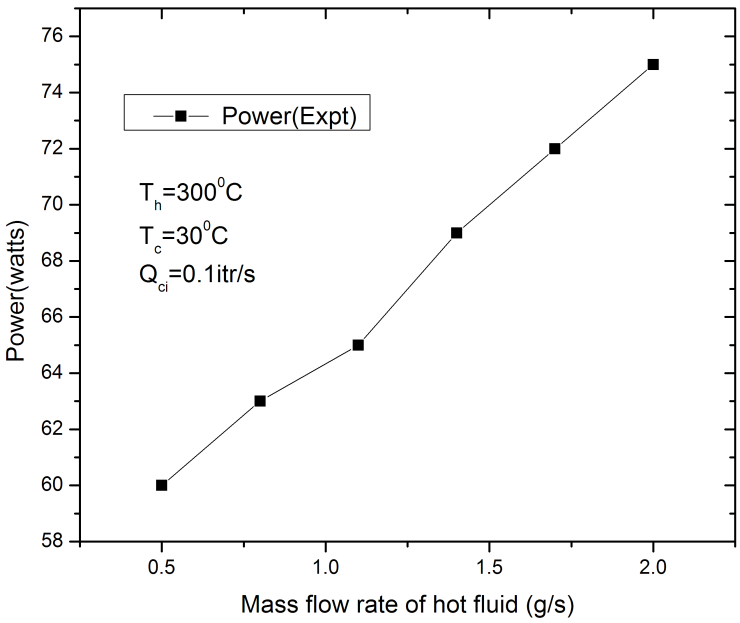

Figure 4.48: Power versus mass flow rate of hot fuid

4.9 Conclusions

This chapter presented a characterization of Thermoelectric Generators (TEGs). To achieve this, a experimental technique is employed to calculate equivalent material properties. Theoretical methods are utilized to determine the effective material properties. Performance evaluation of a commercially available TEG is done. The experimental analysis results, are compared with those obtained from of theoretical and numerical modeling using effective material properties, They are comparable with a maximum deviation of 13% and 12% respectively. As a result, the subsequent work adopts the use of effective material properties.

A single leg TEG made of $CoSb_3$ is tested. A single leg TEG made of In filled $CoSb_3$ is taken.Open circuit voltage is very low, about 7 mv at a temperature difference of 50 C. Low voltage is due to electric contact resistance between leads to measure voltage and the TEG leg.

The experimental analysis further extended to evaluate the performance of commercially available TEG models, namely Marlow, TEC12706, and TEC SP 27145. A detailed experimental setup was utilized to measure electrical and thermal parameters, such as voltage, current, and temperature differentials. The power output of these TEG models was assessed under specific operating conditions. For instance, the TEG 12706 exhibited a peak power output of 168 milliwatts at a load resistance of 2.4Ω. MARLOW TEG produced a power of 485mW under same boundary conditions.These experimental results were then compared to analytical simulations, showing a good agreement overall.

Additionally, the chapter explored the performance and optimization of Hi-Z TEGs and single P-N pair TEGs through mathematical modeling and finite element simulations. The simulations provided insights into the power generation capabilities of these TEG configurations under different geometries, material properties, and temperature differentials. Square shaped TEG produce high power for low load resistance, circular section TEG produced high power at high load resistance due to tuning of internal to load resistance. For Hi-Z TEGs, the power output was found to increase as the leg length decreased. The simulations were in good agreement with analytical and experimental results obtained from previous studies.

The optimization analysis of single P-N pair TEGs considered the effect of geometry, including variations in leg shapes such as square, circular, cone-shaped, and cascaded legs. Trapezoid shaped leg has higher efficiency. Thermal stress analysis revealed that

the von Mises stress increased as the leg length decreased. Different leg shapes exhibited varying stress levels, with the pyramid shape showing the highest stress. The Cone-up TEG consistently demonstrates the highest power output compared to other shapes across different load resistances.

Uni-couple leg is simulated for Bi_2Te_3, $CoSb_3$ materials. The results are compared with the segmented leg. It is observed that after segmentation, the power output increases by 14.7% compared to $CoSb_3$. There is a 178% increase compared to the single Bi_2Te3 leg.

From analysis of Thermoelectric Generator with heat exchanger mounted on hot air blower. It is observed that at a load resistance of 81 Ω experimental power produced is 59 watts. There is deviation of 11.94% when compared with numerical and theoretical values.

Overall, the results obtained from experimental measurements, simulations, and analytical models provide valuable insights into the characterization, analysis, and optimization of TEGs. These findings contribute to a better understanding of the factors influencing the power output and efficiency of TEG devices, facilitating their further development and application in thermoelectric energy conversion.

.

.

Chapter 5

Application of Thermoelectric Generator to Automotive Exhaust System

5.1 Introduction

Automotive vehicles utilize only about 25% of the energy produced. 40% of energy is available in the form of heat in exhaust gases; this heat can be trapped & converted to electrical energy using a Thermoelectric generator[TEG].

Section 5.2 presents a performance analysis of the Automotive Exhaust Thermoelectric Generator[AETEG]. An AETEG is designed and fabricated to the exhaust pipe of a single-cylinder diesel engine. A neural network is trained with experimental results and studied. The experimental, ANN and validated numerical model [3.3.2] to simulate AETEG results are compared. Experimental results are used to train the neural network. The effect of external load resistance, the mass flow rate of hot & cold fluid, and hot junction temperatures are analyzed and reported.

5.2 Experimental Analysis of Automotive Exhaust thermoelectric Generator Mounted on Exhaust of IC engine

This section reports the Experimental Analysis of an Automotive Exhaust thermoelectric Generator Mounted on the Exhaust of an IC engine. Numerical analysis, ANN model

and experimental study of TEG are reported in section 3.3.2, section5.2.2, section5.2.1 respectively. Effective material properties are used for analysis. Effective material properties are discussed in section 4.2.2. The numerical model is validated in section 3.3.2. A heat exchanger is designed and fabricated. The experimental setup is shown in Fig.5.1. Figure 5.2 shows a schematic diagram of a heat exchanger with TEG.

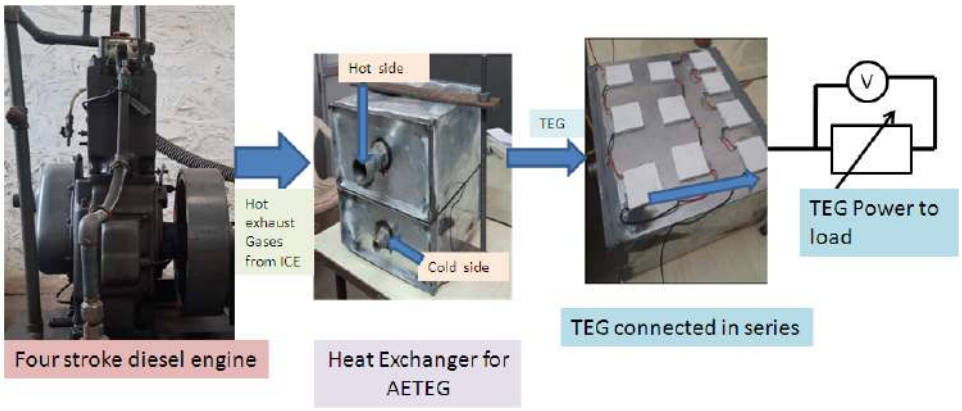

Figure 5.1: AETEG Set-Up

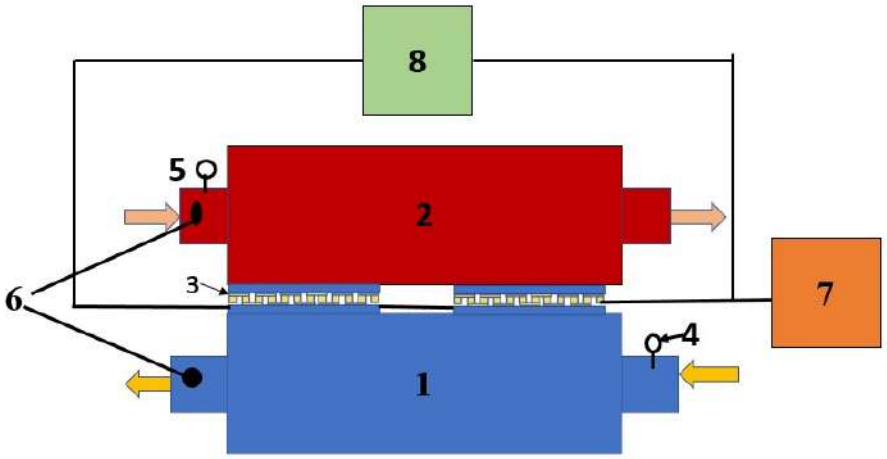

1. Cold Side 2.Hot Side 3. TEG 4.Cold side flow meter 5.Exhaust gas Flow meter 6.Thermocouple 7. Digital Multi meter 8. Rheostat

Figure 5.2: Heat exchanger for AETEG

The effective material properties are listed in table 4.2.

For simulation, a heat exchanger is modeled as shown in Fig. 5.3. Numerical analysis is done in the commercial software ANSYS. For heat exchanger analysis Fluent is used. Fluent uses the Finite volume method to analyze the fluid flow and heat transfer. TEG analysis is done using coupled thermal electric equations solved using the FEA method. The temperature calculated from the FVM method is imported to ANSYS thermal electric. Thermal electric uses the Finite element method to analyze. The numerical

model used is discussed in the section 3.3.2.Temperature distribution of heat exchanger after simulation in software is shown in fig. 5.4. For FVM, a Semi-Implicit Method for Pressure-Linked Equations [SIMPLE] algorithm is used, and Second-order upwind is used for discretization.

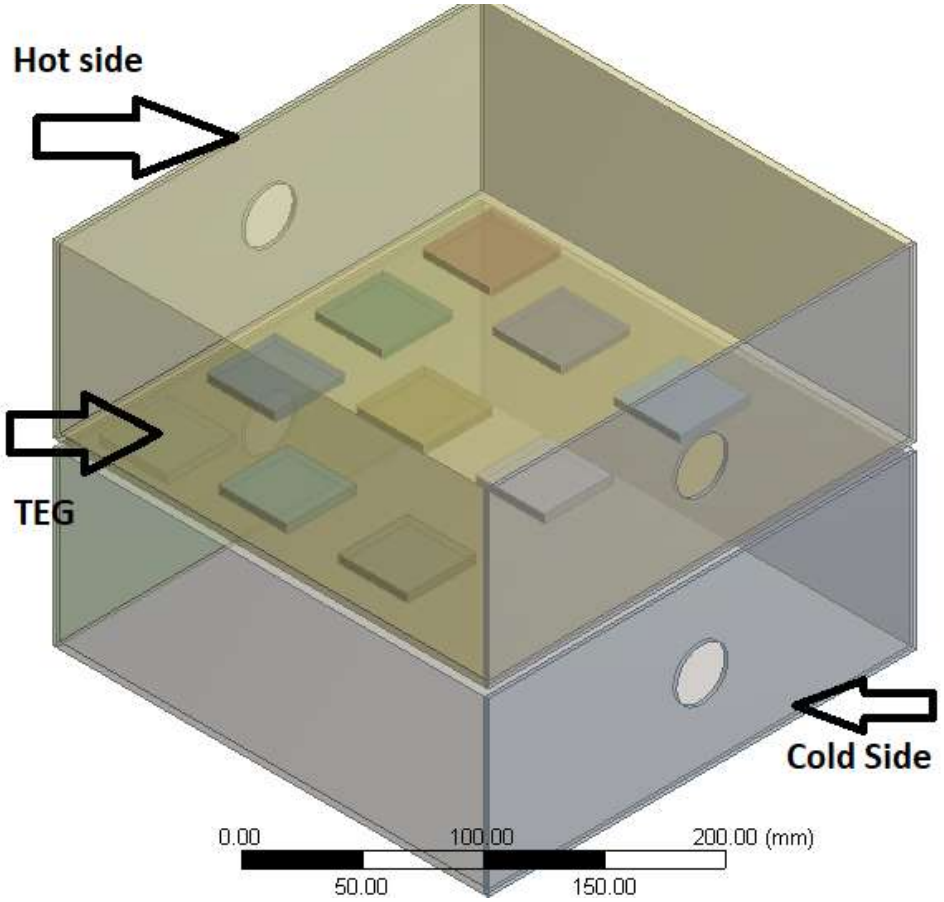

Figure 5.3: Model of Heat Exchanger for TEG

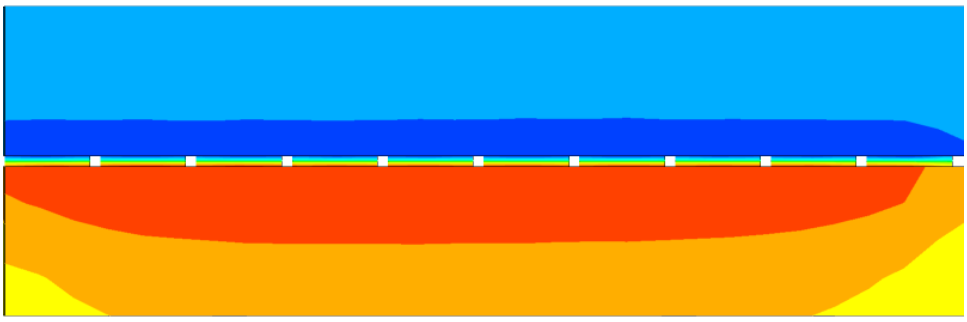

Figure 5.4: Temperature profile of Heat exchanger

5.2.1 Experimental Analysis

Engine is operated for different speeds to get different exhaust gas temperature which are taken as boundary conditions. In table 5.1 exhaust gas temperature for different

speed is tabulated. The heat exchanger is insulated, and heat transfer takes place only from hot fluid to cold fluid. On one side, hot exhaust gases are made to flow; on the other side, cold water. Ten commercially available thermoelectric generators TEM12706 are connected in series as shown in Fig.5.5. By measuring the temperatures at the inlet and outlet of the hot side of the heat exchanger, heat supplied is calculated by Equation. 5.1. Voltage and current of 10 TEG in series are noted, and power is calculated with Equation 5.2. Efficiency is calculated by equation 5.3. Experiments are conducted for the different flow rates of hot fluid, cold fluid, external load resistance, and exhaust gas temperatures. The cold fluid inlet temperature is varied from $Q_c = 0.1ltr/s$ to $Q_c = 0.2ltr/s$ at a time step of 0.05ltr/s. The mass of exhaust gas is varied from 6g/s to 12g/s at regular intervals of 2g/s. Load resistance is varied from 2Ω to 30Ω. Performance evaluation is based on power and conversion efficiency and is reported in the section 5.3.

$$\dot{Q} = \dot{m}_e(T_{hi} - T_{ci}) \tag{5.1}$$

$$Power = V * I \tag{5.2}$$

$$\eta = \frac{\dot{Q}}{power} \tag{5.3}$$

Table 5.1: Engine parameter for AETEG

Engine Speed (RPM)	**Exhaust Gas Temperature (°C)**	**Air-Fuel Ratio**
1000	300	20:1
1500	350	18:1
2000	400	16:1
2500	450	14:1
3000	500	12:1

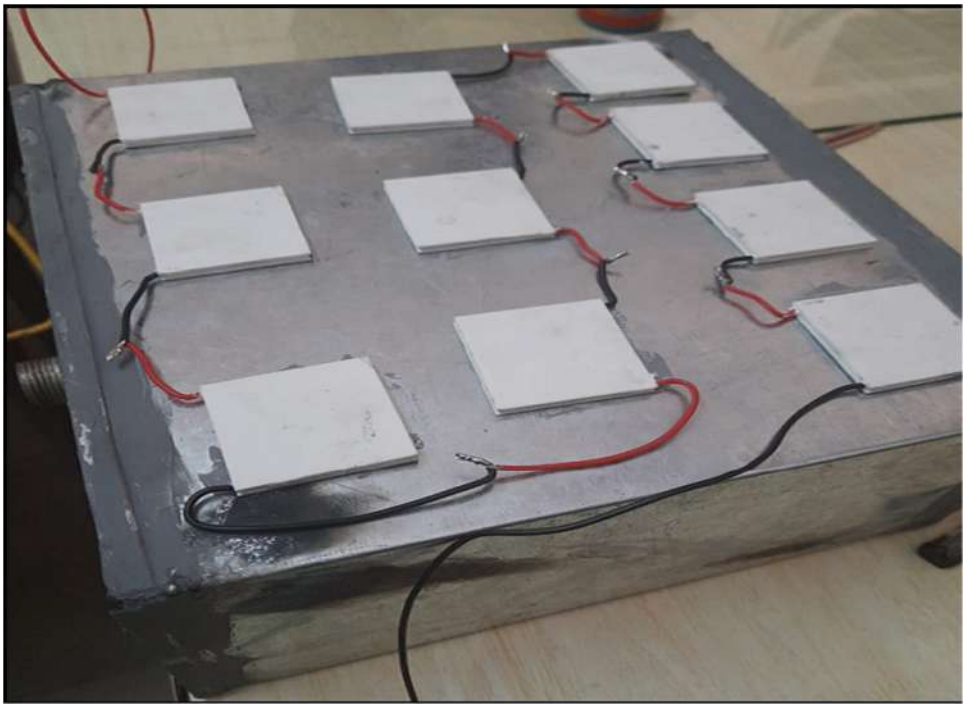

Figure 5.5: Heat Exchanger with TEG

5.2.2 Artificial Neural network model

Experimental data is used for modeling ANN model. Levenberg-Marquardt's back-propagation Algorithm is used for the present study. Weights are assigned from one layer to another. In each neuron, the summation of weights is calculated with bias by equation 5.4. The summation of weights with bias is calculated. The sigmoid activation function is evaluated by Equation 5.5. If the activation function calculated is higher than the specified activation value, a neuron gets activated, and output is sent. Mean square error is calculated from Equation 5.6. A neural network is constructed using MATLAB. Fig.5.7 shows the regression curves of ANN. It shows the relationship between the ANN model's predicted output and the training set's output. Training data is taken from experimental results. From Fig.5.7 for training, R is 99.9% means it can predict at the accuracy of 99.9%. 70% data is taken for training and 15% each for testing and validation. The performance of the ANN model is discussed in section 5.3.

$$\hat{Y} = W_1 x_1 + W_2 X_2 + X_3 .....X_m + bias \tag{5.4}$$

$$S(x) = \frac{1}{1 - e^{-\hat{Y}}} \tag{5.5}$$

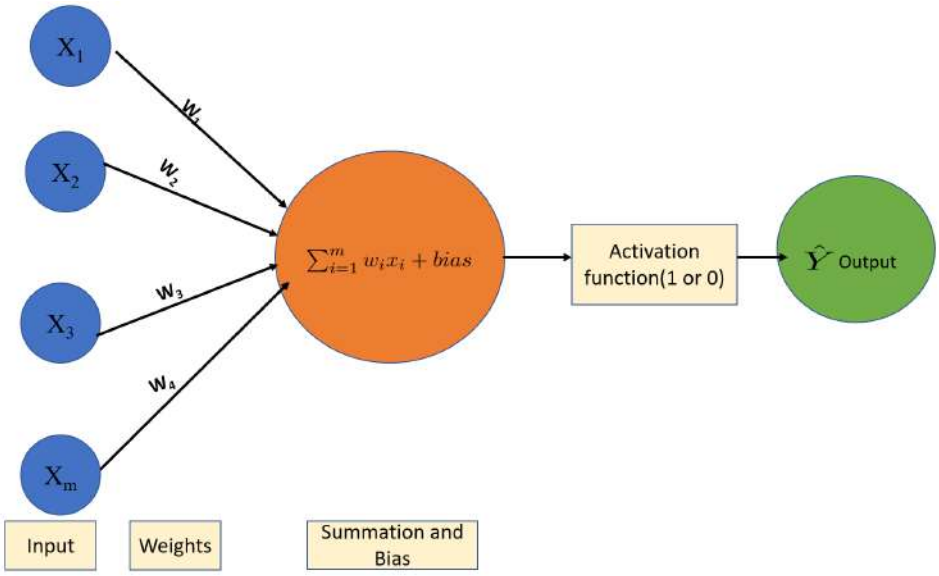

Figure 5.6: Artificial Neural Network

$$MSE = \frac{1}{m}\sum_{i=1}^{m}(Y_i - \hat{Y}_i)^2 \tag{5.6}$$

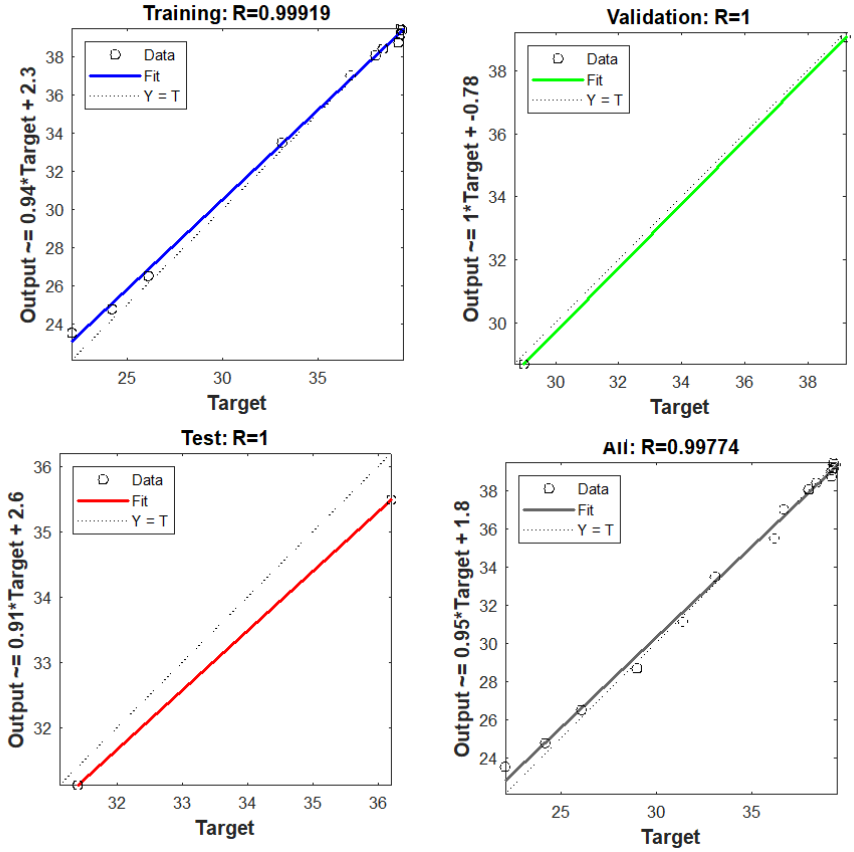

Figure 5.7: Regression Plots

5.3 Results

The results of the analysis of are reported in this section. Figure 5.8 shows the variation of mass flow of exhaust gases with power produced by TEG. For different exhaust mass flow rates from $m_{ex} = 6g/s$ to $m_{ex} = 12g/s$ at regular intervals of 2g/s power is evaluated. The mass flow of exhaust gases is directly proportional to the power produced by AETEG. As the mass flow rate of exhaust gases increases, the temperature and heat flux increase; hence power increases. For exhaust gas mass flow of 12gm/s. The power of 10 TEG in series at matched load resistance is 31 watts. The matched load resistance is 24Ω.

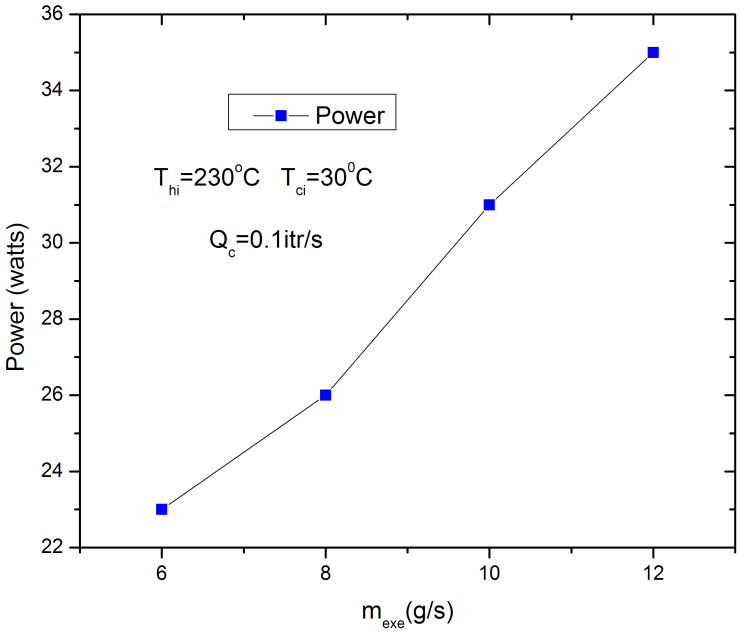

Figure 5.8: Exhaust gases mass verses Power

For inlet temp of exhaust gases at 230^0C. Cold water inlet temp if 30^0C variation of power with load resistance is shown in Fig. 5.9. The flow rate of cold fluid is varied from 0.1ltr/s to 0.2ltr/s at 0.05lts/s intervals. It is observed that the mass flow rate of cold fluid is directly proportional to the power developed. The power of AETEG depends on the amount of heat rejected at the cold junction. As the mass flow rate of the cold side increases, more heat is rejected, and more power is generated. The curve power produced versus load resistance is parabolic in nature. Maximum power is produced when the load resistance is equal to internal resistance due to electrical resonance.

For flow rate of $Q_c = 0.1itr/s$ $T_h = 230^0C$, $T_c = 30^0C$, and $m_{ex} = 10g/s$. Figure 5.10

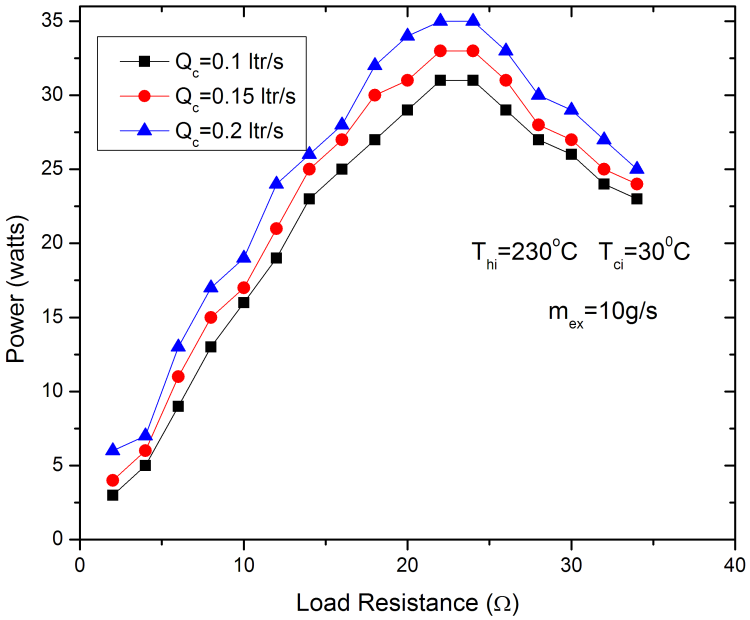

Figure 5.9: Load resistance verses power

shows the comparison of experimental results with numerical and ANN model results. Experimental and ANN results match. For experimental with a numerical analysis, there is a deviation of 12.9% at peak power. The difference in experimental and numerical results is due to the use of effective material properties and heat loss in experiments. Variation of current with voltage is shown in Fig. 5.11, and it is linear according to ohms law. For matched load resistance power versus hot side inlet temperature, is shown in Fig.5.12 for constant cold side temperature. As the hot side inlet temperature increases, power output also increases as the Seebeck coefficient is directly proportional to the power generated. Efficiency versus load resistance is plotted in Fig.5.14. It is observed that the efficiency is maximum at a load resistance of 34Ω. Peak efficiency is 3.5%. The peak power and peak efficiency are not at the same external load. This is due to Thomson and Peltier's effect.

Figure 5.13 shows the power produced versus load resistance when TEGs are connected in series. As more TEGs are connected in series, power output increases. Peak power is produced at electrical resonance when internal resistance is equal to load resistance. It is observed that peak power is 31 watts for 10TEG in series. Peak power is at a load resistance of 24Ω. The peak power for 5TEG in series is 12.5 watts. Peak power is at 12Ω load resistance as the number of TEG is reduced; peak power shifts for low load resistance. The energy produced by one TEG is 1.4 watts for 2Ω load resistance. It is

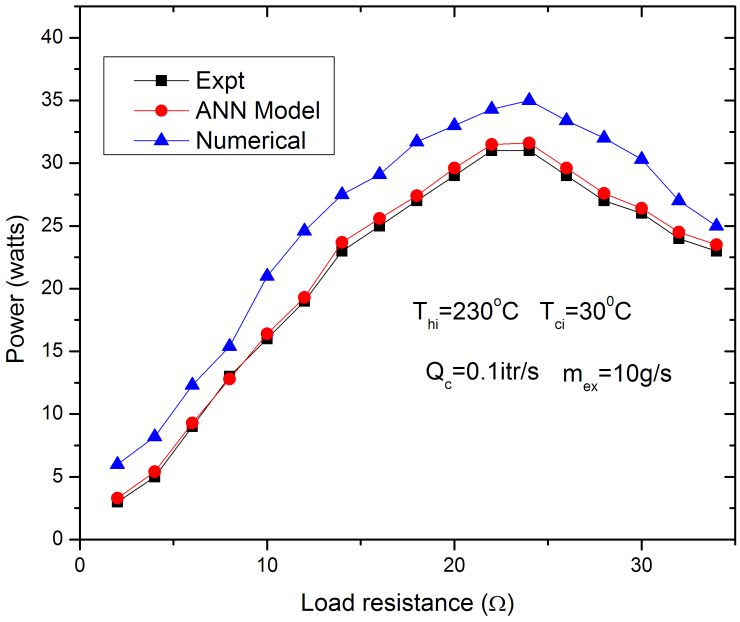

Figure 5.10: Comparison of numerical & experimental results

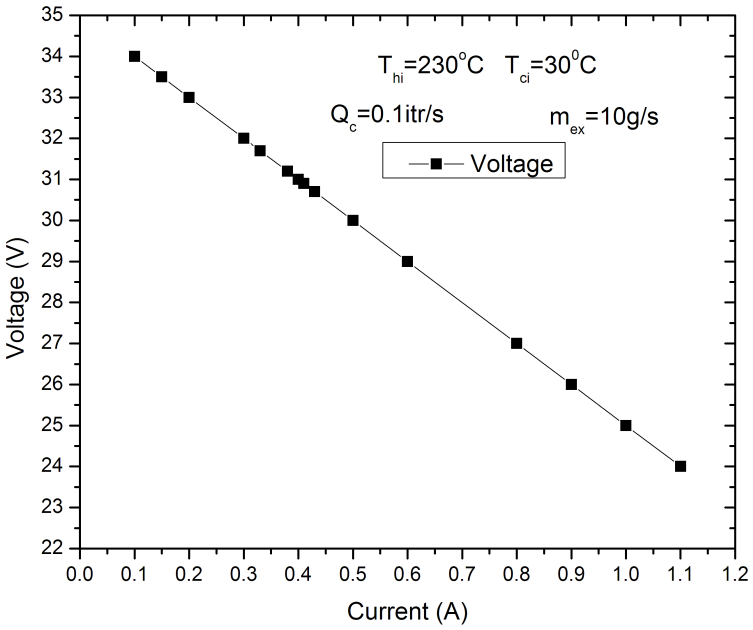

Figure 5.11: Current verses voltage

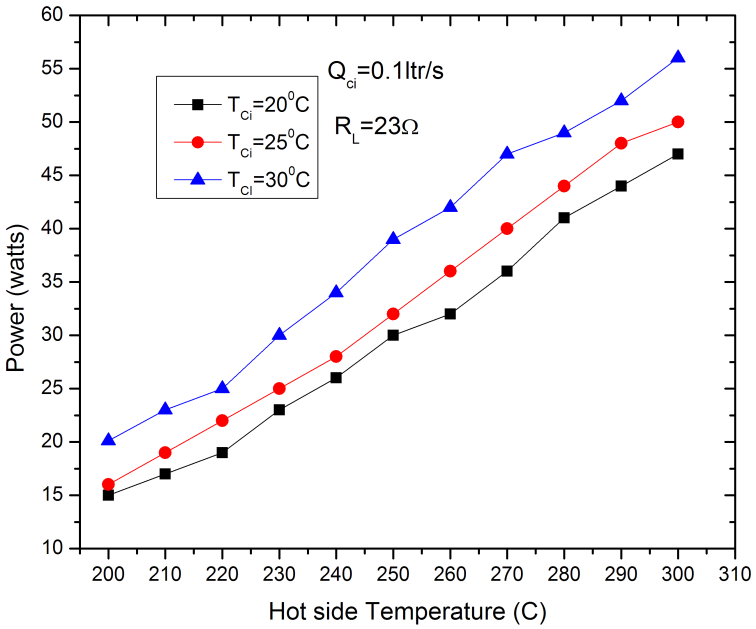

Figure 5.12: Power verses Hot side temperature

observed from Fig. 5.9 that as the number of TEG reduces, the peak power point shifts towards the left. AETEG needs to design based on the load resistance.

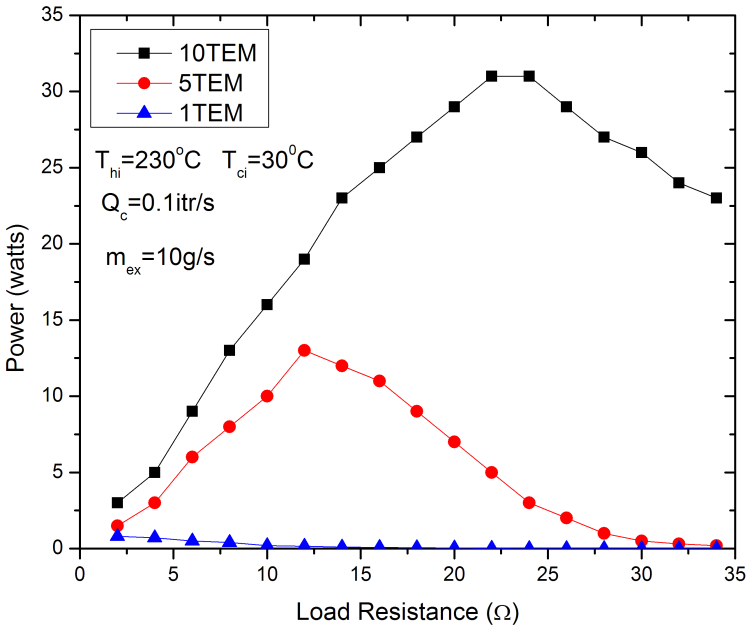

Figure 5.13: Power for different number of TEG in series

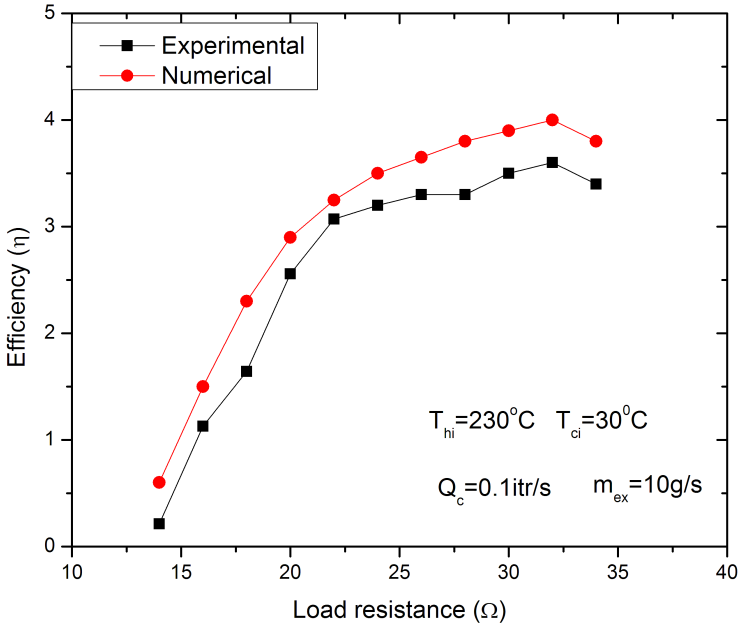

Figure 5.14: Efficiency verses load resistance

5.4 Conclusion

The performance analysis of AETEG on exhaust of IC engine. The peak power and peak efficiency are not at same load resistance. Peak power occurs at a point when internal resistance is equal to load resistance due to electrical resonance. Maximum efficiency occurs when the load resistance is 1.4 times the internal resistance and is due to Thomson and Peltier effect. Based on the external load, AETEG needs to be designed. For inlet temp of exhaust gases at 230^0C. Cold water inlet temp if 30^0C. For flow rate of $Q_c = 0.1itr/s$ $T_h = 230^0C$, $T_c = 30^0C$, and $m_{ex} = 10g/s$. Peak power is 31 watts at 24Ω and peak efficiency is 3.5% at 34Ω.

A numerical model is validated with results in the literature and used to simulate the experimental setup. Experimental results are compared with numerical results. The results agree with an acceptable deviation of 12.9% for peak power. The difference in experimental and numerical results is due to effective material properties used for simulation and unaccounted heat loss in experiments. An artificial neural network is trained with experimental data. Artificial neural network model results are compared with experimental and numerical results. ANN results and experimental results are similar. Hence ANN can predict AETEG performance. The performance of AETEG depends on TEG material and heat exchanger design parameters. As the mass flow rate

and exhaust gas temperature increase, power output from AETEG increases because heat flux increases. The mass flow rate of cold fluid is directly proportional to power output since the convective heat transfer coefficient increases. Peak power increases as the hot side temperature increases. Because as Seebeck effect is directly proportional to the temperature difference between the hot and cold sides. Effective material properties can be used to simulate TEG.

Chapter 6

Conclusions and Future Scope

6.1 Conclusions

In conclusion, this comprehensive study on Thermoelectric Generators (TEGs) and Automotive Exhaust Thermoelectric Generators (AETEGs) has demonstrated the importance of theoretical and numerical modeling for investigating and validating their performance. The results obtained have been promising and shed light on various factors that influence the power generation capabilities of these energy conversion systems.

Theoretical and numerical modeling of TEG and AETEG can be used for performance investigation and validation of the TEG and AETEG revealed promising results. The power generated by the TEG was analyzed in relation to load resistance, leg length, and temperature difference. For a hot side temperature $T_h = 300^0C$ and cold side temperature $T_h = 30^0C$ the peak power produced is 20 watts. The results showed an initial increase in power until reaching a maximum at the peak power point, attributed to electrical resonance. Further increasing the load resistance resulted in a gradual decline in power.

The evaluation of AETEGs using theoretical and numerical models on a test bench with a hot air blower demonstrated a theoretical and numerical power output of 67 watts at a load resistance of 81 Ω. The close similarity between theoretical and numerical simulation results validated the accuracy of the AETEG model. Moreover, the utilization of effective material properties in the theoretical and numerical modeling allowed for reliable comparisons with experimental data, with maximum deviations of 13% and 12% respectively.A single leg TEG made of $CoSb_3$ is tested. A single leg TEG made of In filled $CoSb_3$ is taken.Open circuit voltage is very low, about 7 mv at a temperature difference of 50 C. Low voltage is due to electric contact resistance between leads to measure voltage and the TEG leg. Commercially available TEG models, such as Marlow, TEC12706, and

TEC SP 27145, were also analyzed experimentally. TEG 12706 exhibited a peak power output of 168 milliwatts at a load resistance of 2.4Ω. MARLOW TEG produced a power of 485mWatts under same boundary conditions.

With simulation of HiZ TEG it is observed that square shaped TEG produce high power for low load resistance, circular section TEG produced high power at high load resistance due to tuning of internal to load resistance. The optimization analysis of single P-N pair TEGs considered the effect of geometry, including variations in leg shapes such as square, circular, cone-shaped, and cascaded legs. Trapezoid shaped leg has higher efficiency. Thermal stress analysis revealed that the von Mises stress increased as the leg length decreased. Different leg shapes exhibited varying stress levels, with the pyramid shape showing the highest stress. The Cone-up TEG consistently demonstrates the highest power output compared to other shapes across different load resistances.

Uni-couple leg is simulated for Bi_2Te_3, $CoSb_3$ materials. The results are compared with the segmented leg. It is observed that after segmentation, the power output increases by 14.7% compared to $CoSb_3$. There is a 178% increase compared to the single Bi_2Te3 leg. From analysis of Thermoelectric Generator with heat exchanger mounted on hot air blower. It is observed that at a load resistance of 81 Ω experimental power produced is 59 watts. There is deviation of 11.94% when compared with numerical and theoretical values.

The performance analysis of AETEG on exhaust of IC engine. For inlet temp of exhaust gases at 230^0C. Cold water inlet temp if 30^0C. For flow rate of $Q_c = 0.1itr/s$ $T_h = 230^0C$, $T_c = 30^0C$, and $m_{ex} = 10g/s$. Peak power is 31 watts at 24Ω and peak efficiency is 3.5% at 34Ω. Maximum efficiency occurs when the load resistance is 1.4 times the internal resistance and is due to Thomson and Peltier effect. An artificial neural network (ANN) was trained with experimental data, and its predictions closely matched both experimental and numerical results, indicating the potential of ANN in predicting AETEG performance.

In conclusion, this study demonstrated the importance of theoretical and numerical modeling in the characterization and evaluation of TEGs and AETEGs. Effective material properties were found to be a reliable approach in simulating TEGs, and ANN proved to be a promising tool for predicting AETEG performance. This study has provided valuable insights into the design, optimization, and characterization of TEGs and AETEGs.

6.2 Future Work

An automotive exhaust gas thermoelectric generator needs commercialization. High performance materials such as Selenide Polycrystalline TEG needs to be analyzed and optimized. High temperature materials such as half Heusler and skutterudite need to be used to produce commercial TEGs. Device fabrication with half Heusler and skutterudite is a challenging task that needs to be addressed. Heat exchanger to enhance heat tranfer coefficient are to be designed and explored. Machine learning techniques can be used to explore and optimization of AETEG. Uncertainty analysis, using Kline-McClintock method can be done.

Appendix-A

A.1 Simulation of Thermoelectric Generator For Hybrid electric Vehicle

The simulated hybrid electric vehicle consists of an internal combustion engine, battery, transmission, and wheels. The HEV is simulated for different speeds from 100km/hr to 200km/hr. The exhaust temperature is calculated and reported in section A.1.2. Figure A.1 shows different blocks of the simulated thermoelectric generator.

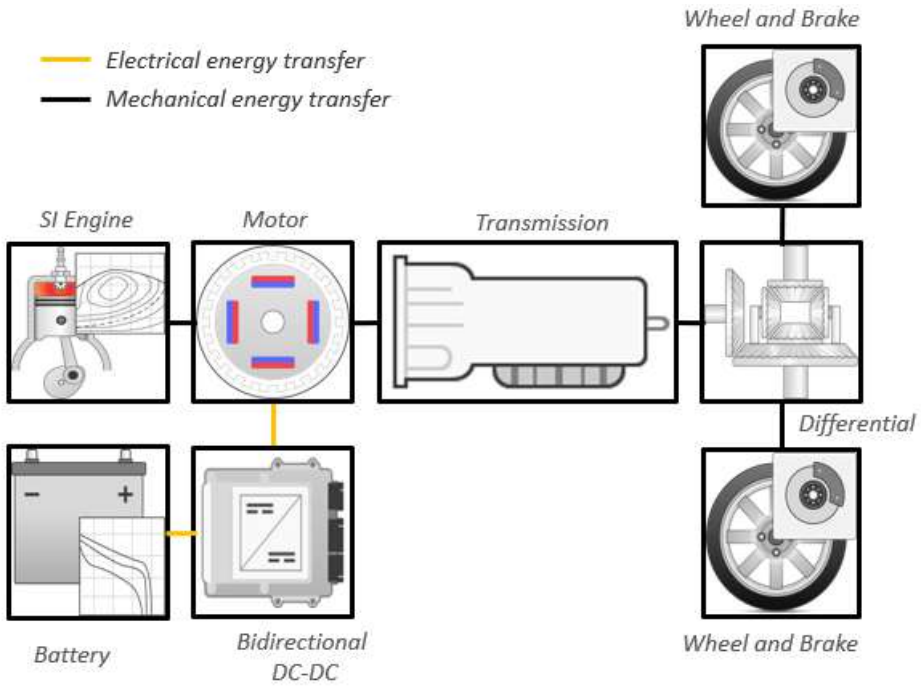

Figure A.1: Shematic diagram of hybrid electric vehicle

A.1.1 Simulation of Thermoelectric Generator For Hybrid Electric Vehicle

Taking the input from the exhaustgas temperaturesof the hybrid electric vehicles. A heat exchanger is modeled as shown with dimensions in fig.A.2. The heat exchanger is modeled with vortex generators. As the vortex generator increases the heat transfer coefficient, the heat transfer rate increases hence performance of TEG increases. 32 bismuth telluride thermoelectric modules are simulated [109] . The temperatureprofile of the heat exchanger is shown in Fig.A.3. Fluid flow and heat transfer analysis is carried out with finite volume. Finite element analysis is used for Thermoelectric generator analysis using coupled heat transfer and electric equation. Power developed by the thermoelectric generator is reported in section A.1.2.

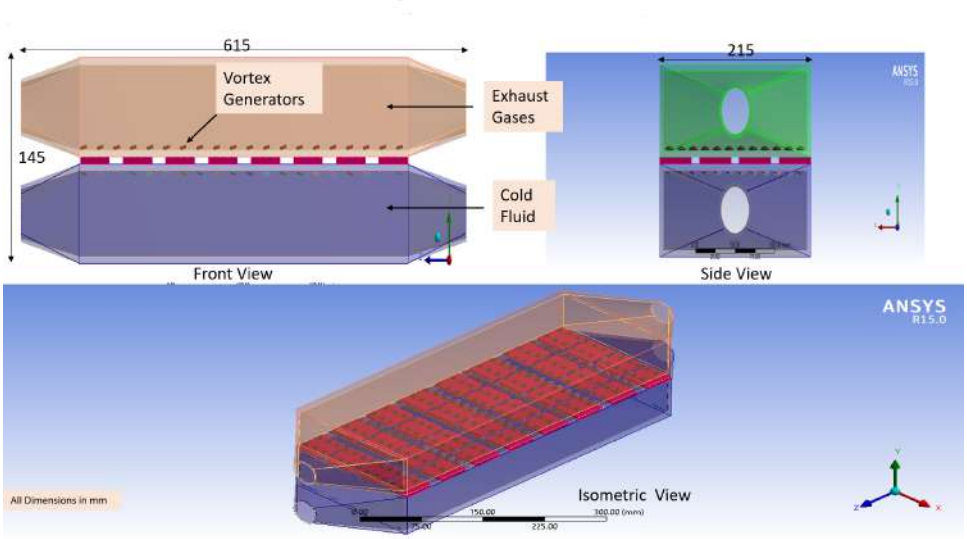

Figure A.2: Heat exchanger

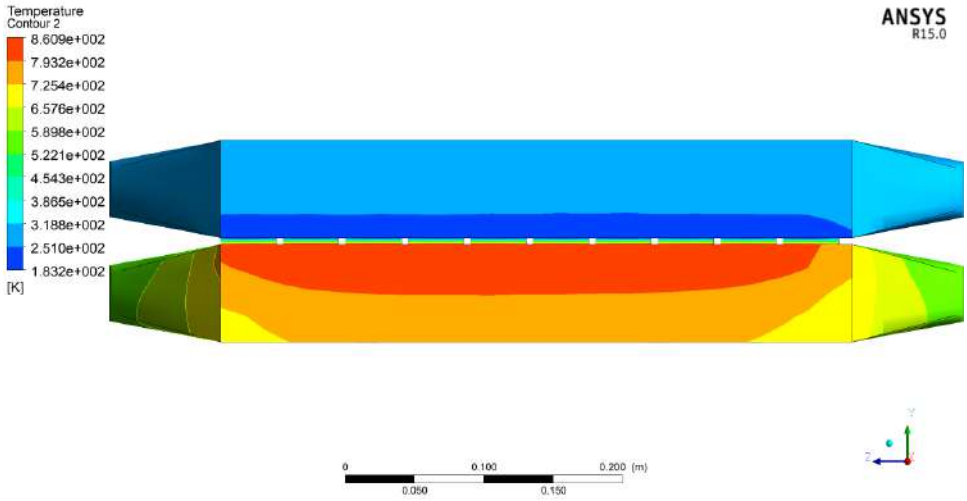

Figure A.3: Temp profile of Heat exchanger

A.1.2 Results

The hybrid electric vehicle is simulated in MATLAB Simulink. Exhaust gas temperature versus vehicle speed and mass of exhaust gases versus vehicle speed are plotted as in Fig. A.4. It is observed that for variation of speed from 100km/hr to 200km/hr, exhaust gas temperature increases from 650K to 750K. Exhaust gas temperature and mass flow rate increase with temperature. These temperatures are taken as input to simulate the heat exchanger. 32 Thermoelectric modules were simulated, and power versus load resis-tance is plotted in Fig. A.5. The temperature of the exhaust gas is 700K mass flow rate of the exhaust gas is 87.5g/s. Water is selected as cold fluid with an inlet temperature of 313K. It is observed that the variation of power with load resistance is parabolic. At 75ohms load resistance, the maximum power produced is 72watts.

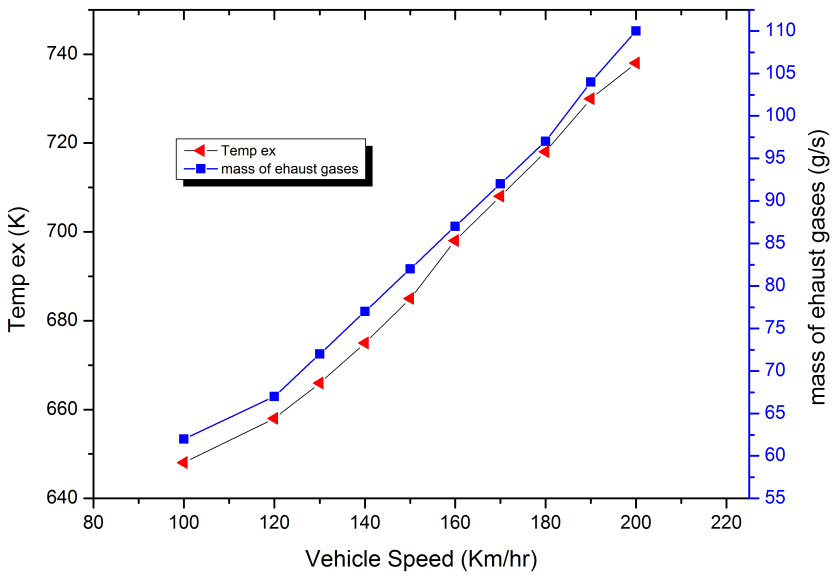

Figure A.4: Vehicle speed verses Exhautsgas temp

A.1.2 Results

In this section results of the automotive exhaust thermoelectric generator are discussed. Initially from analysis with a thermoelectric generator mounted on a hot air blower. It is observed that at a load resistance of 82Ω power produced is 61 watts for the hot side average temperature of 300^0C and cold side average temperature of 30^0C. The mass flow rate of hot gases is $m_{hi} = 0.5$g/s. The cold side mass flow rate is $Q_{ci} = 0.1$ltr/s. The theoretical and numerical simulation results are compared with experimental results.

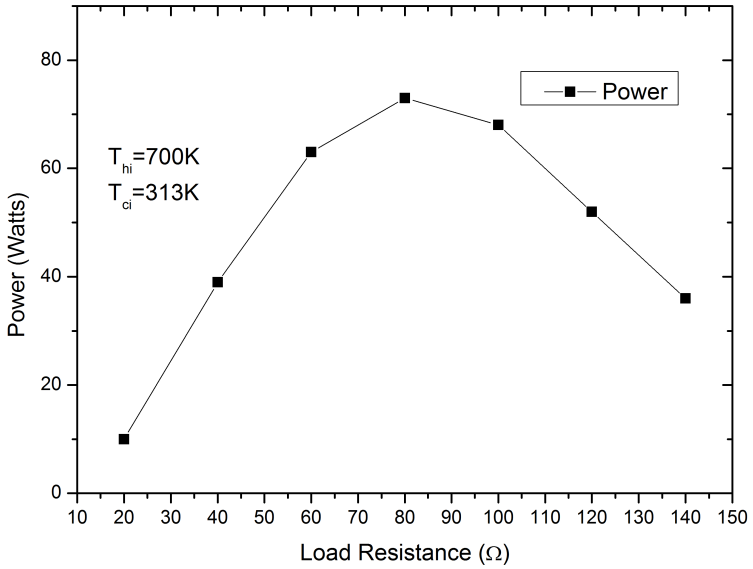

Figure A.5: power verses load resistance

Theoretical and numerical results are almost similar. There is a small deviation in experimental results due to heat losses and the assumption of equivalent material properties.

From the analysis of AETEG mounted on the exhaust of an internal combustion engine. It is observed that when 10 TEGs are connected in series a power of 31 watts was produced at a matched load resistance of 24Ω. The results are validated with numerical and ANN results.

The hybrid electric vehicle is simulated in MATLAB Simulink. With the increase in speed of the engine mass flow rate and exhaust gas temperature increase. These temperatures are taken as input to simulate the heat exchanger in ANSYS. 32 Thermoelectric modules were simulated, and power versus load resistance is plotted. For the temperature of the exhaust gas of 700K and the mass flow rate of the exhaust gas of 87.5g/s. At 75ohms load resistance, the maximum power produced is 72watts.

List of Publications

Journal Papers Published and accepted:

1. Kondaguli, R. S., and P. V. Malaji. "Geometry Design and Performance Evaluation of Thermoelectric Generator." *The European Physical Journal Special Topics*, 2021. (Quartile 2 (Q2), Scopus Indexed)

2. Kondaguli, R. S., C R Hiremath, and P. V. Malaji. "Thermoelectric Generator for Hybrid Electric Vehicle." *Journal of Mines Metals and Fuels*, [Accepted]. (Scopus Indexed)

Journal Papers Under Review

3. Kondaguli, R. S., C R Hiremath, and P. V. Malaji. "Experimental Analysis of Thermoelectric Generator and its Application to Hybrid Electric Vehicle." *Suranaree Journal of Science and Technology*, [Under Review]. (Scopus Indexed)

4. Kondaguli, R. S., C R Hiremath, and P. V. Malaji."Performance Analysis of Automotive Exhaust Gas Thermoelectric Generators[AETEG] and application of segmented leg to enhance performance of AETEG". (Submitted to Q1 Journal)

Conference Proceedings Papers

5. Kondaguli, R. S., and P. V. Malaji. "Analysis of Bismuth Telluride (Bi2Te3) Thermoelectric Generator." *2020 IEEE Bangalore Humanitarian Technology Conference*

(B-HTC). IEEE, 2020. (Scopus Indexed)

6. Kondaguli, R. S., and P. V. Malaji. "Mathematical Modeling and Numerical Simulation of Thermoelectric Generator." *AIP Conference Proceedings*, Vol. 2274, No. 1. AIP Publishing LLC, 2020. (Scopus Indexed)

Journal Papers Under Preparation

7. Kondaguli, R. S., and P. V. Malaji. "Performance Analysis of Automotive exhaust Gas thermoelectric generator" will be submitted to Q1 or Q2 journal.

Bibliography

[1] "IEA Reports," https://www.iea.org/reports/world-energy-outlook-2017, 2022, accessed June 16, 2022.

[2] B. Mahlalela *et al.*, "Electric power generation potential based on waste heat and geothermal resources in south africa, pangea."

[3] "Lawrence Livermore National Laboratory Report," 2021.

[4] "magazine report," http://cesa-automotive-electronics.blogspot.co.uk/2012/09/dual-voltage-power-supply-system-with.html.Accessed:2017-11-10., 2022, accessed June 17, 2022.

[5] "Thermoelectrics Lab," http://thermoelectrics.matsci.northwestern.edu/, 2022, accessed April 26, 2022.

[6] Online, "Exhaust system," http://http://www.kevinbodentyresales.co.uk/Exhausts, 2022, accessed April 26, 2022.

[7] M. Karri, E. Thacher, B. Helenbrook, M. Compeau, A. Kushch, N. Elsner, M. Bhatti, J. O'Brien, and F. Stabler, "Thermoelectrical energy recovery from the exhaust of a light truck," Mechanical and Aeronautical Engineering Department, Clarkson University ..., Tech. Rep., 2003.

[8] A. F. Agudelo, R. García-Contreras, J. R. Agudelo, and O. Armas, "Potential for exhaust gas energy recovery in a diesel passenger car under european driving cycle," *Applied Energy*, vol. 174, pp. 201–212, 2016.

[9] J. LaGrandeur, D. Crane, and A. Eder, "Vehicle fuel economy improvement through thermoelectric waste heat recovery," in *DEER conference*, 2005, pp. 1–24.

[10] Q. Yan and M. G. Kanatzidis, "High-performance thermoelectrics and challenges for practical devices," *Nature materials*, vol. 21, no. 5, pp. 503–513, 2022.

[11] G. Nie, W. Li, J. Guo, A. Yamamoto, K. Kimura, X. Zhang, E. B. Isaacs, V. Dravid, C. Wolverton, M. G. Kanatzidis *et al.*, "High performance thermoelectric module through isotype bulk heterojunction engineering of skutterudite materials," *Nano Energy*, vol. 66, p. 104193, 2019.

[12] A. J. Tomarchio, "A feasibility study of replacing an electrical generator of a standard american automobile with a thermoelectric generator: a thesis," Ph.D. dissertation, Clarkson College of Technology, 1964.

[13] F. J. Lesage, É. V. Sempels, and N. Lalande-Bertrand, "A study on heat transfer enhancement using flow channel inserts for thermoelectric power generation," *Energy Conversion and Management*, vol. 75, pp. 532–541, 2013.

[14] "DIYhz Aluminum Computer Graphics Card Cooler," https://www.amazon.in/DIYhz-Aluminum-Computer-Graphics-Endothermic/dp/B07FZWM4Z7/ref=sr_1_6?keywords=DIYhz&qid=1690413809&sr=8-6, accessed on Month Day, Year.

[15] "New material breaks," https://phys.org/news/2019-11-material-world-electricity.html, 2022, accessed June 16, 2022.

[16] T. J. Seebeck, "Magnetic polarization of metals and minerals," *Abhandlungen der Deutschen Akademie der Wissenschaften zu Berlin*, vol. 265, pp. 1822–1823, 1822.

[17] J. C. A. Peltier, *Nouvelles expériences sur la caloricité des courans électriques*, 1834.

[18] A. F. Ioffe, L. Stil'Bans, E. Iordanishvili, T. Stavitskaya, A. Gelbtuch, and G. Vineyard, "Semiconductor thermoelements and thermoelectric cooling," *Physics Today*, vol. 12, no. 5, p. 42, 1959.

[19] W. Thomson, "4. on a mechanical theory of thermo-electric currents," *Proceedings of the Royal society of Edinburgh*, vol. 3, pp. 91–98, 1857.

[20] E. Altenkirch, "Über den nutzeffekt der thermosäule," *Physikalische Zeitschrift*, vol. 10, no. 560, p. 12, 1909.

[21] M. Telkes, "Power output of thermoelectric generators," *Journal of Applied Physics*, vol. 25, no. 8, pp. 1058–1059, 1954.

[22] R. Kondaguli and P. Malaji, "Mathematical modeling and numerical simulation of thermoelectric generator," in *AIP Conference Proceedings*, vol. 2274, no. 1. AIP Publishing LLC, 2020, p. 030037.

[23] D. Rowe, "General principles and basic considerations," in *Thermoelectrics Handbook*. CRC press, 2018, pp. 26–40.

[24] L.-D. Zhao, S.-H. Lo, Y. Zhang, H. Sun, G. Tan, C. Uher, C. Wolverton, V. P. Dravid, and M. G. Kanatzidis, "Ultralow thermal conductivity and high thermoelectric figure of merit in snse crystals," *Nature*, vol. 508, no. 7496, pp. 373–377, 2014.

[25] P.-P. Shang, J. Dong, J. Pei, F.-H. Sun, Y. Pan, H. Tang, B.-P. Zhang, L.-D. Zhao, and J.-F. Li, "Highly textured n-type snse polycrystals with enhanced thermoelectric performance," *Research*, vol. 2019, 2019.

[26] W. Liu, Q. Jie, H. S. Kim, and Z. Ren, "Current progress and future challenges in thermoelectric power generation: From materials to devices," *Acta Materialia*, vol. 87, pp. 357–376, 2015.

[27] A. L. Eiss, "Thermoelectric bonding study," Tech. Rep., 1966.

[28] H.-C. Hsieh, C.-H. Wang, W.-C. Lin, S. Chakroborty, T.-H. Lee, H.-S. Chu, and A. T. Wu, "Electroless co-p diffusion barrier for n-pbte thermoelectric material," *Journal of Alloys and Compounds*, vol. 728, pp. 1023–1029, 2017.

[29] X. Hu, P. Jood, M. Ohta, M. Kunii, K. Nagase, H. Nishiate, M. G. Kanatzidis, and A. Yamamoto, "Power generation from nanostructured pbte-based thermoelectrics: comprehensive development from materials to modules," *Energy & Environmental Science*, vol. 9, no. 2, pp. 517–529, 2016.

[30] A. Singh, S. Bhattacharya, C. Thinaharan, D. Aswal, S. Gupta, J. Yakhmi, and K. Bhanumurthy, "Development of low resistance electrical contacts for thermoelectric devices based on n-type pbte and p-type tags-85 ((agsbte2) 0.15 (gete) 0.85)," *Journal of Physics D: Applied Physics*, vol. 42, no. 1, p. 015502, 2008.

[31] Z. Bu, X. Zhang, B. Shan, J. Tang, H. Liu, Z. Chen, S. Lin, W. Li, and Y. Pei, "Realizing a 14% single-leg thermoelectric efficiency in gete alloys," *Science Advances*, vol. 7, no. 19, p. eabf2738, 2021.

[32] L. Chen, D. Mei, Y. Wang, and Y. Li, "Ni barrier in bi2te3-based thermoelectric modules for reduced contact resistance and enhanced power generation properties," *Journal of Alloys and Compounds*, vol. 796, pp. 314–320, 2019.

[33] H.-j. Wu, A. T. Wu, P.-c. Wei, and S.-w. Chen, "Interfacial reactions in thermoelectric modules," *Materials Research Letters*, vol. 6, no. 4, pp. 244–248, 2018.

[34] S. Harish, D. Sivaprahasam, B. Jayachandran, R. Gopalan, and G. Sundararajan, "Performance of bismuth telluride modules under thermal cycling in an automotive exhaust thermoelectric generator," *Energy Conversion and Management*, vol. 232, p. 113900, 2021.

[35] D. Champier, "Thermoelectric generators: A review of applications," *Energy Conversion and Management*, vol. 140, pp. 167–181, 2017.

[36] "Website," https://hi-z.com/, 2022, accessed June 16, 2022.

[37] "Website," https://ii-vi.com/thermoelectrics/, 2022, accessed June 16, 2022.

[38] M. Brignone and A. Ziggiotti, "Impact of novel thermoelectric materials on automotive applications," in *AIP Conference Proceedings*, vol. 1449, no. 1. American Institute of Physics, 2012, pp. 493–496.

[39] A. D. LaLonde, Y. Pei, H. Wang, and G. J. Snyder, "Lead telluride alloy thermoelectrics," *Materials today*, vol. 14, no. 11, pp. 526–532, 2011.

[40] T. Hogan, T. Shih, and D. Rowe, "Thermoelectrics handbook: macro to nano," *CRC, Boca Raton, FL*, vol. 12, no. 1, 2005.

[41] P. Jood, M. Ohta, A. Yamamoto, and M. G. Kanatzidis, "Excessively doped pbte with ge-induced nanostructures enables high-efficiency thermoelectric modules," *Joule*, vol. 2, no. 7, pp. 1339–1355, 2018.

[42] E. Hazan, O. Ben-Yehuda, N. Madar, and Y. Gelbstein, "Functional graded germanium–lead chalcogenide-based thermoelectric module for renewable energy applications," *Advanced Energy Materials*, vol. 5, no. 11, p. 1500272, 2015.

[43] Z.-Z. Luo, S. Hao, X. Zhang, X. Hua, S. Cai, G. Tan, T. P. Bailey, R. Ma, C. Uher, C. Wolverton *et al.*, "Soft phonon modes from off-center ge atoms lead to ultralow thermal conductivity and superior thermoelectric performance in n-type pbse–gese," *Energy & Environmental Science*, vol. 11, no. 11, pp. 3220–3230, 2018.

[44] J. M. Hodges, S. Hao, J. A. Grovogui, X. Zhang, T. P. Bailey, X. Li, Z. Gan, Y.-Y. Hu, C. Uher, V. P. Dravid *et al.*, "Chemical insights into pbse–x% hgse: high power factor and improved thermoelectric performance by alloying with discordant atoms," *Journal of the American Chemical Society*, vol. 140, no. 51, pp. 18 115–18 123, 2018.

[45] B. Jiang, Y. Yu, J. Cui, X. Liu, L. Xie, J. Liao, Q. Zhang, Y. Huang, S. Ning, B. Jia *et al.*, "High-entropy-stabilized chalcogenides with high thermoelectric performance," *Science*, vol. 371, no. 6531, pp. 830–834, 2021.

[46] Z. Liu, N. Sato, W. Gao, K. Yubuta, N. Kawamoto, M. Mitome, K. Kurashima, Y. Owada, K. Nagase, C.-H. Lee *et al.*, "Demonstration of ultrahigh thermoelectric efficiency of 7.3% in mg3sb2/mgagsb module for low-temperature energy harvesting," *Joule*, vol. 5, no. 5, pp. 1196–1208, 2021.

[47] Y. Sadia, D. Ben-Ayoun, and Y. Gelbstein, "Evaporation–condensation effects on the thermoelectric performance of pbte-based couples," *Physical Chemistry Chemical Physics*, vol. 19, no. 29, pp. 19 326–19 333, 2017.

[48] W. Li, J. Wang, Y. Xie, J. L. Gray, J. J. Heremans, H. B. Kang, B. Poudel, S. T. Huxtable, and S. Priya, "Enhanced thermoelectric performance of yb-single-filled skutterudite by ultralow thermal conductivity," *Chemistry of Materials*, vol. 31, no. 3, pp. 862–872, 2019.

[49] Z. Zhou, J. Li, Y. Fan, Q. Zhang, X. Lu, S. Fan, K. Kikuchi, N. Nomura, A. Kawasaki, L. Wang *et al.*, "Uniform dispersion of sic in yb-filled skutterudite nanocomposites with high thermoelectric and mechanical performance," *Scripta Materialia*, vol. 162, pp. 166–171, 2019.

[50] P.-a. Zong, R. Hanus, M. Dylla, Y. Tang, J. Liao, Q. Zhang, G. J. Snyder, and L. Chen, "Skutterudite with graphene-modified grain-boundary complexion enhances zt enabling high-efficiency thermoelectric device," *Energy & Environmental Science*, vol. 10, no. 1, pp. 183–191, 2017.

[51] Q. Zhang, J. Liao, Y. Tang, M. Gu, C. Ming, P. Qiu, S. Bai, X. Shi, C. Uher, and L. Chen, "Realizing a thermoelectric conversion efficiency of 12% in bismuth telluride/skutterudite segmented modules through full-parameter optimization and

energy-loss minimized integration," *Energy & Environmental Science*, vol. 10, no. 4, pp. 956–963, 2017.

[52] G. Skomedal, N. R. Kristiansen, R. Sottong, and H. Middleton, "Evaluation of thermoelectric performance and durability of functionalized skutterudite legs," *Journal of Electronic Materials*, vol. 46, no. 4, pp. 2438–2450, 2017.

[53] J. Chu, J. Huang, R. Liu, J. Liao, X. Xia, Q. Zhang, C. Wang, M. Gu, S. Bai, X. Shi *et al.*, "Electrode interface optimization advances conversion efficiency and stability of thermoelectric devices," *Nature communications*, vol. 11, no. 1, pp. 1–8, 2020.

[54] M. Daniel, M. Friedemann, J. Franke, and M. Albrecht, "Thermal stability of thermoelectric cosb3 skutterudite thin films," *Thin Solid Films*, vol. 589, pp. 203–208, 2015.

[55] C. Fu, S. Bai, Y. Liu, Y. Tang, L. Chen, X. Zhao, and T. Zhu, "Realizing high figure of merit in heavy-band p-type half-heusler thermoelectric materials," *Nature communications*, vol. 6, no. 1, pp. 1–7, 2015.

[56] W. S. McCulloch and W. Pitts, "A logical calculus of the ideas immanent in nervous activity," *The bulletin of mathematical biophysics*, vol. 5, no. 4, pp. 115–133, 1943.

[57] A. M. Turing and J. Haugeland, "Computing machinery and intelligence," *The Turing Test: Verbal Behavior as the Hallmark of Intelligence*, pp. 29–56, 1950.

[58] A. L. Samuel, "Some studies in machine learning using the game of checkers. ii—recent progress," *Computer Games I*, pp. 366–400, 1988.

[59] J. McCarthy, M. Minsky, N. Rochester, and C. Shannon, "The dartmouth summer research project on artificial intelligence," *Artificial intelligence: past, present, and future*, 1956.

[60] F. Rosenblatt, "The perceptron: a probabilistic model for information storage and organization in the brain." *Psychological review*, vol. 65, no. 6, p. 386, 1958.

[61] D. Michie, "Experiments on the mechanization of game-learning part i. characterization of the model and its parameters," *The Computer Journal*, vol. 6, no. 3, pp. 232–236, 1963.

[62] S. Linnainmaa, "Alogritmin kumulatiivinen pyöristysvirhe yksittäisten pyöristysvirheiden taylor-kehitelmänä," Ph.D. dissertation, Master's thesis, University of Helsinki, 1970.

[63] K. Fukushima, "Neural circuit model of pattern recognition mechanism unaffected by misalignment -neocognitron-," *Journal of the Institute of Electronics, Information and Communication Engineers A*, vol. 62, no. 10, pp. 658–665, 1979.

[64] J. C. Bass, N. B. Elsner, and F. A. Leavitt, "Performance of the 1 kw thermoelectric generator for diesel engines," in *AIP conference proceedings*, vol. 316, no. 1. American Institute of Physics, 1994, pp. 295–298.

[65] K. Ikoma, M. Munekiyo, K. Furuya, M. Kobayashi, T. Izumi, and K. Shinohara, "Thermoelectric module and generator for gasoline engine vehicles," in *Seventeenth International Conference on Thermoelectrics. Proceedings ICT98 (Cat. No. 98TH8365)*. IEEE, 1998, pp. 464–467.

[66] K. Matsubara, "Development of a high efficient thermoelectric stack for a waste exhaust heat recovery of vehicles," in *Twenty-First International Conference on Thermoelectrics, 2002. Proceedings ICT'02.* IEEE, 2002, pp. 418–423.

[67] M. A. Karri, "Modeling of an automotive exhaust thermoelectric generator: A thesis," Ph.D. dissertation, Clarkson University, 2005.

[68] E. Thacher, B. Helenbrook, M. Karri, and C. J. Richter, "Testing of an automobile exhaust thermoelectric generator in a light truck," *Proceedings of the Institution of Mechanical Engineers, Part D: Journal of Automobile Engineering*, vol. 221, no. 1, pp. 95–107, 2007.

[69] K. Wojciechowski, M. Schmidt, R. Zybala, J. Merkisz, P. Fuć, and P. Lijewski, "Comparison of waste heat recovery from the exhaust of a spark ignition and a diesel engine," *Journal of electronic materials*, vol. 39, no. 9, pp. 2034–2038, 2010.

[70] G. Meisner, "Program final report-develop thermoelectric technology for automotive waste heat recovery," General Motors Corporation, Tech. Rep., 2011.

[71] M. Mori, T. Yamagami, M. Sorazawa, T. Miyabe, S. Takahashi, and T. Haraguchi, "Simulation of fuel economy effectiveness of exhaust heat recovery system using

thermoelectric generator in a series hybrid," *SAE International journal of materials and manufacturing*, vol. 4, no. 1, pp. 1268–1276, 2011.

[72] D. Crane, J. LaGrandeur, V. Jovovic, M. Ranalli, M. Adldinger, E. Poliquin, J. Dean, D. Kossakovski, B. Mazar, and C. Maranville, "Teg on-vehicle performance and model validation and what it means for further teg development," *Journal of electronic materials*, vol. 42, no. 7, pp. 1582–1591, 2013.

[73] X. Liu, Y. Deng, Z. Li, and C. Su, "Performance analysis of a waste heat recovery thermoelectric generation system for automotive application," *Energy conversion and management*, vol. 90, pp. 121–127, 2015.

[74] S. Yu, Q. Du, H. Diao, G. Shu, and K. Jiao, "Effect of vehicle driving conditions on the performance of thermoelectric generator," *Energy Conversion and Management*, vol. 96, pp. 363–376, 2015.

[75] T. Y. Kim, A. A. Negash, and G. Cho, "Waste heat recovery of a diesel engine using a thermoelectric generator equipped with customized thermoelectric modules," *Energy Conversion and Management*, vol. 124, pp. 280–286, 2016.

[76] J. Merkisz, P. Fuc, P. Lijewski, A. Ziolkowski, M. Galant, and M. Siedlecki, "Analysis of an increase in the efficiency of a spark ignition engine through the application of an automotive thermoelectric generator," *Journal of Electronic Materials*, vol. 45, no. 8, pp. 4028–4037, 2016.

[77] F. Brito, J. Martins, E. Hançer, N. Antunes, and L. Gonçalves, "Thermoelectric exhaust heat recovery with heat pipe-based thermal control," *Journal of Electronic Materials*, vol. 44, no. 6, pp. 1984–1997, 2015.

[78] İ. Temizer and C. İlkılıç, "The performance and analysis of the thermoelectric generator system used in diesel engines," *Renewable and Sustainable Energy Reviews*, vol. 63, pp. 141–151, 2016.

[79] S. Vale, L. Heber, P. Coelho, and C. Silva, "Parametric study of a thermoelectric generator system for exhaust gas energy recovery in diesel road freight transportation," *Energy conversion and management*, vol. 133, pp. 167–177, 2017.

[80] A. Ziolkowski, "Automotive thermoelectric generator impact on the efficiency of a

drive system with a combustion engine," in *MATEC Web of Conferences*, vol. 118. EDP Sciences, 2017, p. 00024.

[81] R. Stobart, M. Wijewardane, and Z. Yang, "Comprehensive analysis of thermoelectric generation systems for automotive applications," *Applied Thermal Engineering*, vol. 112, pp. 1433–1444, 2017.

[82] X. Liu, Y. Deng, S. Chen, W. Wang, Y. Xu, and C. Su, "A case study on compatibility of automotive exhaust thermoelectric generation system, catalytic converter and muffler," *Case Studies in Thermal Engineering*, vol. 2, pp. 62–66, 2014.

[83] A. Massaguer, E. Massaguer, M. Comamala, T. Pujol, J. González, M. Cardenas, D. Carbonell, and A. Bueno, "A method to assess the fuel economy of automotive thermoelectric generators," *Applied Energy*, vol. 222, pp. 42–58, 2018.

[84] B. Orr, A. Akbarzadeh, M. Mochizuki, and R. Singh, "A review of car waste heat recovery systems utilising thermoelectric generators and heat pipes," *Applied thermal engineering*, vol. 101, pp. 490–495, 2016.

[85] P. Fernández-Yáñez, O. Armas, R. Kiwan, A. Stefanopoulou, and A. Boehman, "A thermoelectric generator in exhaust systems of spark-ignition and compression-ignition engines. a comparison with an electric turbo-generator," *Applied Energy*, vol. 229, pp. 80–87, 2018.

[86] B. Orr, A. Akbarzadeh, and P. Lappas, "An exhaust heat recovery system utilising thermoelectric generators and heat pipes," *Applied Thermal Engineering*, vol. 126, pp. 1185–1190, 2017.

[87] N. Kempf and Y. Zhang, "Design and optimization of automotive thermoelectric generators for maximum fuel efficiency improvement," *Energy Conversion and Management*, vol. 121, pp. 224–231, 2016.

[88] R. Poshekhonov, G. Arutyunyan, S. Pankratov, A. Osipkov, D. Onishchenko, and A. Leontyev, "Development of a mathematical model for optimizing the design of an automotive thermoelectric generator taking into account the influence of its hydraulic resistance on the engine power," *Semiconductors*, vol. 51, no. 8, pp. 981–985, 2017.

[89] C. Lu, S. Wang, C. Chen, and Y. Li, "Effects of heat enhancement for exhaust heat exchanger on the performance of thermoelectric generator," *Applied Thermal Engineering*, vol. 89, pp. 270–279, 2015.

[90] H. Lu, T. Wu, S. Bai, K. Xu, Y. Huang, W. Gao, X. Yin, and L. Chen, "Experiment on thermal uniformity and pressure drop of exhaust heat exchanger for automotive thermoelectric generator," *Energy*, vol. 54, pp. 372–377, 2013.

[91] X. Liu, C. Yu, S. Chen, Y. Wang, and C. Su, "Experiments and simulations on a heat exchanger of an automotive exhaust thermoelectric generation system under coupling conditions," *Journal of electronic materials*, vol. 43, no. 6, pp. 2218–2223, 2014.

[92] X. Liu, Y. Deng, K. Zhang, M. Xu, Y. Xu, and C. Su, "Experiments and simulations on heat exchangers in thermoelectric generator for automotive application," *Applied Thermal Engineering*, vol. 71, no. 1, pp. 364–370, 2014.

[93] B. Li, K. Huang, Y. Yan, Y. Li, S. Twaha, and J. Zhu, "Heat transfer enhancement of a modularised thermoelectric power generator for passenger vehicles," *Applied Energy*, vol. 205, pp. 868–879, 2017.

[94] J. He and T. M. Tritt, "Advances in thermoelectric materials research: Looking back and moving forward," *Science*, vol. 357, no. 6358, 2017.

[95] S. Bai, H. Lu, T. Wu, X. Yin, X. Shi, and L. Chen, "Numerical and experimental analysis for exhaust heat exchangers in automobile thermoelectric generators," *Case Studies in Thermal Engineering*, vol. 4, pp. 99–112, 2014.

[96] S. Lohani, "Energy and exergy analysis of fossil plant and heat pump building heating system at two different dead-state temperatures," *Energy*, vol. 35, no. 8, pp. 3323–3331, 2010.

[97] R. Ramírez, A. S. Gutiérrez, J. J. C. Eras, K. Valencia, B. Hernández, and J. D. Forero, "Evaluation of the energy recovery potential of thermoelectric generators in diesel engines," *Journal of Cleaner Production*, vol. 241, p. 118412, 2019.

[98] M. E. Demir and I. Dincer, "Performance assessment of a thermoelectric generator applied to exhaust waste heat recovery," *Applied Thermal Engineering*, vol. 120, pp. 694–707, 2017.

[99] Q. Cao, W. Luan, and T. Wang, "Performance enhancement of heat pipes assisted thermoelectric generator for automobile exhaust heat recovery," *Applied Thermal Engineering*, vol. 130, pp. 1472–1479, 2018.

[100] C. Tao, G. Chen, Y. Mu, L. Liu, and P. Zhai, "Simulation and design of vehicle exhaust power generation systems: The interaction between the heat exchanger and the thermoelectric modules," *Journal of Electronic Materials*, vol. 44, no. 6, pp. 1822–1833, 2015.

[101] Y. Wang, S. Li, X. Xie, Y. Deng, X. Liu, and C. Su, "Performance evaluation of an automotive thermoelectric generator with inserted fins or dimpled-surface hot heat exchanger," *Applied Energy*, vol. 218, pp. 391–401, 2018.

[102] Y. Wang, S. Li, Y. Zhang, X. Yang, Y. Deng, and C. Su, "The influence of inner topology of exhaust heat exchanger and thermoelectric module distribution on the performance of automotive thermoelectric generator," *Energy Conversion and Management*, vol. 126, pp. 266–277, 2016.

[103] W. He, R. Guo, H. Takasu, Y. Kato, and S. Wang, "Performance optimization of common plate-type thermoelectric generator in vehicle exhaust power generation systems," *Energy*, vol. 175, pp. 1153–1163, 2019.

[104] C. Su, W. Wang, X. Liu, and Y. Deng, "Simulation and experimental study on thermal optimization of the heat exchanger for automotive exhaust-based thermoelectric generators," *Case Studies in Thermal Engineering*, vol. 4, pp. 85–91, 2014.

[105] A. Massaguer, E. Massaguer, M. Comamala, T. Pujol, L. Montoro, M. Cardenas, D. Carbonell, and A. Bueno, "Transient behavior under a normalized driving cycle of an automotive thermoelectric generator," *Applied Energy*, vol. 206, pp. 1282–1296, 2017.

[106] G. J. Snyder and E. S. Toberer, "Complex thermoelectric materials," in *Materials for sustainable energy: a collection of peer-reviewed research and review articles from Nature Publishing Group*. World Scientific, 2011, pp. 101–110.

[107] R. Kondaguli and P. Malaji, "Geometry design and performance evaluation of thermoelectric generator," *The European Physical Journal Special Topics*, pp. 1–11, 2022.

[108] H. Yang, G. Shu, H. Tian, X. Ma, T. Chen, and P. Liu, "Optimization of thermoelectric generator (teg) integrated with three-way catalytic converter (twc) for harvesting engine's exhaust waste heat," *Applied Thermal Engineering*, vol. 144, pp. 628–638, 2018.

[109] R. Kondaguli and P. Malaji, "Analysis of bismuth telluride (bi2te3) thermoelectric generator," in *2020 IEEE Bangalore Humanitarian Technology Conference (B-HTC)*. IEEE, 2020, pp. 1–5.

[110] G. J. Snyder and T. S. Ursell, "Thermoelectric efficiency and compatibility," *Physical review letters*, vol. 91, no. 14, p. 148301, 2003.

[111] T. Ming, Y. Wu, C. Peng, and Y. Tao, "Thermal analysis on a segmented thermoelectric generator," *Energy*, vol. 80, pp. 388–399, 2015.

[112] Z. Ouyang and D. Li, "Modelling of segmented high-performance thermoelectric generators with effects of thermal radiation, electrical and thermal contact resistances," *Scientific reports*, vol. 6, no. 1, pp. 1–12, 2016.

[113] S. Walczak, "Artificial neural networks," in *Encyclopedia of Information Science and Technology, Fourth Edition*. IGI global, 2018, pp. 120–131.

[114] G. Hinton, S. Osindero, M. Welling, and Y.-W. Teh, "Unsupervised discovery of nonlinear structure using contrastive backpropagation," *Cognitive science*, vol. 30, no. 4, pp. 725–731, 2006.

[115] P. Wang, K. Wang, L. Xi, R. Gao, and B. Wang, "Fast and accurate performance prediction and optimization of thermoelectric generators with deep neural networks," *Advanced Materials Technologies*, vol. 6, no. 7, p. 2100011, 2021.

[116] Y. Zhu, D. W. Newbrook, P. Dai, C. K. de Groot, and R. Huang, "Artificial neural network enabled accurate geometrical design and optimisation of thermoelectric generator," *Applied Energy*, vol. 305, p. 117800, 2022.

[117] X. Niu, J. Yu, and S. Wang, "Experimental study on low-temperature waste heat thermoelectric generator," *Journal of Power Sources*, vol. 188, no. 2, pp. 621–626, 2009.

[118] A. Elarusi, N. Illendula, and H. Fagehi, "Performance prediction of commercial thermoelectric generator modules using the effective material properties," *Western Michigan University*, 2014.

[119] Y. Wang, C. Dai, and S. Wang, "Theoretical analysis of a thermoelectric generator using exhaust gas of vehicles as heat source," *Applied Energy*, vol. 112, pp. 1171–1180, 2013.

[120] J. Pandit, M. Thompson, S. V. Ekkad, and S. T. Huxtable, "Effect of pin fin to channel height ratio and pin fin geometry on heat transfer performance for flow in rectangular channels," *International Journal of heat and mass transfer*, vol. 77, pp. 359–368, 2014.

[121] Z. Niu, H. Diao, S. Yu, K. Jiao, Q. Du, and G. Shu, "Investigation and design optimization of exhaust-based thermoelectric generator system for internal combustion engine," *Energy Conversion and Management*, vol. 85, pp. 85–101, 2014.

[122] T. J. Hendricks, "Integrated thermoelectric–thermal system resistance optimization to maximize power output in thermoelectric energy recovery systems," *MRS Online Proceedings Library (OPL)*, vol. 1642, 2014.

[123] A. Montecucco, J. Siviter, and A. R. Knox, "The effect of temperature mismatch on thermoelectric generators electrically connected in series and parallel," *Applied Energy*, vol. 123, pp. 47–54, 2014.

[124] S. Bhattacharya, A. Chattopadhyay, and S. Bandyopadhyay, "Experimental investigation on the performance of automotive exhaust thermoelectric generators," *Applied Energy*, vol. 185, pp. 115–123, 2017.

[125] A. Alavi, A. Rahimi, and B. Mohammadi, "Experimental investigation of thermoelectric performance of automotive exhaust gas," *Energy Conversion and Management*, vol. 157, pp. 139–149, 2018.

[126] S. Jadhav, A. Chattopadhyay, and S. Bandyopadhyay, "Experimental and numerical analysis of automotive exhaust thermoelectric generators," *Energy Conversion and Management*, vol. 183, pp. 154–164, 2019.

[127] W. Yang, Y. Li, X. Wang, and Y. Zhang, "Effect of thermoelectric materials on

the performance of thermoelectric generators," *Renewable Energy*, vol. 130, pp. 596–603, 2019.

[128] X. Wu, H. Liu, W. Li, X. Wang, and Y. Zhang, "Effect of heat exchanger design on the performance of thermoelectric generators," *Applied Thermal Engineering*, vol. 133, pp. 148–155, 2018.

[129] Z. Chen, X. Wang, and Y. Zhang, "Working fluid on the cold side of thermoelectric generators," *Renewable Energy*, vol. 138, pp. 1209–1215, 2019.

[130] Y. Zhang, X. Wang, and W. Li, "Strategies to enhance heat transfer coefficient in thermoelectric generators," *Journal of Power Sources*, vol. 376, pp. 108–115, 2018.

[131] X. Li, Q. Huang, J. Zhang, Z. Wang, X. Liu, and F. Wang, "Thermoelectric generators for waste heat recovery: A review," *Renewable and Sustainable Energy Reviews*, vol. 106, pp. 1035–1053, 2019.

[132] J. Liu, X. Li, L. Xu, and Y. Zhou, "Thermoelectrics for waste heat recovery: Current status and future prospects," *Energy*, vol. 180, pp. 1158–1177, 2019.

[133] L. Xu, X. Li, and Y. Zhou, "Review of thermoelectric materials and devices for waste heat recovery," *Renewable and Sustainable Energy Reviews*, vol. 104, pp. 266–283, 2019.

[134] X. Wang, R. Yu, Q. Wang, W. Chen, and X. Zhang, "Design and experimental investigation of an aeteg-based exhaust heat recovery system for heavy-duty diesel engines," *Applied Energy*, vol. 221, pp. 1221–1231, 2018.

[135] X. Li, Q. Wang, R. Yu, W. Chen, and X. Zhang, "Experimental investigation on performance of an aeteg based exhaust heat recovery system for heavy-duty diesel engines," *Energy*, vol. 140, pp. 118–127, 2017.

[136] Y. Liu, Q. Wang, R. Yu, W. Chen, and X. Zhang, "Experimental investigation of an aeteg-based exhaust heat recovery system for a heavy-duty diesel engine," *Energy Conversion and Management*, vol. 184, pp. 186–197, 2019.

[137] ——, "Performance analysis of an aeteg-based exhaust heat recovery system for a heavy-duty diesel engine," *Applied Energy*, vol. 196, pp. 125–134, 2017.

[138] J. Wang, L. Zhang, J. Sun, and W. Zhang, "Heat transfer enhancement of exhaust heat exchangers using modified shapes and vortex generators," *Applied Thermal Engineering*, vol. 65, pp. 429–437, 2014.

[139] Y. Li, X. Yu, and D. Yu, "Experimental investigation on heat transfer enhancement of exhaust heat exchangers using vortex generators," *Applied Thermal Engineering*, vol. 36, pp. 117–124, 2012.

[140] Z. Luo, Y. Niu, and J. Li, "Heat transfer enhancement of a circular exhaust heat exchanger using vortex generators," *Applied Thermal Engineering*, vol. 31, pp. 391–397, 2011.

[141] L. Zhang, J. Wang, J. Sun, and W. Zhang, "Heat transfer enhancement of a circular exhaust heat exchanger using a combination of vortex generators and pin fins," *Applied Thermal Engineering*, vol. 30, pp. 1388–1396, 2010.

[142] J. Sun, L. Zhang, and W. Zhang, "Heat transfer enhancement of a circular exhaust heat exchanger using pin fins," *Applied Thermal Engineering*, vol. 29, pp. 3091–3097, 2009.

[143] S. Zhang, J. Li, and Q. Li, "A review on thermoelectric working fluids for high temperature applications," *Applied Thermal Engineering*, vol. 177, p. 115904, 2023.

[144] L. Wang, Z. Yang, J. Li, and Q. Li, "Thermoelectric performance of a water-cooled thermoelectric generator with a novel heat exchanger," *Energy*, vol. 230, p. 121701, 2023.

[145] X. Li, Y. Shen, J. Li, and Q. Li, "Thermoelectric performance of a water-cooled thermoelectric generator with a novel heat pipe heat exchanger," *Energy Conversion and Management*, vol. 225, p. 113691, 2023.

[146] X. Zhang, Y. Zhang, J. Li, and Q. Li, "Thermoelectric performance of a water-cooled thermoelectric generator with a novel heat exchanger and a micro-channel structure," *Journal of Power Sources*, vol. 481, p. 228760, 2023.

[147] H. Lee, J. Sharp, D. Stokes, M. Pearson, and S. Priya, "Modeling and analysis of the effect of thermal losses on thermoelectric generator performance using effective properties," *Applied Energy*, vol. 211, pp. 987–996, 2018.

[148] Y. Feng, X. Liu, W. Chen, Q. Lu, B. Li, and W. Wang, "Experimental study of the thermoelectric performance of thermoelectric generators under dynamic conditions," *Energy*, vol. 246, p. 123384, 2022.

[149] A. Bhandari, H. Wang, and Q. Zhang, "On-road testing of thermoelectric generators," *Applied Energy*, vol. 223, pp. 1295–1303, 2018.

[150] J. Zhou, Q. Zhang, H. Wang, and A. Bhandari, "Experimental characterization of the performance of thermoelectric generators under dynamic conditions," *Energy Conversion and Management*, vol. 137, pp. 117–125, 2017.

[151] C. Goupil, *Continuum theory and modeling of thermoelectric elements*. John Wiley & Sons, 2015.

[152] R. C. Mallik, J.-Y. Jung, S.-C. Ur, and I.-H. Kim, "Transport properties on sn-filled and te-doped cosb3 skutterudites," *Metals and Materials International*, vol. 14, no. 5, pp. 615–620, 2008.

[153] R. Courant, "Variational methods for the solution of problems of equilibrium and vibrations," *Bulletin of the American Mathematical Society*, vol. 49, no. 1, pp. 1–23, 1943.

[154] P. G. Lau and R. J. Buist, "Temperature and time dependent finite-element model of a thermoelectric couple," in *Fifteenth International Conference on Thermoelectrics. Proceedings ICT'96*. IEEE, 1996, pp. 227–233.

[155] H.-Z. maunfacturer, "Hiz data sheet," *Hi Z*, vol. 1, no. 1, p. 1, 2019.

[156] S. Weera, H. Lee, and A. Attar, "Utilizing effective material properties to validate the performance of thermoelectric cooler and generator modules," *Energy Conversion and Management*, vol. 205, p. 1427, 2020.

[157] G. Rogl, A. Grytsiv, P. Heinrich, E. Bauer, P. Kumar, N. Peranio, O. Eibl, J. Horky, M. Zehetbauer, and P. Rogl, "New bulk p-type skutterudites dd0. 7fe2. 7co1. 3sb12-xxx (x= ge, sn) reaching zt> 1.3," *Acta Materialia*, vol. 91, pp. 227–238, 2015.

[158] B. Poudel, Q. Hao, Y. Ma, Y. Lan, A. Minnich, B. Yu, X. Yan, D. Wang, A. Muto, D. Vashaee *et al.*, "High-thermoelectric performance of nanostructured bismuth antimony telluride bulk alloys," *Science*, vol. 320, no. 5876, pp. 634–638, 2008.

[159] J. Dismukes, L. Ekstrom, E. Steigmeier, I. Kudman, and D. Beers, "Thermal and electrical properties of heavily doped ge-si alloys up to 1300 k," *Journal of Applied Physics*, vol. 35, no. 10, pp. 2899–2907, 1964.

[160] Q. Yan, C. Shen, W. Wang, S. Wang, G. Chen, and Z. Xing, "Near infrared emission and energy transfer of bismuth–thulium co-doped chalcohalide glasses," *Journal of the American Ceramic Society*, vol. 93, no. 11, pp. 3539–3541, 2010.